MODEL EXPERIMENTS FOR THE DESIGN OF A SIXTY-INCH WATER TUNNEL

PART V

VANED ELBOW STUDIES

by

St. Anthony Falls Hydraulic Laboratory
University of Minnesota

Project Report No. 14

Submitted by

Lorenz G. Straub
Director

Prepared by

James S. Holdhusen
and
Owen P. Lamb

September, 1948

Prepared for the
David Taylor Model Basin
Department of the Navy
Washington, D.C.

Bureau of Ships Contract NObs-34208
Task Orders 2 and 3

PREFACE TO REPORT SERIES

Contract NObs-34208 between the University of Minnesota and the Bureau of Ships, Department of the Navy, provides for making hydrodynamic studies in compliance with specific task orders issued by the David Taylor Model Basin calling for services to be rendered by the St. Anthony Falls Hydraulic Laboratory. Certain of these task orders related to model experiments for the design of a 60-in. water tunnel.

The end result of the studies related to the 60-in. water tunnel proposed eventually to be constructed at the David Taylor Model Basin was crystallized as a series of six project reports, each issued under separate cover as follows:

Part I DESCRIPTION OF APPARATUS AND TEST PROCEDURES (Project Report No. 10)

Part II CONTRACTION STUDIES (Project Report No. 11)

Part III TEST SECTION AND CAVITATION INDEX STUDIES (Project Report No. 12)

Part IV DIFFUSER STUDIES (Project Report No. 13)

Part V VANED ELBOW STUDIES (Project Report No. 14)

Part VI PUMP STUDIES (Project Report No. 15)

The investigational program was under the general direction of Dr. Lorenz G. Straub, Director of the St. Anthony Falls Hydraulic Laboratory, and the work was supervised by John F. Ripken, Associate Professor of Hydraulics.

PREFACE TO PART V

Part V of the water tunnel report series was prepared in accord with Task Order 2 of Contract NObs-34208 but, in addition, serves as one part of a report series dealing with fluid flow diversion studies as conducted in the Laboratory under Task Order 3 of Contract NObs-34208.

In the latter series, this report has been preceded by Project Report No. 5 entitled THE NATURE OF FLOW IN AN ELBOW, and will be followed by a report covering a comprehensive study of flow diversion by guide vanes. In this respect, Part V is designed to stand apart and may be used independently of the other parts of the water tunnel series.

Mr. E. Silberman, Research Associate, supervised the flow diversion experimental studies. The report was jointly written by James S. Holdhusen and Owen P. Lamb, Research Fellows. Elaine Hulbert and Ethel Swan assisted in preparation of the manuscript. Mr. Holdhusen was project leader on the water tunnel experimental work and was assisted by Clyde O. Johnson and Harry D. Purdy. Mr. Lamb served as project leader on the flow diversion experiments and was assisted by Feng Hsiao, Alexander Rodionov, and June Brevdy.

S Y N O P S I S

A study of vaned elbows was made at the St. Anthony Falls Hydraulic Laboratory as part of the research program for the design of the proposed 60-in. water tunnel of the David Taylor Model Basin, Bureau of Ships, Department of the Navy. The shape, size, and spacing of the vanes to be used in the elbows were determined from the work of previous investigators, and model studies of the vane cascade were performed at the Laboratory as part of a broad research program in fluid flow diversion. Additional model studies of the assembled elbow were performed on a 1:10 scale model of the 60-in. tunnel.

From the model studies on the vane cascade, the optimum angular setting of the vanes was obtained, as well as data regarding pressure distribution and energy loss. The validity of the application of model results to a prototype was examined in the additional studies on the elbows in the model water tunnel.

On the basis of this study, a cascade of vanes of the proportions shown in Fig. 44 of this report is recommended for use in the prototype tunnel. The vanes are to be used at a spacing-chord ratio of 0.48 and a stagger angle of 99° to 101°. The miter line is to cross each vane at about 37 1/2 per cent of the chord from the leading edge. Structural analysis of these vanes indicates that they may be of either solid or hollow cross section without detrimental effects on stresses, deflections, or vibrations. The studies also indicate that the vaned elbows in the prototype tunnel will be free from cavitation.

CONTENTS

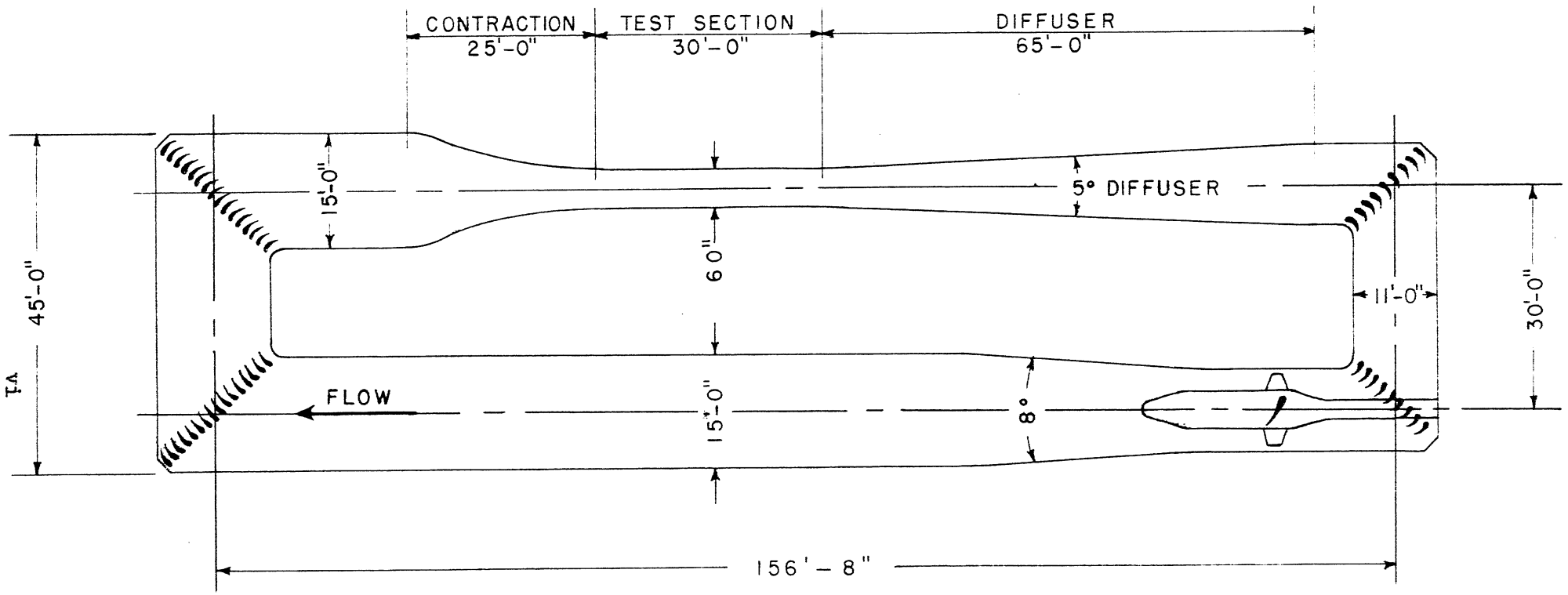

PROPOSED 60" WATER TUNNEL

VANED ELBOW STUDIES

I. INTRODUCTION

This paper is concerned primarily with the application of a guide vane cascade to the elbows in a proposed 60-in. water tunnel at the David Taylor Model Basin. It is proposed to select a vane shape, size, and spacing with reference to work of previous investigators; to determine experimentally the hydrodynamic performance of the resulting cascade of vanes; to check the final cascade in an elbow of a model water tunnel to determine the correlation between model and prototype; and to check the suitability of the proposed vanes for the 60-in. tunnel with regard to stresses, deflection, and vibrations.

The primary function of a guide vane elbow is to produce a given change in the stream direction, in this case a 90° change, with as little disturbance as possible in the resulting flow. Secondarily, the flow diversion should take place with small energy loss, and without cavitation, vibration, or poor loading characteristics on the vanes. The goal of this paper is the selection of a cascade to satisfy these criteria.

Although many published reports were referred to in the course of this investigation, only a few of the reports were so closely related to the immediate problems that separate mention of them need be made. An enumeration of the contributions of all of the previous investigators of this subject would not be warranted in an objective report of this nature, since reference has been made to a rather complete summary and bibliography of the literature of fluid flow diversion compiled at the St. Anthony Falls Laboratory [1].* The reports to which particular reference has been made in designing the cascade for the water tunnel are those of Klein, Tupper, and Green [2], Collar [3], and Kröber [4].

---

*Numbers in brackets refer to the corresponding numbers in the list of references, p. 35.

II. SELECTION OF THE GUIDE VANE CASCADE

A. Definition of Terms

The terms used to describe a given cascade sometimes vary among different investigators. Those used in this report are defined in Fig. 1 and in the statements below.

The vanes of a cascade are assumed to be of uniform cross section throughout so that the vanes may be replaced by their profile in a plane. The vane profile is defined by its chord length (c) and certain relative shape characteristics such as maximum camber and maximum thickness. Only the chord is of importance at this time. The chord line is defined as the line obtained by placing a straight edge against the pressure side of the vane profile; it is tangent to the leading and trailing edges. The chord length is the distance between the projections of the extreme ends of the vane on the chord line.

A cascade of vane profiles is obtained by first selecting a straight line as a cascade axis. To form the cascade, vane profiles are placed on the cascade axis so that corresponding points on the profile fall at regular intervals along the axis and so that the chords of all the profiles make the same angle with the cascade axis. The distance between corresponding points on the axis is then the vane spacing (s) and the angle between the chord and the axis is the vane stagger (θ). A given cascade is defined by the profile of the vanes, the chord length, the dimensionless spacing-chord ratio (s/c), and the stagger angle (θ). Other investigators sometimes use the gap-chord ratio, where the gap is the projection of the spacing in the direction of approaching flow, in place of the spacing-chord ratio.

The aspect ratio of the passage between vanes is important in determining whether two-dimensional flow exists around the vanes. Aspect ratio is defined as the average span of the two adjacent vanes divided by the free distance between them.

A cascade of vanes is installed in an elbow so that the cascade axis falls in a plane parallel to the miter plane of the elbow, where the miter plane is that plane formed by the intersection of the elbow walls. For a 90° bend, the cascade axis is placed at 45° to the direction of the approaching flow. The angle of attack between the approaching flow and the chord, designated by the symbol α, is then 45° less than the stagger angle; $\alpha = \theta - 45^\circ$.

B. Vane Shape

The vane profile selected (Fig. 2) was formed with a minimum number of simple circular curves. In practice, this is considered preferable because of ease of fabrication to the more complex theoretical curvatures and bent airfoil shapes used by previous investigators. The investigation of Klein, Tupper, and Green tended to show that vane shape is not a critical factor in producing good flow quality. Consequently these tests utilized a vane with a thickened section that has good structural qualities and reduces the free width between vanes to an approximately uniform value. The vane was designed with a rounded leading edge, since experiments of other investigators indicated that a vane stagger greater than 90° might have to be used. This design reduces the possibility of cavitation and separation of the flow from the vane surface at the leading edge because it is relatively insensitive to changes in the vane stagger.

The vanes were also fitted with end trunnions to permit adjustment of the stagger angle. The axis of rotation chosen for the experimental models was near the center of pressure, estimated from preliminary considerations, but this point proved to be downstream of the center of pressure found by the subsequent experiments. This discrepancy would of course cause mechanical difficulties with a large-scale prototype vane designed to pivot on trunnions, but inasmuch as the proposed tunnel design is to have fixed vanes, the location of the trunnion in the preliminary studies is immaterial.

These vanes are designated as Type 1 vanes for future reference and to avoid confusion with vanes to be tested in another program.

C. The Vane Cascade

Two general requirements appear to govern the choice of number of vanes and length of chord of each vane in a cascade:

1. From previous experimental work it appears that a spacing-chord ratio of the order of magnitude of 1/2 is desirable for minimum energy loss.

2. Minimum energy loss also involves the prevention of secondary spirals in the flow between the vanes. This requires an aspect ratio of the order of magnitude of 6 or larger.

Graphical divisions of a circular area into strips of equal width indicated that at least 6 or 8 vanes are required to approximate this aspect ratio in the greater portion of a circular duct. Increasing the number of

vanes leads to a superior discharge velocity distribution and reduction in individual vane size. However, if the number is increased immoderately, flimsy proportions, large deflections, and vibration and noise under high water impact loadings may result. These can be alleviated by tying adjacent vanes together at points between the end supports, thus reducing the free span. However, such webs or tie plates, even though faired, tend to reduce the aspect ratio and increase the energy loss.

These dimensional relations led to a division of the circular tunnel area into 18 spaces, requiring 17 vanes, a larger number than is used in most tunnels. The smaller spacing, however, results in a better velocity distribution and in a chord length of practicable dimensions in a large tunnel.

For the 60-in. prototype tunnel these considerations lead to a spacing of 14.14 in. between vanes. A choice of spacing-chord ratio of 0.48 then gives a chord of 29.5 in. and leads to fabricating dimensions in even inches (Fig. 44). Figure 2 shows the fabricating dimensions of the same vane as used on a 1:10 scale model of the prototype tunnel where the spacing is 1.414 in. and the chord is 2.95 in.

The vanes are to be assembled in cascade along an axis passing through the trunnions of each vane (Fig. 1). The stagger angle is to be adjusted by rotating the vanes about their trunnions. Since the center of pressure is actually forward of the trunnions, the cascade axis will be placed parallel to, but slightly to the rear of, the miter plane, a distance of about 1/4 in. in the model tunnel.

The selection of the cascade was made by J. F. Ripken in the preliminary design of the 60-in. water tunnel at the Taylor Model Basin in 1945 [5].

D. Vanes Used in Experiments

Two sets of vanes were actually fabricated to the dimensions shown in Fig. 2. One set was for use in all the elbows in a 1:10 scale model water tunnel and the other for a separate elbow in a flow diversion test bend. It was determined that approximately 70 ft of vane stock would be needed to outfit the vaned turns of the model water tunnel. Vane stock of extruded aluminum with the profile dimensions shown in Fig. 2 was procured in 10-ft lengths from the Aluminum Company of America. The desired lengths of span were cut from this stock and fitted into the cascade frames. The vanes used in the flow diversion apparatus are described in a subsequent section of this report

but it should be noted here that they were cast to the dimensions of Fig. 2 from "Cerrobend", a low melting temperature alloy.

A final check of the shape of the experimental vanes disclosed a very close adherence of the Cerrobend vanes to all of the specified dimensions but it also revealed certain significant discrepancies in the shape of the extruded aluminum vanes. These differences were found to be at the leading edges and region near the trailing edges of the aluminum vanes; the thicker sections of the vanes satisfied the specifications. The leading edge appeared to vary somewhat at different points along the spans but in general the nose was slightly more pointed than the radius of 0.08 in. specified. The tail of the vane was thinner than the design called for with a small ridge at the trailing edge. This thin section was bent around towards the center of curvature so that the profile presented a turn of about 95°. The overturning of the geometrical profile and the ridge were corrected before the installation of the vanes in the cascade frames. The verification of the performance of the aluminum vanes in relation to the dimensionally correct Cerrobend vanes is included in the experimental data.

The Cerrobend vanes were polished smooth and then waxed before they were tested, but a slight roughness could be detected on the surfaces of the aluminum vanes. The effect of any differences in roughness between the vanes was not apparent in the evaluation of energy loss in the cascades nor in the observations of the flow on the surfaces of the vanes as interpreted in a later section.

III. EXPERIMENTAL APPARATUS, PROCEDURE, AND DATA

A. Experiments in the Flow Diversion Apparatus

1. The Apparatus

The first studies of the proposed vane cascade were performed in a transparent 90° elbow in a square duct. The apparatus for these experiments consisted of a test stand with suitable piping and measuring facilities that had been set up for all types of flow diversion experiments. For these studies a miter elbow, in which banks of guide vanes could be tested, was fitted in the flow diversion apparatus. A photograph of the flow diversion test stand is reproduced in Fig. 3, and one of the test elbows is shown in Fig. 4.

a. The Experimental Elbow

Details of the miter elbow are given in Fig. 5. The elbow and its two tangent pieces were fabricated of transparent lucite with an inside cross section 6 in. square and a bend deflection angle of 90°. The elbow was fitted with holes to receive the vane trunnions along a line 1/4 in. downstream from the miter line for reasons previously explained. The elbow was rounded to a 2 1/2-in. radius at the outer corner and a 1 1/2-in. radius at the inner corner to provide a uniform gap between the walls and the adjacent vanes.

The elbow was installed in the test stand with the bend in the horizontal plane. The entrance to the upstream tangent of the elbow was bolted to a plate on the end of a 12-in. diameter supply pipe. A 6-in. square hole was centered in the plate to match the cross section of the lucite pipe. Bolts through this plate served to hold a bell-mouthed contraction and a distributor ring in place in the 12-in. pipe. This distributor ring was used in conjunction with a supply of compressed air to introduce dyes or air bubbles into the flow.

For making measurements of the velocity and pressure in the elbow, three measuring stations as well as two measuring discs and many separate piezometer taps were provided. These are shown in detail in Fig. 5. The discs were used to permit insertion of a pitot cylinder to obtain velocity and energy measurements immediately before and after the vanes, while the separate piezometer taps were used to obtain wall pressure measurements at many points around the bend. All 1/16-in. holes designed for wall pressure readings were carefully rounded at the inside edge to about 1/64-in. radius to remove all burrs. At the measuring stations, the 1/4-in. holes allowed entry of a pitot cylinder into the flow. These measuring sections made possible the obtaining of wall pressure readings at 24 points and velocity and energy readings at 45 points within the section in the course of a normal traverse.

b. The Test Stand

The 12-in. diameter supply pipe carrying fluid to the test elbow was connected to an air blower, and also to the main Laboratory supply channel, drawing water directly from the Mississippi River. This arrangement is shown in Fig. 6. The regulating valves in the 12-in. line were placed about

40 ft upstream from the elbow. A long honeycomb in the entrance pipe rectified the flow before it entered the bellmouth of the 6-in. duct. Flow of water through the elbow up to 4.5 cu ft per sec was measured by a discharge measuring flume, while the capacity of the blower limited the flow of air to 30 cu ft per sec. The variations of the flow from either source were sufficiently small to be neglected entirely in the analysis and computation.

The discharge from the downstream tangent of the lucite duct was led through a diffuser and a short length of 12-in. round pipe into a vertical pipe. The portion of this vertical pipe above the elevation of the lucite duct served as a standpipe, and the lower portion conducted the water flow to the previously calibrated measuring flume. A valve in this lower pipe regulated the pressure in the lucite duct while the standpipe protected the duct from an excess of pressure.

c. Instrumentation

Instruments used in making readings were a long pitot cylinder and a shorter cantilevered cylinder. The reliability of these same instruments is discussed in a report issued by the St. Anthony Falls Hydraulic Laboratory [9]. Pressure readings with water flowing in the duct were recorded by a 100-in. U-tube using air as the indicating fluid, and a 50-in. U-tube using kerosene as the indicating fluid. An inclined manometer draft gauge was used to record the pressures for the flow of air and a very large manometer bank was used as a method of obtaining simultaneous photographic readings when using water.

d. The Experimental Vanes

The guide vane elbow was designed to receive a bank of five Type 1 vanes at the 1.414-in. spacing previously determined. The free span of the vanes was 6 in., the full height of the duct. Thus the spacing-chord ratio is 0.48, the gap between the vanes is one inch, and the aspect ratio is 6 for these experiments. The aspect ratio of 6 assures two-dimensional flow near the centers of the vanes where measurements were to be made.

As previously noted, the vanes were cast from Cerrobend, a low melting temperature alloy, to the dimensions of Fig. 2, and were finished with a smooth surface. Pressure lines of 1/8-in. OD copper tubing were cast into all five of the vanes. These tubes extended out through a trunnion to provide a connection outside the duct for attaching the tubes to the manome-

ters. Wall-mounted set screws bearing on the ends of the vanes prevented the vanes from turning about the vane trunnions. This arrangement allowed a rigid support for the vanes in the simplest manner possible without disturbing the flow. Figure 7 is a photograph of a cast vane used in these experiments.

A second set of five Type 1 vanes was cut from the extruded aluminum stock secured for the model water tunnel. These were arranged for mounting in the same manner as the Cerrobend vanes but contained no piezometer holes.

2. Experimental Procedure and Data

Values of Reynolds number in this paper are based on a length parameter which is arbitrarily taken as the length of a side of the square duct, or 0.50 ft. Based on the chord length of a vane, which is approximately 0.25 ft, the Reynolds numbers are one-half of those quoted in the experiments. Mean velocity is considered as the velocity obtained by dividing the discharge through the duct by the cross-sectional area of 0.25 sq ft.

a. Visual and Photographic Methods

The first flow observations as well as many of the subsequent findings were made by visual means and recorded photographically. Figures 8 and 9 incorporate six photographs taken of the guide vanes at two different water flows. Air bubbles introduced into the flow through the distributor ring along the duct bottom rise to mid-depth and appear as streaks around the bend in the photographs, furnishing a basis for a first comparison of the three trial staggers of 90°, 96°, and 101°. The two flows had mean velocities of 7.9 ft per sec, and 16.7 ft per sec, corresponding to Reynolds numbers of 300,000 and 640,000 respectively. The photographs indicate the existence of a more nearly axial flow immediately before and after the bend for a stagger of 101° than is true for the other two settings. For staggers of 90° or 96° there was an apparent deflection of the flow towards the inside of the bend in the upstream tangent. These photographs of air bubbles in the flow must not be interpreted too literally in the gap between the vanes where centrifugal forces affect the ability of the air bubbles to follow the streamlines. In the approach flow, however, they should yield reliable results and they should locate the front stagnation point of the vanes quite accurately.

In the course of the experiments a number of photographs were taken of the vanes and other bounding surfaces with strings, dyes, and streaks used to indicate the direction of the boundary streamlines. Figure 10 includes photographs of the vanes at stagger angles of 96° and 101° with threads glued on their suction sides. A flow of air with a mean velocity of 100 ft per sec corresponding to a Reynolds number of 310,000 was passing through the duct at the times the pictures were taken.

Figures 11 and 12 are photographs of the same air flow, using a filament of colored water to examine the boundary layer. Figures 11 [a] and 11 [b] were made at a stagger angle of 96°. In the former the colored fluid is introduced through a piezometer hole about 2 in. from the trailing edge of the central vane, while in the latter it is introduced through a hole about 1/2 in. from the trailing edge, both on the suction surface of the vane. Figure 11 [c] was made at a stagger angle of 101° and fluid is introduced near the leading edge. Figure 12 contains photographs taken as dye was introduced through holes near the trunnions at the bottoms of the vanes for the stagger angles of 96° and 101°. In each case the vane observed was either the central vane of the cascade or the next one towards the inside of the bend.

Similar visual observations of the flow near the surface of the vanes were made in a water flow with a mean velocity of 11.52 ft per sec and a Reynolds number of 300,000. A mixture of aluminum dust and SAE 30 machine oil was carefully applied to the vane surface as well as the duct wall at the inside of the bend. When this paste had been applied, the flow of water was started and photographs were made at 5- to 10-minute intervals. Since the photographs did not show any basic difference in the design worn in the paste with time other than a sharper contrast, the photographs reproduced (Fig. 13) are the clearest ones taken at each stagger angle.

By fastening threads on a fine steel wire, it was possible to traverse directly behind the vanes in a plane at mid-depth and in a plane about one inch from the duct floor. This was done in an air flow with the same average velocity and Reynolds number as before. Although it was not possible to record these observations photographically, they were helpful in obtaining a better understanding of the flow close to the vanes.

The traverse at mid-depth at the 96° stagger showed an extremely turbulent region from a point directly behind the trailing edge of a vane to

a point about 3/8 in. from the suction side. The same region at the 101° stagger was very smooth except directly behind the trailing edge, where moderate disturbances of the strings were noted. The flow behind the portion of the gap closest to the pressure side of a vane was very smooth at the 96° stagger angle and exhibited a slight fluctuation at the 101° stagger. For the mid-depth traverse the strings streamed parallel to the top and bottom duct walls and also parallel to the side walls except that a slight component towards the outside of the bend was observable adjacent to the suction side of a vane. The traverse at one inch from the bottom of the duct indicated vertical direction components existing close to the vanes, upwards on the suction sides and downwards on the pressure sides.

Streams of colored water were released in an air flow along the bottom of the duct. Both stagger angles had a direction component towards the inside of the duct in the downstream tangent, with the 96° stagger exhibiting a greater deviation from an axial flow. These are boundary phenomena. However, the difference in flow directions exhibited by dye particles which lie in the boundary layers, as opposed to particles in the core of the moving stream, is explainable by reasoning that boundary particles are motivated largely by pressure gradients, whereas core flow particles are motivated largely by their own inertia forces.

b. Measurements in the Duct

The cross section at each of the three measuring sections in the duct was divided into elementary square and rectangular areas. There were twenty-five one-in. squares, twenty 1/2 by one-in. rectangles, and four 1/2-in. squares. By obtaining a relative static pressure, a relative total head, and the magnitude and direction of the velocity at the center of each of these elementary areas, the flow could be adequately defined in the cross section. Previous investigations with the flow diversion apparatus in connection with work on a radius elbow [6] indicated that the best integration of the discharge over the section could be obtained by neglecting the flow through the 1/2-in. squares in the corners, this omission being balanced by the small excess in readings obtained in the twenty 1/2 by one-in. rectangles next to the walls. The previous work on the flow diversion apparatus also established the fact that a very close approximation to the static pressure at an internal point could be obtained by assuming linear variation between wall pressures directly above and below the point in question. The

static pressures used for calculations were, therefore, interpolated at each internal point from the wall pressures measured at the 36 piezometer taps around the cross section. The direction angles were obtained by inserting the long pitot cylinder from the top and then from the side to the point of measurement. The stagnation head of the fluid at the point was measured with the cylinder in both the horizontal and vertical positions. The positions of all the points where actual measurements were made in a typical measuring station are indicated in Fig. 5.

The circular disc mounting at the bottom of the duct was used to facilitate intrusion of the cantilevered pitot cylinder into a flow as close as 1/4 in. to trailing edges of the inner vanes, and to read wall pressures just upstream and downstream of the vanes. Measurements taken this close to the vanes with the pitot cylinder must be considered only qualitative, because of the vibrations of the cylinder at mid-depth in moderate velocities, and because of the relatively large diameter of the cylinder (1/4 in.) compared to the distances over which there is an appreciable change in the magnitude and direction of the velocities.

All of the measured pressures in all of the runs are with reference to the static pressure at a section located near the upstream end of the approach tangent. This eliminated local errors resulting from the presence of measuring tubes in the flow or small changes in the total head on the system.

The series of runs in the flow diversion apparatus which yielded numerical data are indexed in Table I. Series 19 is a special series used to compare the performance of the extruded aluminum vanes with the performance of the cast Cerrobend vanes.

Table I

Series No.	Fluid	Reynolds No.	Vane Material	Vane Stagger	Average Velocity Ft Per Sec	Data on Fig. No.
10	Water	119,000	Cerrobend	96°	2.40	14
11	Water	307,000	Cerrobend	96°	11.43	15
12	Air	308,000	Cerrobend	96°	101.90	16
13	Water	353,000	Cerrobend	96°	7.82	17
14	Water	707,000	Cerrobend	96°	16.68-18.55	18
15	Water	833,000	Cerrobend	96°	16.78	19
16	Water	111,000	Cerrobend	101°	4.23	20
17	Water	302,000	Cerrobend	101°	11.42	21
18	Water	478,000	Cerrobend	101°	18.20	22
19	Water	300,000	Aluminum	101°	11.43	23

Each series in the table above consists of complete measurements in the cross sections D-D and M-M indicated on Fig. 5. The readings at Section K-K were in some cases limited to the upper or lower half of the section with the other half assumed symmetrical. The relative pressures around the bend were recorded for every series both at mid-depth and at one inch from the bottom at the points indicated on Fig. 5. In addition to these readings the relative pressures around the vanes were found at mid-depth for all the series except 10, 13, 15, and 19. The holes in the vanes were in the horizontal plane one inch from the floor of the duct for the first three of these, while Series 19 had aluminum vanes installed with no provision to obtain the relative pressures on the surface.

c. Method of Presenting Data

The data obtained at the measuring sections are presented as diagrams in Figs. 14 through 23. The velocities and relative total heads are reduced to the dimensionless form in the figures. In each case the magnitude of the velocity component is listed as the quotient $\frac{V}{\overline{U}}$ where V is the velocity component and $\overline{U}$ is the average longitudinal velocity through the section. Total heads are given in terms of the stagnation head of the average velocity through the section. The individual wall pressures at the measuring sections are not presented in the diagrams, although they were measured in every case.

Each total head and longitudinal velocity component is entered on the diagrams at the point where the measurement was taken. The velocity components in the plane of measurement are in the form of vectors originating at the point of measurement. The scale for the magnitude of these vectors is listed on each diagram (one inch = one unit). Contour lines were interpolated between the measured points of longitudinal velocity components and relative total heads to complete the illustration of the flow at the sections of measurement. The diagrams are to be examined with the observer looking downstream at the cross section, with the inside of the bend on his left.

To obtain the velocity head at a point, the relative static pressure was subtracted from the relative total head at that point. This velocity head was then corrected by first dividing by the square of the cosine of the angle between the velocity and the plane of measurement and then multiplying by the pitot cylinder coefficient of 0.98 as recommended in the appendix. The corrected total head at a point was obtained by adding the static pressure to the corrected velocity head.

The velocity at a point was computed using the corrected velocity head and was then resolved into longitudinal, horizontal, and vertical components using the previously obtained direction angles. To obtain the average velocity through a cross section, each elementary area was multiplied by the local longitudinal velocity component at its center; these products were totalled for the cross section and the sum was divided by the total area of the cross section. These averages generally compared within 1 1/2 per cent with the averages obtained by flume discharge measurements. To obtain energy flowing through a cross section, each elementary area was multiplied by the local longitudinal velocity components and total heads at the center of the area; these products were totalled for the cross section and the sum was divided by the integrated discharge data obtained in the previous step. The average total head through a section as obtained by integration is listed beneath each relative total head diagram, and the integrated average velocity through the section is listed beneath each velocity diagram.

Relative pressures taken around the bend at mid-depth are plotted in dimensionless form normal to the duct walls in Fig. 24. Positive pressures are plotted out from the walls and negative pressures are directed into the fluid. There are six diagrams of this type in Fig. 24, covering Series 10, 15, 16, 17, 18, and 19. The diagrams for Series 11, 12, 13, and 14 are not included because they differ very little from those of Series 10 and 15, the smallest and largest Reynolds numbers taken at the same stagger angle of 96°. Wall pressures near the bottom wall were also obtained but those are not presented here. They were roughly 10 per cent smaller than those at mid-depth.

Figures 25 and 26 present dimensionless data from pressure measurements on the vanes near mid-depth, the former for a stagger angle of 96° and the latter for an angle of 101°. Originally both individual readings, using the measuring manometers, and simultaneous readings, using the large manometer board, were taken for each flow series. The small discrepancies between the data obtained by the two methods were attributed to difficulties in maintaining tight pressure lines to the manometer board. Simultaneous readings were discontinued during the later series, since the change in average pressures at a point on the vane with time was found to be negligible. In Figs. 25 and 26 the pressures are plotted as outward normals to the vane profile from the location of the tap where the measurement was taken. Positive pressures are shown as solid lines and negative pressures are plotted as broken lines. The

dimensionless data plotted are obtained for each series of runs by dividing the measured pressure by the stagnation head of the mean velocity through the duct. Figure 25 is an average of Series 10, 11, and 14, while Fig. 26 is an average of Series 16, 17, and 18. Individual readings usually varied no more than five per cent from the average.

Figure 27 is a conventional diagram of the dimensionless pressures around a vane plotted normal to the chord for the 96° and 101° stagger angles. The same average dimensionless pressures as those used in Figs. 25 and 26 were used for Fig. 27. The measurements at the center vane are plotted in Fig. 27 except that the three taps around the nose at the stagger of 101° were taken on the next vane towards the inside of the bend. This change of vanes is considered valid at the stagger angle of 101° because of the uniformity of loading between the vanes (Fig. 26).

In Fig. 28 the dimensionless pressures around the central vane of the cascade are plotted for three different Reynolds numbers for the stagger of 101°. The pressures are obtained and plotted in the same manner as in Figs. 25 and 26. As noted previously, pressures around the vanes near the bottom walls were also measured. The data are not plotted here but these pressures were roughly ten per cent smaller in absolute magnitude than those near mid-depth.

This report has limited the presentation of data around the guide vanes to the values readily transferable to the problem of vaned turns in the circular ducts of the water tunnel. Hence many of the measurements where particular phenomena depending on the shorter aspect ratio of the cascade and geometrical shape of the duct are apparent have not been included.

B. Experiments in the Model Water Tunnel

Some experiments similar to those conducted in the flow diversion apparatus were also performed on the Type 1 vanes installed in the elbows of a 1:10 scale model of the 60-in. prototype water tunnel. These experiments were performed to check the correlations between data obtained in the more or less idealized, two-dimensional, uniform flow of the flow diversion apparatus and that actually obtaining in a practical duct. These experiments in the model water tunnel were only incidental to a larger testing program on that tunnel, and the description of the tunnel given here contains only those items essential to an understanding of the vane testing program.

1. Description of the Tunnel

The 1:10 scale model of the 60-in. prototype tunnel and one of the large vaned elbows of the model are shown in Figs. 29 and 30, and the dimensions of a sectional elevation in Fig. 31. The model is located on the main Laboratory floor of the St. Anthony Falls Hydraulic Laboratory of the University of Minnesota. Water is circulated through the tunnel by a 12-in. axial flow impeller driven by a 15 hp variable speed drive unit. Water passes from the impeller through straightening vanes to a short 8° diffuser, and from there to an 18-in. diameter settling section, which contains two vaned elbows which turn the stream direction 180°. At the end of the 18-in. diameter section, there is a contraction cone which accelerates the water to nine times its velocity in the settling section, and from this cone the water passes through the 6-in. diameter test section. The test section is followed by a 5° diffuser and a 13.2-in. diameter cylindrical section containing the two vaned elbows which return the water to the impeller.

The pressure in the tunnel was varied by means of a movable pan containing water at atmospheric pressure connected to the throat of the contraction cone. The pan was housed in the pressure control tower and could be elevated 16 ft above or lowered 31 ft below the test section to provide a wide range of pressure variation. The pressure drop across the contraction cone was used to measure the bulk velocity of the flow. The cone had previously been calibrated by a non-recirculating gravity flow which was measured in weighing tanks.

2. Description of Instruments

Velocity traverses pertinent to this report were taken at Stations 5, 6, 7, 10, 11, and 12 (Fig. 31). Each station consisted of a ball-and-socket mounting, hereafter referred to as the main mounting, and three 3/8-in. diameter openings, spaced 90° apart around the tunnel cross section. The main mounting (Fig. 32) was designed to permit traversing of the entire cross section with a 3/8-in. diameter pitot cylinder. The 3/8-in. openings could be used to measure the wall pressure or as taps through which the pitot cylinder could be inserted.

The pitot cylinder used is shown in Fig. 32. The two holes in the nose piece spaced 40° on either side of the center line were connected to opposite sides of a differential manometer, and a pressure reference station

was connected to one side of the same manometer. The direction of flow was determined by rotating the cylinder about its longitudinal axis until the pressures at the two holes in the nose piece were equal. This direction of flow was indicated on Scale and Index C (Fig. 32). After the direction had been determined, the line to the manometer from one of the pitot cylinder holes was shut off and switched to the pressure reference connected to the manometer. The pitot cylinder was rotated 40° from the position just determined as the flow direction, so that the hole still connected to the manometer faced the flow and recorded the total head in the flow (static plus dynamic pressure). The manometer reading was the indicated velocity head, which was later corrected for the difference in static pressure between the station being traversed and the pressure reference station. It was necessary to use the pressure reference instead of the pressure taps at the station being traversed because the wall pressure at the station being traversed was influenced by the proximity of the pitot cylinder to the pressure taps. With the pitot cylinder in the main mounting (Fig. 33), Scales A and B determined the position of the pitot nose in the cross section. When the pitot cylinder was in one of the alternate positions (through one of the 3/8-in. taps), a strap brass index was constructed for Scale C, and Scale A was sufficient to determine the position of the cylinder nose in the cross section.

Although care was exercised in constructing the pitot cylinder and its mountings and indexes, it is believed that the angularity of flow measurement in the tunnel is accurate only to within $1\ 1/2^{\circ}$.

3. Pressure Measurements on a Tunnel Vane

The central vane in Elbow I of the tunnel was fitted for taking pressure readings at ten points on the surface (Fig. 34). Copper tubing (1/8 in. OD) was laid in grooved slots milled in the vane and then led down the inside wall of the vertical circular duct to the instrument access openings in the tunnel at Station 6. The grooves were filled with aluminum solder and the surface was polished, then checked for dimensional accuracy. Small piezometer holes were drilled normal to the surface of the vane in to the copper tubes. These holes were staggered where there might be interference but were confined to a band an inch on either side of the center of the vane span. The manometry arrangement allowed pressure on the vane surface to be recorded relative to the pressure at Station 5, a position close enough to make the static pressure difference a negligible amount.

Measurements in the circular duct immediately before this bend indicated the existence of the typical pointed velocity profile common to the ends of diffusers but with a uniform velocity front over approximately a 3-in. region which included all of the piezometer taps in the measuring vane (Fig. 36).

Pressure readings were taken on the measuring vane at tunnel test section velocities of 18, 30, and 50 ft per sec and at staggers of 96°, 98°, and 100°. The ratio of test section velocity to local velocity approaching the location of the piezometer taps in the vanes was determined from velocity traverse data for the tunnel previously obtained.

The measured pressures on the vane were converted to dimensionless quantities roughly comparable to the data taken from the flow diversion apparatus by using the stagnation head of the local velocity as unity.

A comparison of the data taken at a given stagger and temperature for the three different velocities showed no appreciable change with Reynolds number that could not be attributed to some other cause such as a change of the ratio of local velocity to test section velocity. The dimensionless values at the three velocities for each stagger were averaged together with no separate value differing by more than five per cent from the average. Figure 35 is a diagram of these composites at the three staggers plotted perpendicular to the chord in the conventional manner of presenting pressure diagrams around airfoil sections. The discussion and analysis of the data compiled on this measuring vane are included with the discussion of the pressure measurements on the vanes in the flow diversion apparatus in Section IV, C of this report.

IV. ANALYSIS OF THE EXPERIMENTAL DATA

A. Flow Distribution

The velocity and energy distribution downstream from a guide vane elbow depends on size, shape, and spacing of the vanes, the vane stagger, the location of the vanes relative to the miter line, the flow distribution before the vanes, and, to a certain extent, the Reynolds number. Since the size, shape, and spacing of the vanes were fixed before the experimental investigation was inaugurated, it is desirable to verify the particular values chosen while the effects of the remaining variables are being observed.

Actually, each bend in the proposed water tunnel would pose a particular problem of its own if a fairly uniform distribution of velocity and energy is to be expected downstream. However, more practical considerations dictate that turning the flow through 90° without contributing additional maldistribution of velocity or energy should constitute a satisfactory performance of the cascade.

The bulk of the experimental work was conducted with flat turbulent velocity and energy profiles before the cascade so that the downstream velocity and energy distributions can be judged by their proximity to this state. On the other hand, the profiles downstream of the tunnel bend located directly after the diffuser have to be compared with the profiles before the same bend to evaluate the effect of the cascade on the flow.

Preliminary photographs of the flow diversion experiments (Figs. 8 and 9) indicated that the cascade of Type 1 vanes with the chords set perpendicular to the miter line of the bend (90° stagger angle) would considerably underturn the bulk flow. At the vane stagger of 96° the photographs indicated a slight underturning of the flow, while the pictures of the bend with the vane stagger angle of 101° illustrated a desirable condition of flow parallel to the duct walls both downstream and immediately upstream of the cascade. The photographs, of course, yield only superficial data and cannot reveal the energy distribution or the possible shock loss associated with increasing the stagger angle.

The velocity and energy traverses in the 6-in. square duct at the vane staggers of 96° and 101° were made at various Reynolds numbers but with nearly the same upstream flow distribution for all of the series. This can be seen by comparing the contours at Section D-D in Figs. 14 to 23.

The total head contours at the measuring sections downstream of the bend of Series 10 to 15 (96° stagger angle) exhibit a region of very low energy near the inside wall of the duct. The contours at Section K-K for these series are similar to the total head contours just downstream of a radius elbow where the low energy region is divided into two pockets located symmetrically about the mid-depth line of the duct. The distortion of the energy and velocity distribution is still appreciable at Section M-M, five diameters downstream of the bend. The directions and magnitudes of the velocity vectors in the measuring section are not consistent in pattern among the series but do reflect the small disturbances caused by the presence of the vanes and the minor spirals to be expected if each duct between vanes is regarded as a radius elbow.

The downstream velocity and energy contours of Series 16 through 19 (vane stagger 101°) are much closer to those found in a straight duct with a normal turbulent distribution (Figs. 20 to 23). The contours at Section K-K show the lower energy pockets near the inside duct wall, but they are of considerably smaller magnitude relative to the mean energy in the section than those found at the vane stagger of 96°. This small distortion is almost entirely dissipated at Section M-M where the distribution of energy and velocity is well balanced across the section. The distribution downstream of the cascade of aluminum vanes (Series 19) does not differ appreciably from the distribution downstream of the cascade of the cast vanes when tested at the same stagger angle of 101°. This indicates that if some pains are taken in their manufacture, factory-produced vanes will yield the same performance as those made in the laboratory.

The series having the lowest Reynolds numbers (Series 10 and 15) show a slightly greater distortion of the energy profile at Section M-M than the other series with a corresponding vane stagger, but otherwise the downstream distribution remained fairly constant with Reynolds number over the range tested.

Velocity traverses taken at four stations in the model water tunnel are presented in Figs. 36 to 39. Stations 5 and 6 are upstream and downstream respectively of Vaned Elbow I, and Stations 11 and 12 are upstream and downstream respectively of Elbow IV. The average test section velocity for all traverses was approximately 50 ft per sec (29.6 knots), which by continuity considerations gave an average velocity of approach of 10.3 ft per sec in Elbows I and II and 5.5 ft per sec in Elbows III and IV.

The traverses of Stations 11 and 12 were taken with the vanes at a stagger of 96° and show the relative distribution before and after a vaned turn of circular section. The diagrams are to be examined with the observer looking in the upstream direction at the cross section. Although the profile at Station 11 is fairly flat, a distortion of the flow causing the region of highest velocity to be displaced from the center of the section is evident. This displacement seems to be lessened at Station 12, probably because of an ordinary reversion to a normal turbulent profile rather than because of any corrective ability of the cascade. These traverses show that Vaned Elbow IV performs its primary function very well; there is little difference in the flow before and after the elbow.

The traverses taken on diameters of Stations 5 and 6 indicate quite clearly that the elbow is not turning the stream through a large enough angle when the vanes are at a stagger of 96°. The flow coming into the elbow (Station 5) has a distorted velocity distribution due to the action of the diffuser. For the vane stagger of 96° the region of high velocity is not turned far enough, but impinges on the outside wall of the vertical leg. The vane stagger of 100° nearly corrects this difficulty. This is substantially in accordance with the findings of the flow diversion study.

On the basis of this evidence, it is seen that a vane stagger angle of 101° used with the chosen cascade turns the flow through 90° without imparting disturbances in the velocity or energy distributions that would seriously affect the flow downstream.

B. Energy Loss

Although the resistance of the vanes was not determined directly in these experiments, the excess energy loss due to the bend was measured. Except for end effects, which are probably small at the correct stagger angle, the vane resistance produces the entire excess bend loss.

To obtain a total energy curve for each flow diversion series, average total heads at the three measuring sections are plotted against distance from the reference section measured along the center line of the duct (Fig. 40). The computed losses in a straight smooth pipe are also plotted for Reynolds numbers corresponding to three of the flow series. The coefficients used in the computations of these losses are taken from the formula $1/\sqrt{\lambda} = 2 \log R\sqrt{\lambda} - 0.8$* where R is the Reynolds number and λ# is the dimensionless coefficient, giving, in terms of the velocity head, the loss per unit of length measured in diameters. These computed losses checked very closely with previously measured losses for a reach of the lucite duct where parallel flow prevailed [6]. The straight pipe loss curve is drawn through the measured point at Section D-D for the corresponding flow series. The coefficient of loss due to the bend (ξ) can be determined by subtracting the ordinate of the measured loss curve from the ordinate of the straight pipe

*Kármán-Prandtl resistance equation for turbulent flow in smooth pipes.

$h_f = \lambda \frac{\ell}{d} \frac{V^2}{2g}$

friction curve beyond the point where the measured loss curve becomes parallel with the straight pipe friction curve. The two curves are assumed to be parallel at Section M-M, but this assumption is more nearly true for the series at the 101° stagger angle than for those at the 96° stagger angle. Values of ξ are shown on Fig. 40 for the three series where the pipe friction curves are presented.

The loss coefficient of the bend is seen to increase with decreasing Reynolds number in these experiments. This trend is explained by the fact that the principal loss in a cascade is due to additional skin friction over the increased surface area of the vanes. This tends to verify the initial assumption that bend loss and vane resistance are directly related.

There is little difference between the total losses at comparable Reynolds numbers for the two staggers of 96° and 101° but there is an indication that these losses occur in a somewhat different manner. The measured losses at the three stations plot approximately on a straight line for those series conducted with the vanes staggered at 96°, while the other series (101°) show a large slope of the loss curve from Section D-D to K-K and then a slope almost parallel to the straight line friction curve from K-K to M-M. This would indicate that the largest portion of the loss due to the bend at a stagger of 101° has been accomplished before Section K-K, probably in the vanes, and the flow is so nearly axial beyond K-K that little additional loss is experienced. On the other hand, at the vane stagger of 96°, the rate of energy loss beyond K-K indicates that the walls of the channel are still turning the flow as in a radius elbow [6].

Accurate determination of the energy loss in the model water tunnel directly attributable to the vaned turns is somewhat difficult, because of the influence of other tunnel components. According to the law of energy for one-dimensional flow:

$$\int^{A_1} \left(\frac{p}{\gamma} + \frac{U}{2g}\right) U \, dA - \int^{A_2} \left(\frac{p}{\gamma} + \frac{U^2}{2g}\right) U \, dA - \frac{E_t}{\gamma} = 0$$

p = pressure
U = axial velocity
γ = specific weight of fluid
A_1 = area upstream of elbow
A_2 = area downstream of elbow
E_t = total energy loss between Sections 1 and 2

$$\text{Defining} \quad \alpha = \int_A \frac{U^3 \, dA}{A \, \bar{U}^3}$$

the energy equation reduces to

$$\frac{(p_1 - p_2)}{\gamma} - \frac{\alpha_2 \bar{U}_2^2 - \alpha_1 \bar{U}_1^2}{2g} = h_t = \xi \frac{\bar{U}_1^2}{2g} + \lambda \frac{\ell}{d} \frac{U_1^2}{2g}$$

where h_t is the total head loss between Sections 1 and 2, ξ is the bend loss coefficient, and λ is the friction factor (assumed to be 0.0170). Therefore:

$$\xi = \frac{\frac{p_1 - p_2}{\gamma}}{\frac{\bar{U}_1^2}{2g}} + \alpha_1 - \alpha_2 \frac{\bar{U}_2^2}{\bar{U}_1^2} - \lambda \frac{\ell}{d}$$

Values of ξ for Elbows I, II, III and IV at a stagger of 96° are tabulated in Table II, using values of α determined from velocity traverses at a test section velocity of 49.62 ft per sec and a friction factor (λ) of 0.0170. The Reynolds number listed is based on chord length.

The high value of ξ in Elbow I is mainly due to the energy lost in converting the abnormally high kinetic energy of Station 5 to a lower and more normal kinetic energy at Station 6 (reduction of α from 1.812 to 1.308). The high α value at Station 5 results from the distorted energy profile caused by diffuser action, and undoubtedly a large part of the energy lost through the elbow would occur in converting the kinetic energy change to pressure energy even if the diffuser were followed by a straight pipe. Actually, then, most of the energy loss in this elbow is caused by the diffuser.

Elbow II (duct diameter = 13.2 in.) is bisected by a 3-in. wide pump shaft fairing (Fig. 41) which lessens the aspect ratio of the cascade and causes additional energy loss for the bend. The fairing also causes a contraction of the stream, thereby increasing the mean velocity through the bend. The total energy loss is therefore quite high, as a result of high skin friction on the fairing and vanes, form loss of the fairing, and eddy loss due to the unfavorable aspect ratio, as well as the bend loss expected in an unobstructed cascade of similar vanes.

Table II

	Test Section Velocity (Ft Per Sec)	18.00	30.00	49.62
Elbow I	Reynolds Number*	90,000	165,000	370,000
	$\bar{U}_5$ (ft per sec)	3.72	6.20	10.25
	$\bar{U}_5^2/2g$ (in.)	2.58	7.16	19.58
	$\bar{U}_6$ (ft per sec)	3.72	6.20	10.25
	$\bar{U}_6^2/2g$ (in.)	2.58	7.16	19.58
	α_5	1.812	1.812	1.812
	α_6	1.308	1.308	1.308
	$\frac{p_5 - p_6}{\gamma}$ (in.)	+ 0.21	- 0.41	+ 0.40
	ξ	0.554	0.416	0.493
Elbow II	Reynolds Number*	90,000	165,000	370,000
	$\bar{U}_6$ (ft per sec)	3.72	6.20	10.25
	$\bar{U}_6^2/2g$ (in.)	2.58	7.16	19.58
	$\bar{U}_7$ (ft per sec)	3.90	6.50	10.77
	$\bar{U}_7^2/2g$ (in.)	2.83	7.87	21.65
	α_6	1.308	1.308	1.308
	α_7	1.090	1.090	1.090
	$\frac{p_6 - p_7}{\gamma}$ (in.)	1.17	3.57	8.8
	ξ	0.527	0.570	0.515
Elbows III & IV	Reynolds Number*	46,000	75,000	138,000
	$\bar{U}_{10}$ (ft per sec)	2.0	3.33	5.51
	$\bar{U}_{10}^2/2g$ (in.)	0.75	2.065	5.66
	$\bar{U}_{12}$ (ft per sec)	2.0	3.33	5.51
	$\bar{U}_{12}^2/2g$ (in.)	0.75	2.065	5.66
	α_{10}	1.050	1.050	1.050
	α_{12}	1.071	1.071	1.071
	$\frac{p_{10} - p_{12}}{\gamma}$ (in.)	0.25	0.70	1.45
	2ξ	0.244	0.250	0.166
	ξ	0.122	0.125	0.083

*Reynolds number is based on chord length (2.95 in.)

The performance of Elbows III and IV is representative of the true energy loss caused by the cascade. The values of ζ as determined for these elbows are in reasonably good agreement with those determined in the flow diversion apparatus. In making this comparison it should be noted that the Reynolds number values of Fig. 40 are based on the 6-in. depth of the duct wall as length parameter, whereas the values of Table II are based on the 2.95-in. vane chord as length parameter.

C. Observations on Vane Surfaces

The pressure measurements and visual observations of the vanes serve to give a better understanding of the flow around the cascade than can be deduced from the downstream flow distribution data and energy loss considerations alone. The data obtained by pressure measurements on the vanes are also useful in the analysis concerning loading and cavitation.

Figures 25 and 26 indicate that at the stagger of 101° the pressures are approximately equal at corresponding points on all the vanes, while at the 96° stagger the negative pressures on the vanes increase in magnitude towards the inside of the bend. When the upstream velocity distribution is fairly flat, the equal pressure on the vanes indicates an orderly axial turning of the stream with no lateral flow.

The loading of the vanes was determined by integration of the pressure diagrams (Fig. 27). For the stagger angle of 101°, the measured loading checked very closely with the theoretical load computed from the change in momentum of the approach stream. The check could not be made at the stagger of 96° because of the unequal loading on the vanes. Integration of the wall pressures at mid-depth (Fig. 24) indicated that the walls carried approximately the load of one vane at the 101° stagger while they carried a great deal more load at the 96° stagger, proving again that the walls were called upon to assist the turn at the 96° stagger angle.

The centers of pressure as determined by integration are indicated by symbol in Fig. 27 for the two staggers. They occur at 44.7 per cent of the chord length at the 96° angle and 37.5 per cent of the chord length at the vane stagger of 101°, measured from the leading edge. For comparison, the vane trunnion and miter line are also indicated in this figure.

The pressure curves about the vane in the model water tunnel (Fig. 35) are in only qualitative agreement with those of Fig. 27. This discrepancy may be explained by the difficulty in determining the stagnation pressure for the tunnel vane. The pressures on the tunnel vane are in units of the stagnation head of the core of high velocity, while the pressures on the vanes of the flow diversion apparatus are in units of the mean velocity of the duct. In both Figs. 27 and 36 corrections have been made for lost head between the respective reference sections and the cascades but no correction was made for any change in profile between the reference section for the tunnel cascade and the cascade itself. The indicated maximum negative pressure on the tunnel vane is also different from that on the flow diversion apparatus vanes because of a slight difference in location of the piezometer taps. The pressure distribution of Fig. 27 is the more reliable because of a closer control of the measurements. Since Figs. 27 and 35 exhibit a close qualitative agreement, the entire correlation would be satisfactory with the above-mentioned corrections in the magnitudes of the pressures around the measuring vane in the tunnel.

Figure 42 illustrates the relation of the velocities near the surface of the vane to the mean free stream velocity computed from the pressure measurements on the vanes in the flow diversion apparatus. The shape of the duct between vanes at a stagger of 101° can be seen in large scale in this figure. It is interesting to observe that the products of radius and velocity at the inside and outside of sections normal to the duct indicate the existence of a nearly potential free vortex flow in the first half of the duct.

The presence of the double spiral in the passages between the vanes can be detected on inspection of the photographs taken of the vane surfaces near the trailing edges. The streaks in the paste (Fig. 13) illustrate the growth of this spiral in the passage closest to the inside of the bend.

An examination of the photographs taken of the convex side of the vane at a stagger angle of 96° reveals a zone of local flow separation near the change of the vane surface curve from a circular arc to a straight line (7/8 in. forward of the trailing edge). At this point the colored liquid stream that has been approaching along the vane surface at mid-span abruptly changes direction and falls to a point on the vane surface about an inch

above the floor of the duct. Apparently the aerodynamic forces of the flow in the duct had dominated the flow of the colored tracing liquid up to the point where the vertical fall suggests the dominance of gravity forces. The aluminum paste forms a ridge along this same transition line. After this zone of separation has been passed, the flow apparently returns to the surface of the vane, since the dye stream in Fig. 11 [b] and strings at the trailing edge approximate the mean direction of the bulk flow in the downstream tangent. This return of the flow to the vane surface after a short region of separation can be indicative of a change of a laminar boundary layer to a turbulent state.

A phenomenon similar to this was noted by Ackeret [7] during experiments with vanes in a flow of air. He coated the suction surface of his vane with lampblack and observed that this coating was eroded by the flow except over a region a short distance forward of the trailing edge. When a thin wire was attached to the surface of the vane near the leading edge to promote the early onset of a turbulent boundary layer this region eroded in the same manner as the rest of the suction surface. It is concluded from this evidence that the zone of local separation occurs when the energy in the laminar boundary layer is no longer able to overcome the increasing pressure and the progress of the boundary flow is halted. The flow returns to the surface of the vane when the boundary layer becomes turbulent and is able to acquire sufficient energy to overcome the adverse pressure gradient.

No such separation was observed with the stagger of 101° (Fig. 11 [c]). This is attributed to the fact that the increase in stagger served to move the beginning of the turbulent boundary layer close to the nose of the vane. The photograph (Fig. 11 [c]) does indicate that the flow leaves the vane slightly before the trailing edge, because the heavier colored liquid does not follow the air stream but gathers on the edge and falls down the trailing edge. The traverses with strings behind the vanes showed that the wake caused by this departure of the flow is small in comparison with the maximum thickness of the vanes.

At both of the stagger settings the dye streams at the bottom of the vanes are picked up by the spiral and discharged off the trailing edge about an inch from the bottom.

D. Application to the Prototype

The foregoing analysis indicates rather conclusively that at a stagger angle of 101° the selected guide vane cascade performs very well in both the flow diversion apparatus and the model tunnel. It now remains to determine whether the same performance may be expected in the 60-in. prototype tunnel. The principal differences to be expected between the model and the prototype are changes in end effects and changes in Reynolds number.

The end effects are proved to be negligible by the satisfactory correlation between the results in the flow diversion apparatus and in the model water tunnel at the stagger angle of 101°. At other stagger angles this is not necessarily true, since then the walls may be called upon to assist the turn, and problems common to radius elbows will arise.

The Reynolds numbers listed in this report, except for those listed in Table II, were intended to be indicative of the general level of turbulence of the flow approaching the vanes and as such were based on the diameter of the approach duct. However, they are readily converted to vane Reynolds numbers with a length parameter based on the chord or to cascade Reynolds numbers using a length parameter such as the vane spacing. The experiments concerned with changes due to Reynolds number were conducted on the flow diversion apparatus because of a closer control of measurements and a smaller variation in temperature than was possible in the model water tunnel.

Flow Series 11 (water velocity 11.4 ft per sec) and Flow Series 12 (air velocity 100 ft per sec) with the same vane stagger of 96° and the same Reynolds number of 300,000 agree very closely when a comparison is made between the respective diagrams of velocity distribution and downstream angularity (Figs. 15 and 16). Also, because of temperature changes during the course of Series 14, the average velocity had to be increased 11 per cent to maintain the same Reynolds number, but spot rechecks of measurements verified the continuity of the series when presented in dimensionless form. As mentioned in a previous section, the velocity and energy distribution downstream of the bend change with Reynolds number, but the change is small above a Reynolds number of 150,000.

Figure 28 shows the effect of a change in Reynolds number on the vane pressures. There is little change with Reynolds number indicated in the diagram except near the leading edge for Reynolds numbers of 150,000 or less,

where the points of maximum positive and negative pressures are not drawn as far around the nose as they are at larger Reynolds numbers.

The length scale of the prototype is ten times that of the vaned turn models, and the average velocities of the prototype are to be as large or larger than the velocities used in the model experiments. This would result in Reynolds numbers in the prototype at least ten times those used in the model tests, assuming that comparable temperatures are to be used in the prototype installation.

Considering the increased length scale and the larger Reynolds numbers of the prototype, it would be difficult to predict the location of a change from laminar to turbulent boundary layer on the prototype vanes by referring to the model studies, unless the point where the boundary layer becomes turbulent on the model vanes is at the point of maximum negative pressure. At the stagger of 101° this would be at the leading edge of the vane. The separation associated with the change in the boundary layer might affect the similarity of the downstream flow distribution as well as the amount and character of the energy loss if the location of this separation is changed. Thus the testing of the model vanes with a turbulent boundary layer on their suction surfaces, when the shape of the vane indicates that a turbulent layer would have to exist on a large-scale prototype vane, would seem to be relevant if similarity is to be attained. The experimental tests at the vane stagger of 101° satisfy this requirement.

From the data appearing in the previous sections, it appears reasonable to assume that there will be no material changes with further increases in Reynolds number. The loss coefficient (ζ) for an elbow with the recommended cascade should be between 0.09 and 0.12 in the prototype over the range of probable Reynolds numbers. The downstream flow distributions in the prototype tunnel should conform very well with the desirable downstream velocity and energy distributions found in the model experiments at the recommended setting of the chosen cascade.

E. Vane Cavitation Analysis

Elbow I will be more susceptible to cavitation than any other elbow, since the lowest absolute pressure and highest velocity occur there. Cavitation cannot occur on the vanes, unless the pressure drops to vapor

pressure at some point on the vane. Experimentally it was determined that the lowest negative pressure on the vanes is $2.25 \frac{\rho}{2} U^2$ (Fig. 27). The coefficient 2.25 is actually the critical cavitation index σ, defined as

$$\sigma = \frac{\frac{p_o}{\gamma} - \frac{p_{vp}}{\gamma}}{\frac{U_o^2}{2g}} \qquad (1)$$

$\frac{p_o}{\gamma}$ = absolute static pressure (ft) in undisturbed stream

$\frac{p_{vp}}{\gamma}$ = vapor pressure (ft)

$\frac{U_o^2}{2g}$ = velocity head in undisturbed stream

Since the point of lowest pressure in the tunnel is at the downstream end of the test section and this pressure cannot drop below vapor pressure, the minimum possible static pressure at Elbow I is therefore:

$$\frac{p_o}{\gamma} = \frac{U_t^2 - U_o^2}{2g} - h_\ell + \frac{p_{vp}}{\gamma}$$

where U_t = test section velocity

h_ℓ = head loss from downstream end of test section to Elbow I

Analytically it was determined that h_ℓ for the diffuser passage between the test section and the elbow would be about $0.12 \frac{U_t^2}{2g}$ and this was verified in the model study. Since the prototype duct diameter at Elbow I is 11 ft, and the prototype test section diameter is 5 ft, Eq. (1) becomes:

$$\frac{p_o}{\gamma} = \frac{19.6\ U_o^2}{2g} + \frac{p_{vp}}{\gamma}$$

Substituting this in Eq. (1)

$$\sigma = 19.6$$

Thus it is seen that for the physical dimensions employed in the prototype design and the consequent pressure regain the vane cannot serve as the initial source of tunnel cavitation. In order for cavitation to occur at an

elbow in the water tunnel, the maximum negative pressure on the vane would have to be 19.6 times the velocity head, which cannot occur on any reasonably shaped vane.

F. Vane Vibration and Stresses

Since trouble has been encountered in some water tunnels due to structural failure and excessive vibration of the guide vanes, a structural analysis of the vane is herein given consideration. The longest vane in each of the four elbows was analyzed, since it would have higher stresses and a lower frequency of vibration than any other vane in the elbow. The vane lengths thus were 15 ft in Elbows III and IV, 11 ft in Elbow I, and 5.5 ft in Elbow II, since this last elbow will be divided by a pump shaft fairing and thus the span will be approximately one-half of the duct diameter. The vanes were assumed to be simply supported for moments and vibrations about the minimum principal axis (approximately parallel to the chord), since there will probably be little restraint in this direction at the supports. Full restraint was assumed for moments about the maximum principal axis. The vane was analyzed both as a solid steel vane, and a hollow vane composed of solid nose and tail pieces and 1/2-in. rolled plate (Fig. 43). Moments of inertia were determined graphically using a full- (prototype-) size drawing of the vane.

The forces acting on the vane are the lift-drag resultant force and the dead weight in water of the vane. The components of the lift-drag resultant force were obtained using the impulse and momentum principle, since the integration of pressure distribution on the vane in the flow diversion apparatus agreed with the results of this principle within a few per cent. The velocities used in the computations were based on a test section velocity of 50 knots; and the velocity impinging on the central vane was assumed to be 20 per cent larger than the bulk velocity of the flow, since the model tests indicated this to be true. The point of application of the lift force was obtained from the integration of the pressure distribution. Since the lift does not act through the center of gravity of the section, a small amount of torsion will be present in the vane. In computing the dead weight in water of the hollow vane, the vane was assumed to be filled with water. The structural analysis of the beam is summarized in Table III. The stresses and moments shown are those in the longest vane of Elbow I, since these stresses were higher than in any other vane. The maximum deflection under the combined loads occurred in Elbow III, and this value is listed in the table.

It should be noted here that large axial compressive stresses will be set up in the vanes if they are not free to expand into the walls of the tunnel when the temperature of the water rises. These stresses could very easily cause failure due to a column buckling action.

Vibration of the vanes will in all probability not be serious unless the natural frequency of one of the vanes is in or near resonance with some regular pulsating force.

The vane having the lowest natural frequency of vibration will be the longest vane in Elbows III and IV. The natural frequency of a beam can be computed from the equation:

$$f = C\sqrt{\frac{g\,E\,I}{w\,L^4}}$$

where C = constant, depending on mode of vibration and support of beam
g = acceleration of gravity
E = modulus of elasticity
I = moment of inertia
w = weight per inch vibrated
L = span

The lowest value C can have for a beam with two supports is 1.57, which is the constant for a simply supported beam vibrating at its fundamental frequency. Vibration of a vane will cause some water to be vibrated with it, thus increasing w, and lowering the frequency of vibration. It is assumed that one vane will vibrate the volume of water contained between it and an adjacent vane ([spacing times chord minus vane area] per inch of span). Thus the lowest frequency of vibration for either a solid or a hollow steel vane is 14.5 cycles per sec. (The hollow vane has the same frequency as the solid vane because its moment of inertia and weight per inch are decreased by the same ratio.) Frequencies of vibration of other beams will range upward from this value since the spans are shorter.

There are two possible sources of excitation of a vane: pulses from the impeller, and the vortices shed from a vane. The impeller will probably be driven at a top speed of 2 revolutions per second, and since it may have as many as 4 blades, the highest frequency of pulsation will be 8 cycles per sec. If 5 straightening vanes follow the impeller, it is possible that a small exciting pulsation of 40 cycles per sec will be generated. However, these pulses will probably be of small magnitude if they do occur, and will be considerably damped before they reach Elbow III.

A rough check was made on the intensity of pulses from the impeller by placing a 1/4-in. diameter cantilevered steel rod in the model tunnel through the taps at Stations 11 and 12. The natural frequency of vibration of the rod was established experimentally by vibrating it under water and determining its frequency with a Strobotac. The rod was then inserted in the tunnel, and the impeller speed adjusted to one-third the natural frequency of the rod. Since the impeller had 3 blades, the number of pulses per second emitted by the impeller was the same as the natural frequency of vibration of the rod. This procedure was repeated for several different lengths of rod, and it was found that the impulses from the impeller were either not present or not strong enough to cause any vibration in the rod. However, the rod was violently excited in a direction transverse to the stream if the velocity of flow was increased until the wake frequency, as determined from the Strouhal number, was in resonance with the rod.

The wake frequency of the vortices shed from the vane can be computed from the Strouhal number, $S = \frac{f\ c}{U}$

S = Strouhal number
f = frequency of vibration
c = chord length
U = velocity of free stream

This dimensionless number is sensibly constant for the range of Reynolds number at which the vanes operate, and experimental evidences [8] indicate a value of $S = 0.15$ for airfoils when c = chord length. The maximum frequency of the wake vortices is thus 1.2 per sec for a velocity of 20.9 ft per sec in Elbow I.

The foregoing analysis indicates that the fundamental frequency of vane vibration is higher than the frequency of the primary forces which might excite the vane. While this does not preclude the possibility of vibration of the vanes, it does give some assurance that resonant vibrations will not occur. There remains the possibility that model propellers mounted in the test section will operate at speeds in the range of resonance of the vanes. It is believed that impulses from this source will be sufficiently damped in traveling the length of the diffuser so that they will not cause serious vibration in the vanes.

Table III

	Cross-Sectional Area of Steel ($in.^2$)	I_{min} ($in.^4$)	I_{max} ($in.^4$)	Moment Abt I_{min} (lb in.)	Moment Abt I_{max} (lb in.)	Max Combined Flexure Stress ($lb/in.^2$) Tens	Comp
Solid Steel	91.4	295.9	4185.9	151,000	4735	1800	3020
Hollow Steel (1/2-in. wall)	39.3	193.8	3022.3	166,000	1180	3910	3100

	Torsional Shear Stress ($lb/in.^2$)	Support Shear Stress ($lb/in.^2$)	Deflection (for lift + dead wt) (in.)	Lowest Freq of Vib (cycles/sec)
Solid Steel	51.3	51	0.0540	14.5
Hollow Steel (1/2-in. wall)	180	13	0.0671	14.5

V. CONCLUSIONS

On the basis of these experimental investigations the following conclusions concerning the vaned turns for the proposed 60-in. prototype tunnel are drawn:

1. The selection of vaned turns and the particular choices of vane shape and spacing-chord ratio ($s/c = 0.48$) were justified by the results of the experiments. The original selection of location of the vanes with respect to the miter line of the bend was changed slightly to conform more closely with the experimental results.

2. The proper setting of the cascade to insure axial flow immediately before and after the turn is a stagger of 99° to 101°; that is, the angle between the chord of the vanes and the miter plane of the bend is 99° to 101° (the angle of attack is 54° to 56° with the approaching flow).

3. Excess losses due to the vaned turns at the recommended setting of the cascade of vanes with a normal turbulent velocity distribution in the approach flow should be 10 per cent of the velocity head in the approach duct plus or minus 2 per cent. For an abnormal velocity distribution entering the cascade (such as would occur at a turn downstream of a diffuser), an additional loss because of the change of velocity profile is apparent.

4. The vanes when installed in the tunnel will not be subject to cavitation.

5. Either a solid steel vane or a hollow steel vane of the dimensions of Fig. 43 will be free from excessive stresses or deflections under all expected conditions of operation, and should not vibrate in resonance with either the tunnel impeller or vortices shed from the vanes.

6. Data obtained with the experimental models should give a very close index of the performance to be expected in the vaned turns of the large tunnel because (a) the Reynolds numbers used in the models were high enough to preclude the possibility of a loss in similarity at the higher Reynolds numbers of the prototype, and (b) the onset of a turbulent boundary layer near the leading edge of the model vanes at the stagger angle of 99° to 101° would be at an approximately similar position on the larger prototype vanes.

7. The dimensions shown in Fig. 44 are the dimensions of the prototype vanes in cascade with the miter line of the bend shown to locate the position of the cascade in the bend. The stagger angle of 99° to 101° will insure that the vanes will be equally loaded and that the centers of pressure will fall in the miter plane.

REFERENCES

[1] Anderson, A. G. FLUID FLOW DIVERSION: A SUMMARY AND BIBLIOGRAPHY OF LITERATURE. St. Anthony Falls Hydraulic Laboratory, University of Minnesota, Project Report No. 1, August, 1947.

[2] Klein, G. J., Tupper, K. F., and Green, J. J. "The Design of Corners in Fluid Channels." CANADIAN JOURNAL OF RESEARCH, Vol. 3, 1930, pp. 272-285.

[3] Collar, A. R. "The Flow of a Perfect Fluid through Cascades of Airfoils." JOURNAL OF THE ROYAL AERONAUTICAL SOCIETY, Vol. 45, 1941, pp. 183-213.

[4] Kröber, G. "Guide Vanes for Deflecting Fluid Currents with Small Loss of Energy." INGENIEUR ARCHIV, Vol. 3, 1932, pp. 516-541, translated and published as Technical Memorandum No. 722, U. S. National Advisory Committee for Aeronautics.

[5] Ripken, J. F. PRELIMINARY WATER TUNNEL DESIGN STUDIES (unpublished). David Taylor Model Basin, 1945.

[6] Silberman, E. THE NATURE OF FLOW IN AN ELBOW. St. Anthony Falls Hydraulic Laboratory, University of Minnesota, Project Report No. 5, December, 1947.

[7] Ackeret, J. "Zum Entwurt ditchstehender Schaufelgitter" (The Design of Closely Spaced Blade Lattices). SCHWEIZERISCHE BAUZEITUNG, Vol. 120, No. 9, August 29, 1942, pp. 103-108.

[8] Freberg, C. R. and Kemler, E. N. AIRCRAFT VIBRATION AND FLUTTER. John Wiley and Sons, 1944, p. 132.

[9] Silberman, E. THE PITOT CYLINDER. St. Anthony Falls Hydraulic Laboratory, University of Minnesota, Circular No. 1, October, 1947.

LIST OF ILLUSTRATIONS

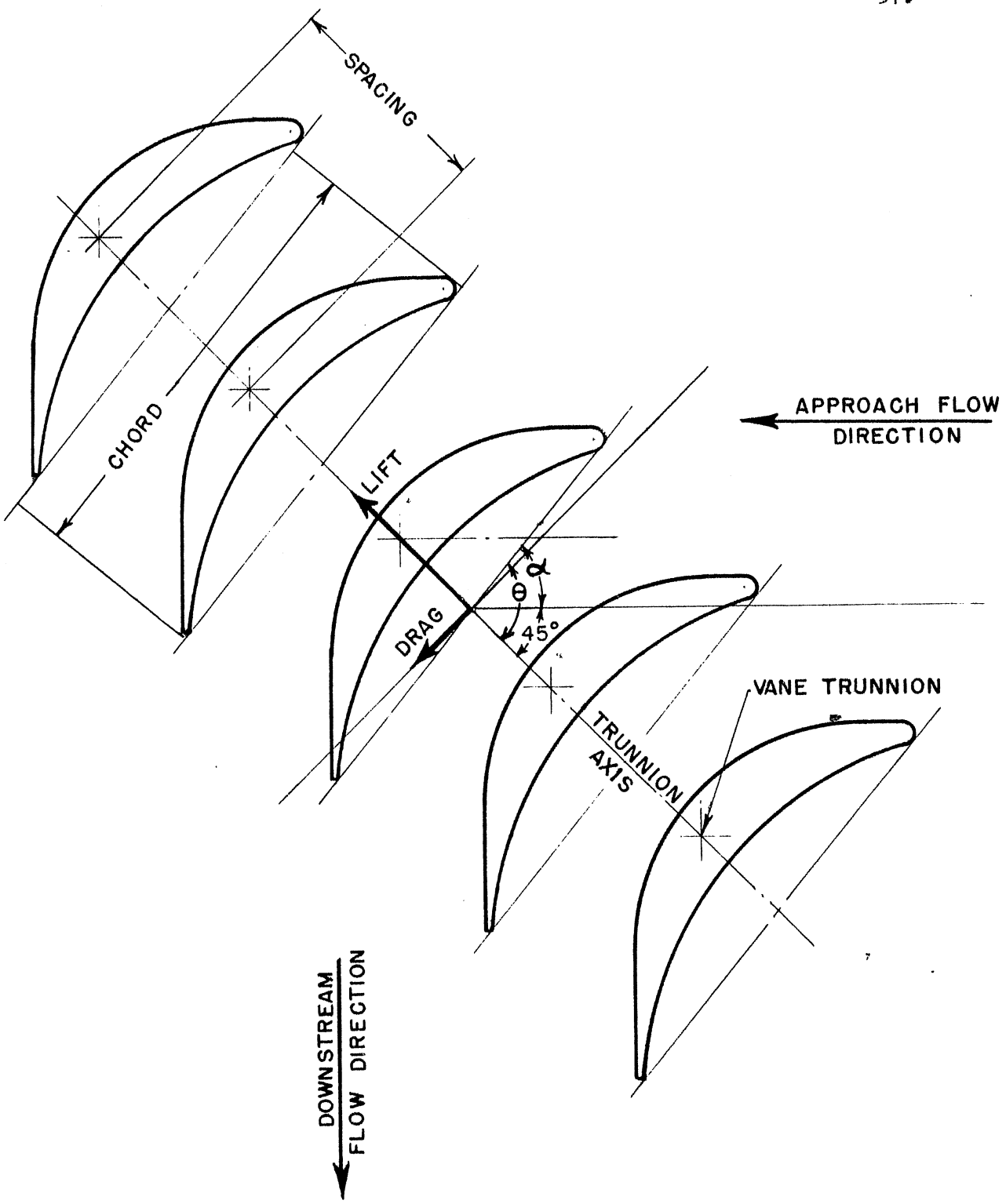

FIG. 1
A CASCADE OF VANES

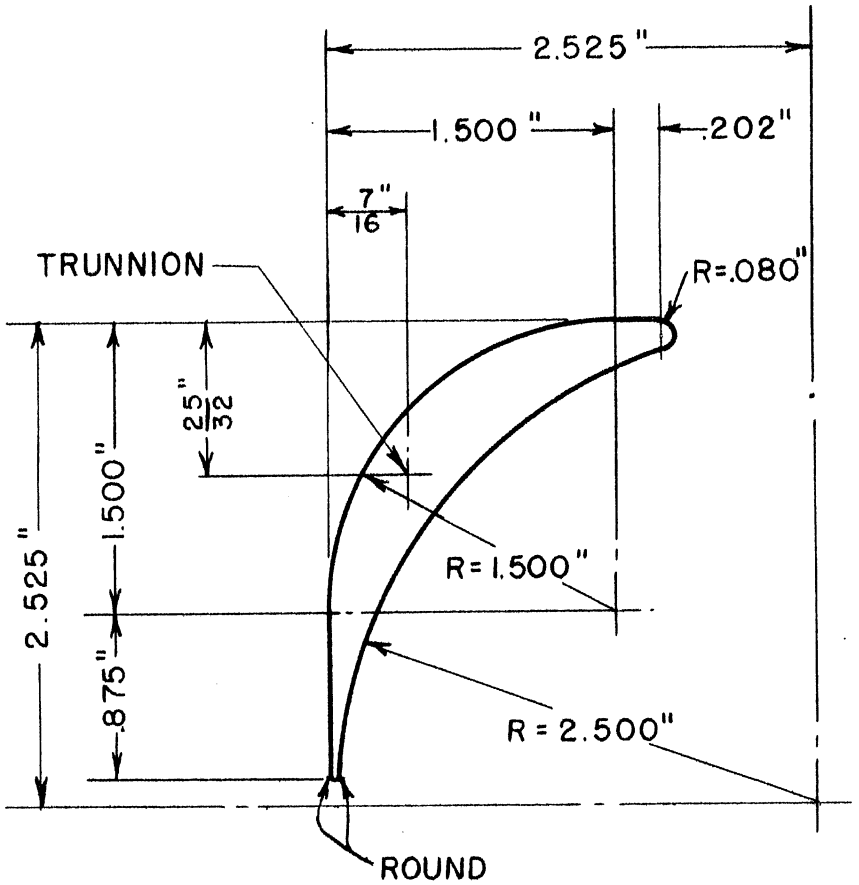

FIG. 2
FABRICATING DIMENSIONS OF TYPE I VANE

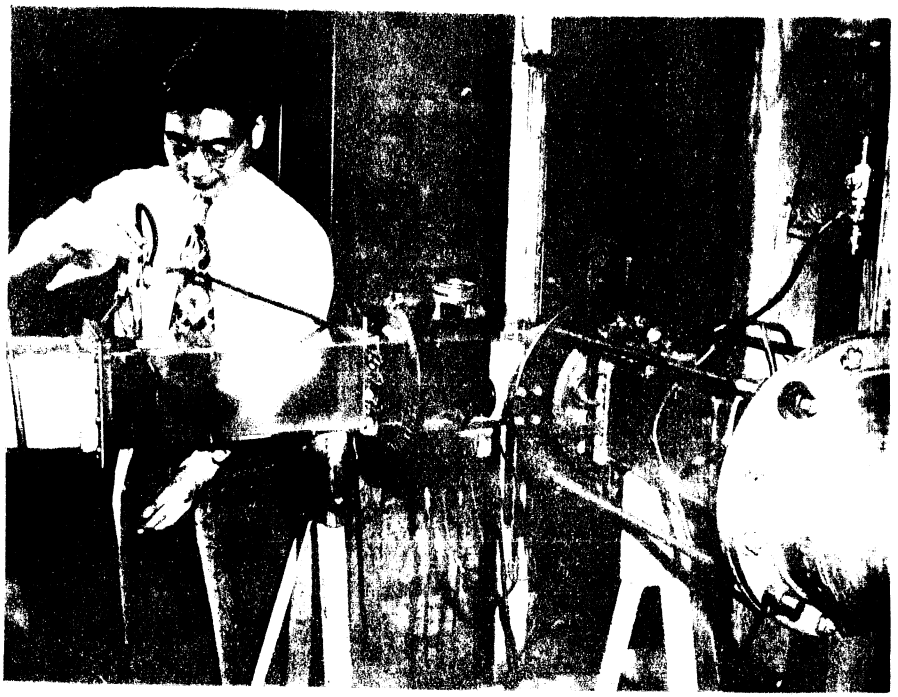

Fig. 3 The New Inverness Jazz Band

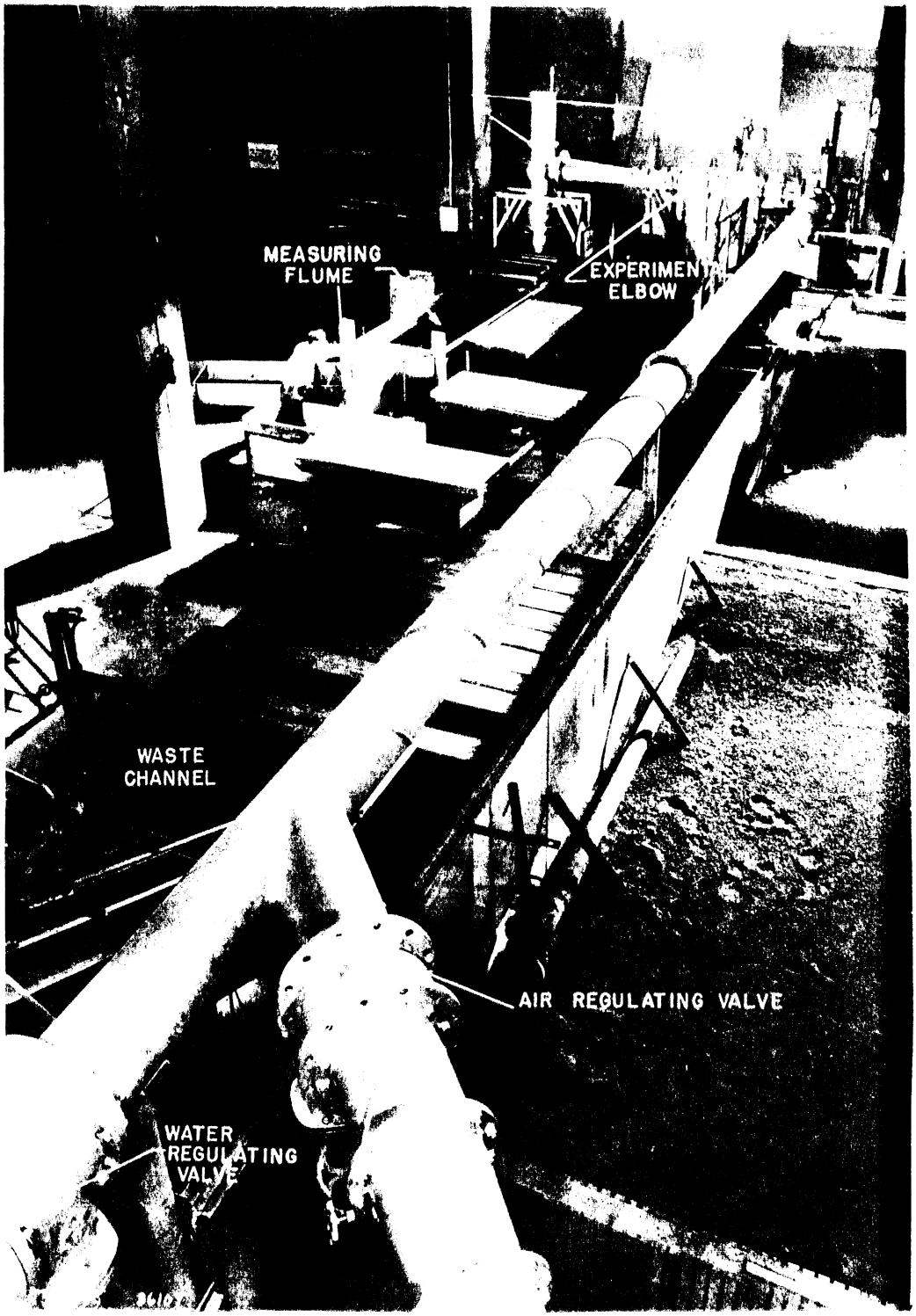

Fig. 4 The Mon Diversion test installation

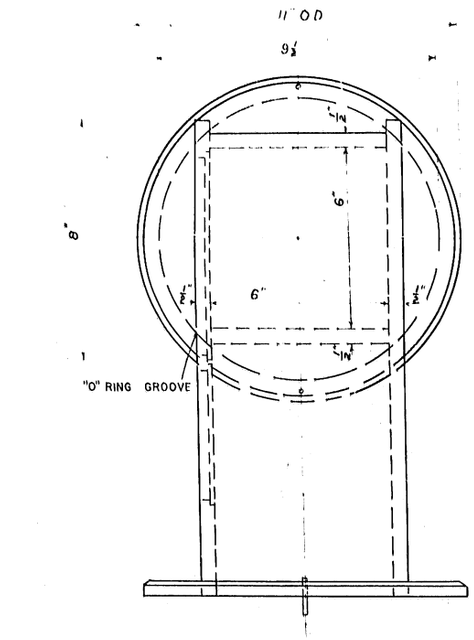

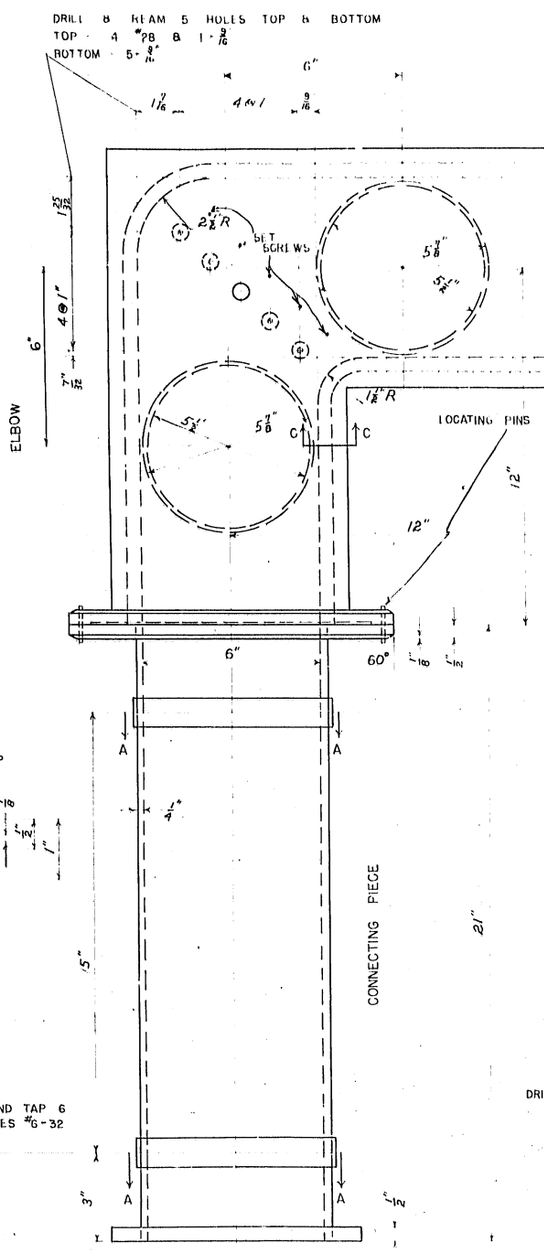

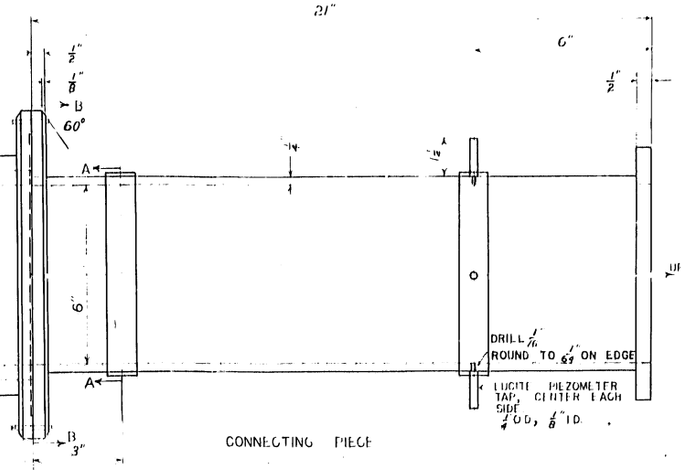

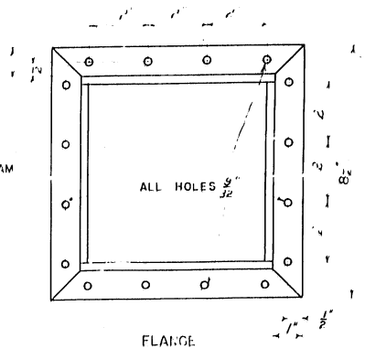

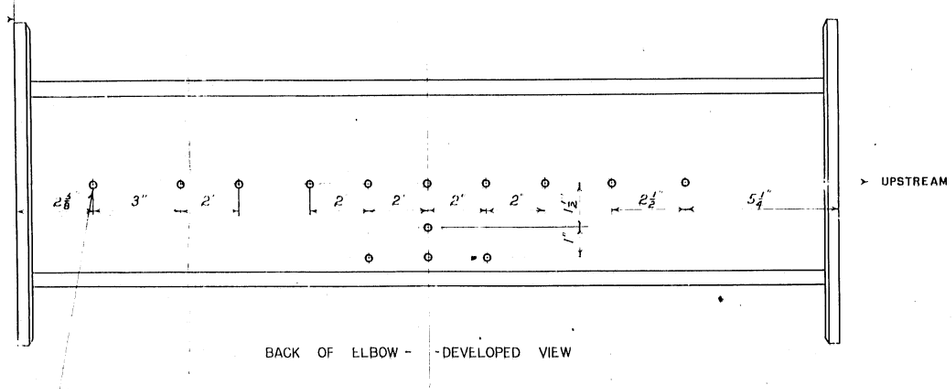

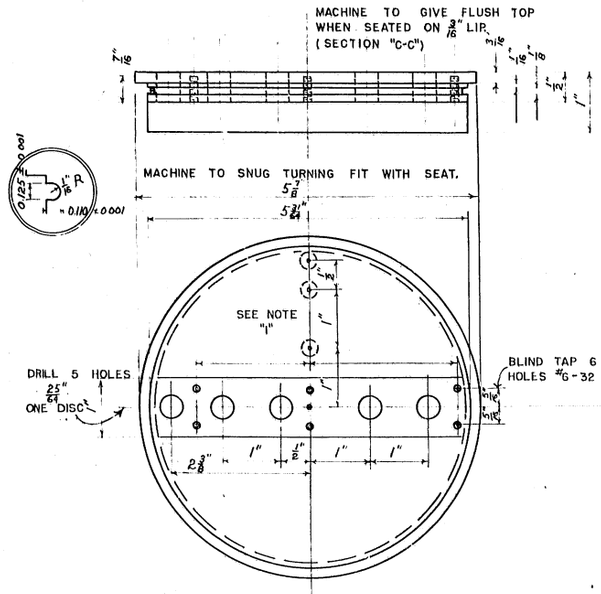

PITOT DISC DETAILS
(2 REQUIRED AS NOTED)

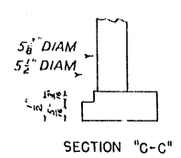

SECTION "C-C"

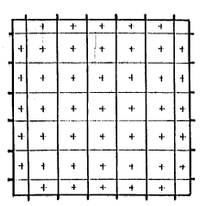

DIVISION OF CROSS SECTION FOR MEASUREMENT

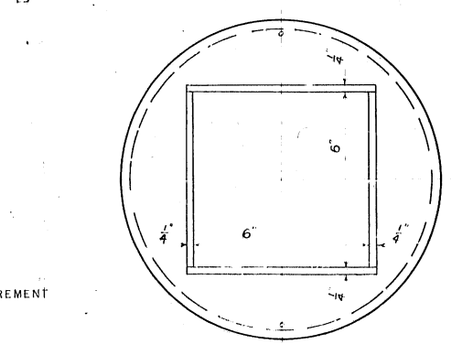

SECTION "B-B"

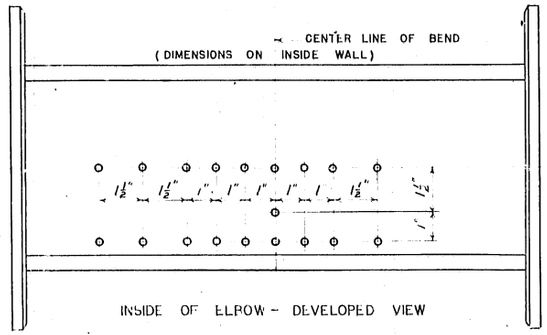

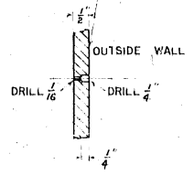

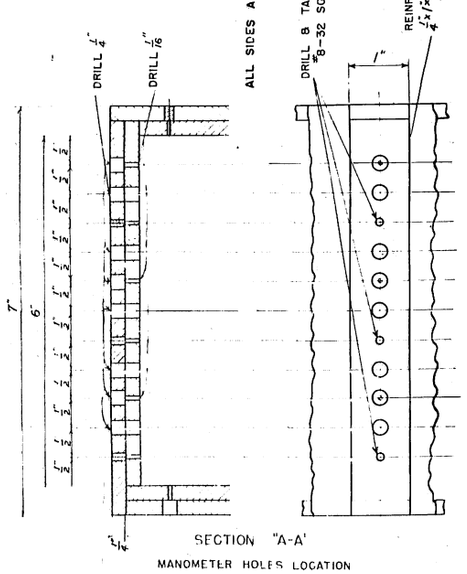

NOTES:

1. PITOT DISC — DRILL 4 HOLES 1/16", ROUND EDGE TO 1/64". COUNTER BORE 3 HOLES 1/4" x 1/4" FOR FRICTION FIT ON TENITE TUBE (BOTH DISCS).
2. ALL DETAIL VIEWS ARE FULL SCALE.
3. MATERIAL - LUCITE.

FIG. 5
BEND AND DUCT DETAILS

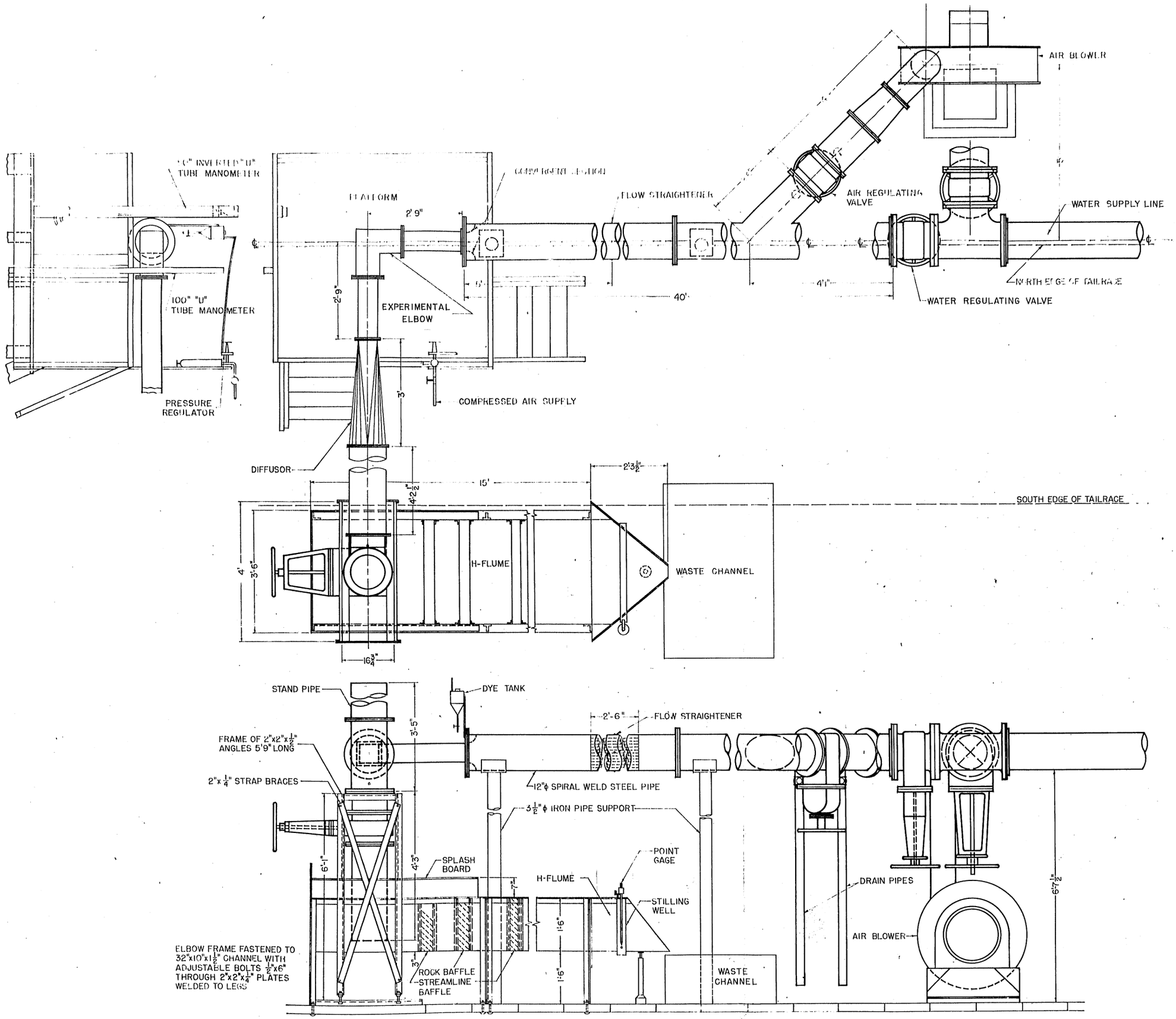

FIG. 6 TEST INSTALLATION

Fig. 7 Type 1 Vane and Trunnions Showing Pressure Taps and Connections

(Vane Surface Is Polished Smooth but Is Slightly Discolored)

(a) Vane Stagger 90°

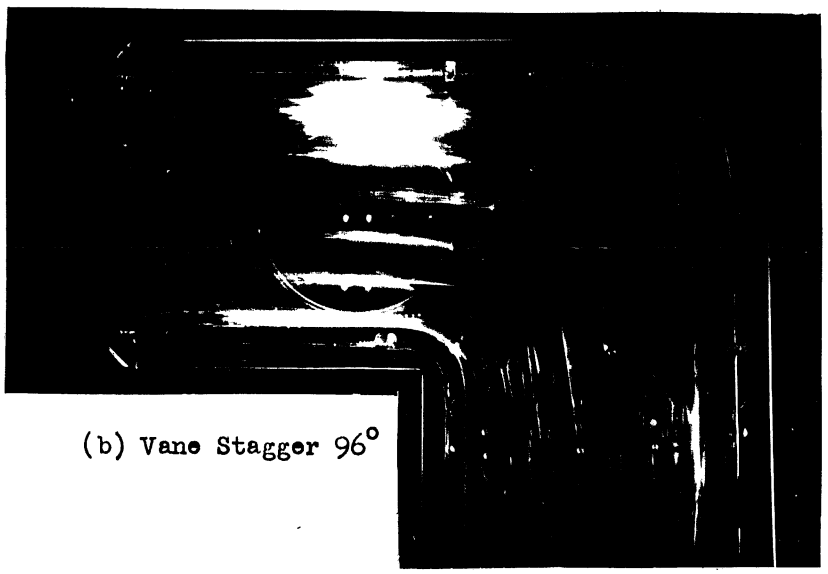

(b) Vane Stagger 96°

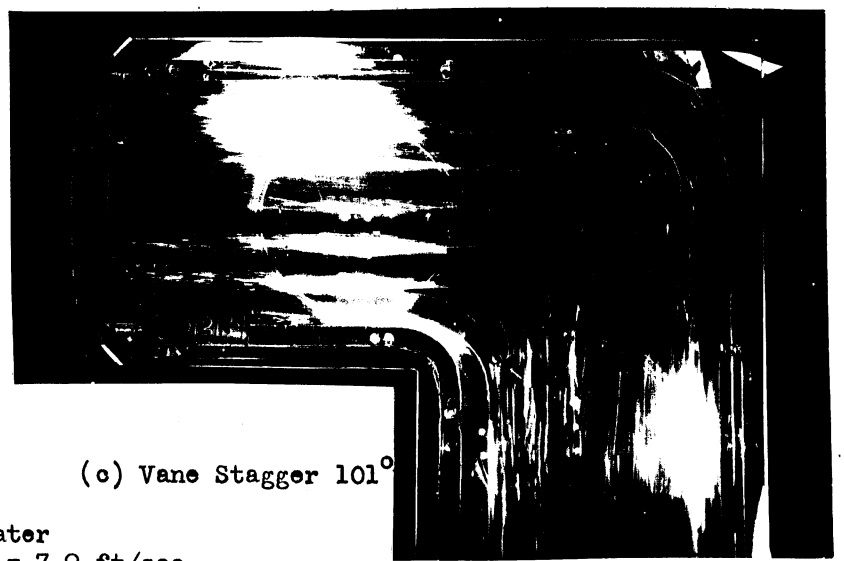

(c) Vane Stagger 101°

Flow of water
avg vel = 7.9 ft/sec

Reynolds no.= 300,000

s/c = 0.48

Fig. 8 Paths of Air Bubbles around Cascade of Type 1 Vanes at Mid-Depth

(a) Vane Stagger 90°

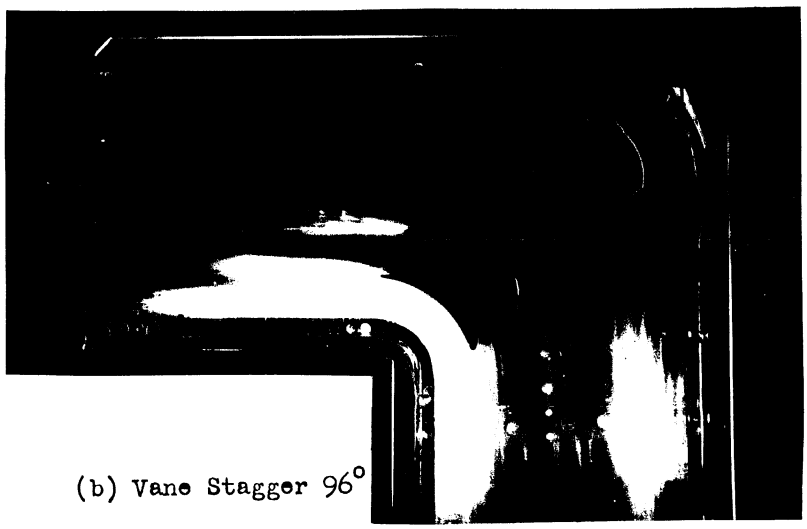

(b) Vane Stagger 96°

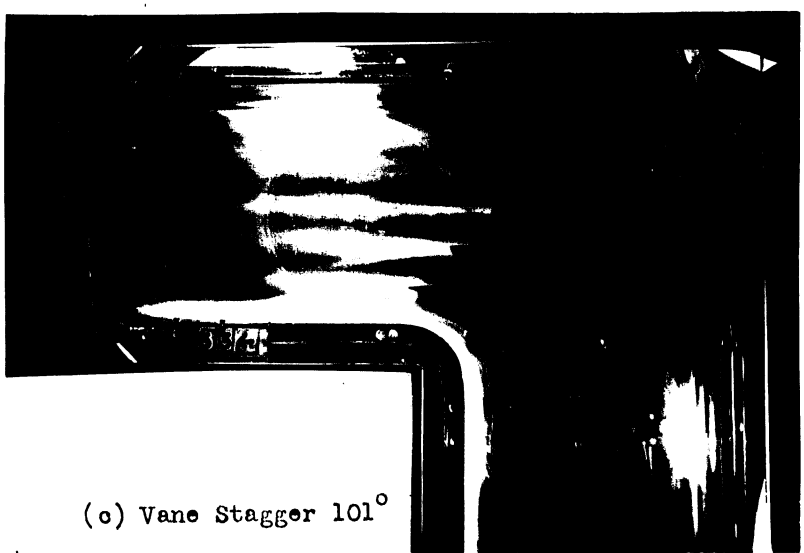

(c) Vane Stagger 101°

Flow of water
avg vel = 16.7 ft/sec
Reynolds no.= 640,000
s/c = 0.48

Fig. 9 Paths of Air Bubbles around Cascade of Type 1 Vanes at Mid-Depth

(a) Vane Stagger 96°

(b) Vane Stagger 101°

Fig. 10 Flow near Trailing Edge of Type 1 Vanes in Cascade as Shown by Strings

Flow of air - avg vel = 100 ft/sec, Reynolds no. 310,000
s/c = 0.48

(a) Dye Introduced near Center of Vane

Vane Stagger 96°

(b) Dye Introduced Immediately before Vane Trailing Edge

Vane Stagger 96°

(c) Dye Introduced Immediately after Vane Leading Edge

Vane Stagger 101°

Flow of air
avg vel = 100 ft/sec
Reynolds no.= 310,000
s/c = 0.48

Fig. 11 Flow near the Trailing Edge of Type 1 Vanes in Cascade as Shown by Colored Fluid

(a) Vane Stagger 96°

(b) Vane Stagger 101°

Fig. 12 Three-Dimensional Flow near the Ends of the Vanes as Shown by Colored Fluid

Flow of air - avg vel = 100 ft/sec Reynolds no. = 310,000
s/c = 0.48

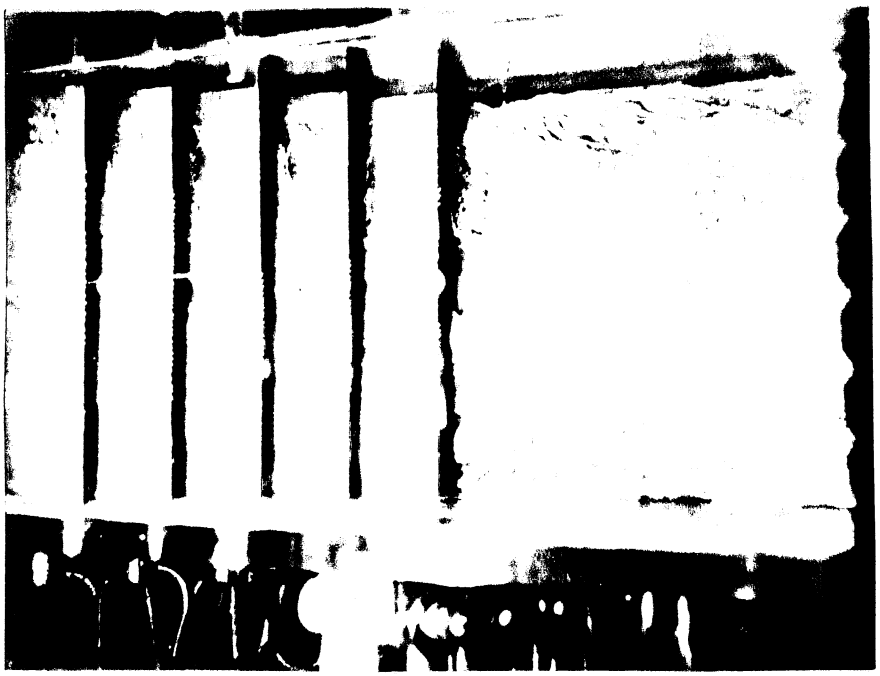

(a) Vane Stagger 90°
(Note Wiper on Vane Surface)

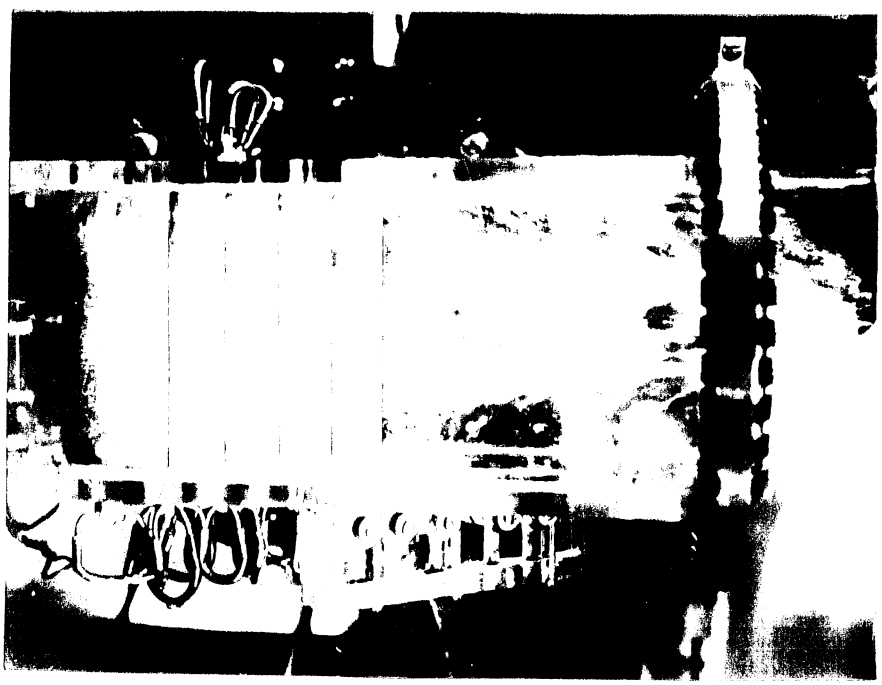

(b) Vane Stagger 101°

Fig. 13 Flow Past Cascade of Type 1 Vanes
Cored with Aluminum Dust and Oil

Flow of water - avg vel = 11.58 ft/sec Reynolds no.= 300,000
t/c = 0.4

SECTION D D

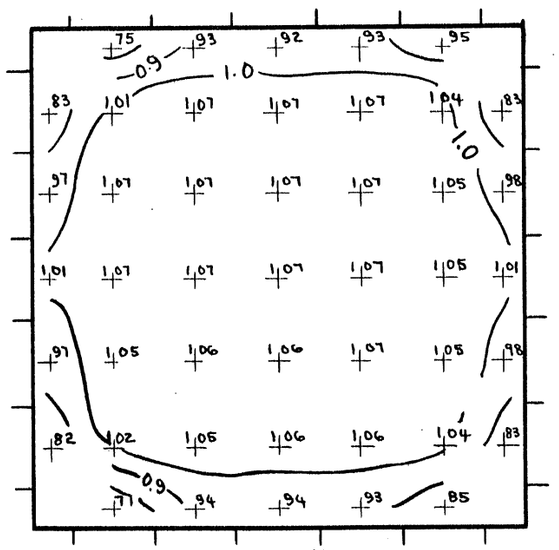

AVERAGE $\frac{H_t}{\bar{U}^2 2g} = 1.014$

SECTION K K

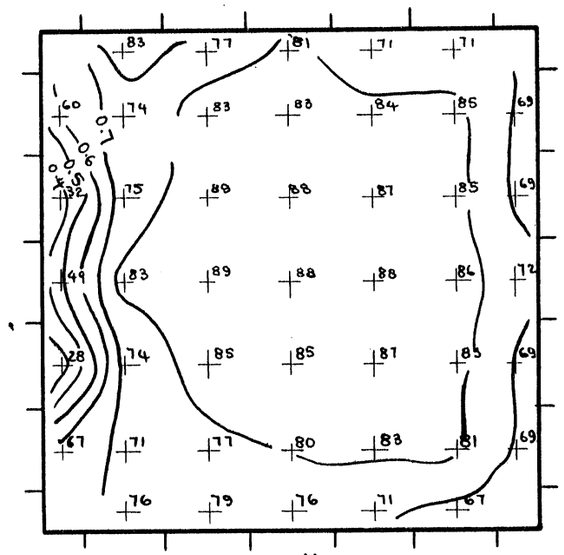

AVERAGE $\frac{H_t}{\bar{U}^2 2g} = 0.790$

SECTION M M

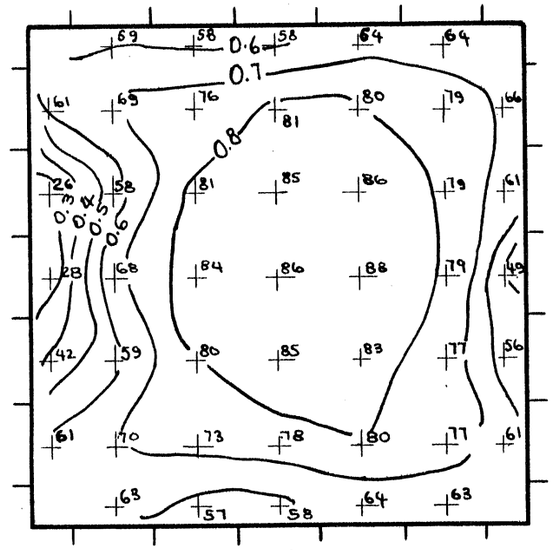

AVERAGE $\frac{H_t}{\bar{U}^2 2g} = 0.723$

TOTAL HEAD CONTOURS

(TOTAL HEADS IN FT. DIVIDED BY MEAN VEL. HEAD IN FT.)

INSIDE OF BEND

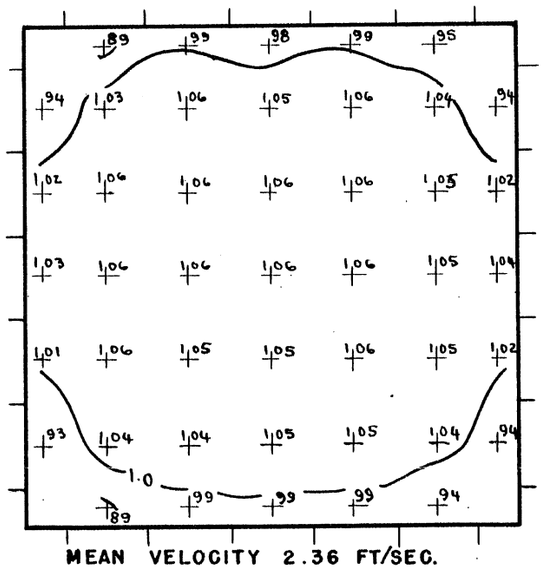

MEAN VELOCITY 2.36 FT/SEC.

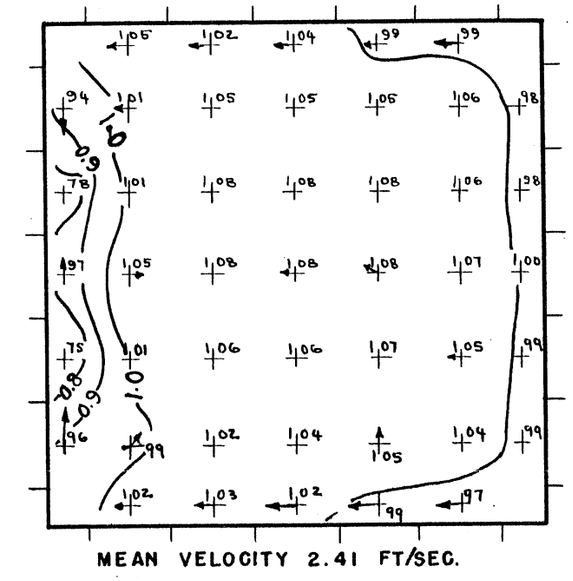

MEAN VELOCITY 2.41 FT/SEC.

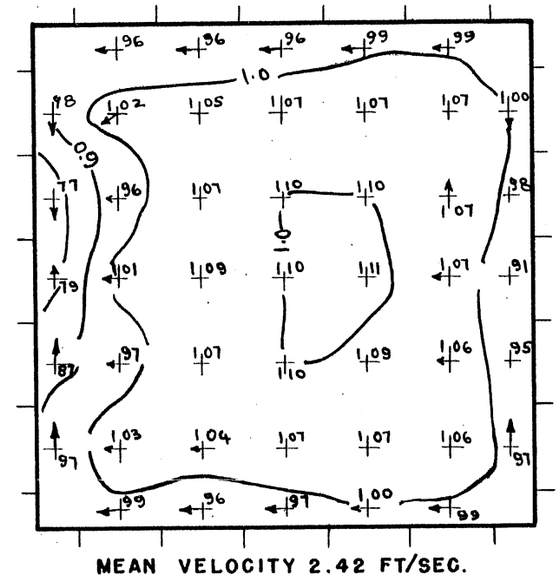

MEAN VELOCITY 2.42 FT/SEC.

OUTSIDE OF BEND

VELOCITY CONTOURS

(VELOCITIES IN FT/SEC DIVIDED BY MEAN VELOCITY IN FT./SEC.)

REYNOLDS NO. 119,000 (WATER)

VANE STAGGER 96°

SCALE OF VELOCITY VECTORS 1" = 0.5 UNIT

FIGURE NO. 14

TOTAL HEAD AND VELOCITY DATA

SERIES NO. 10

SECTION D—D

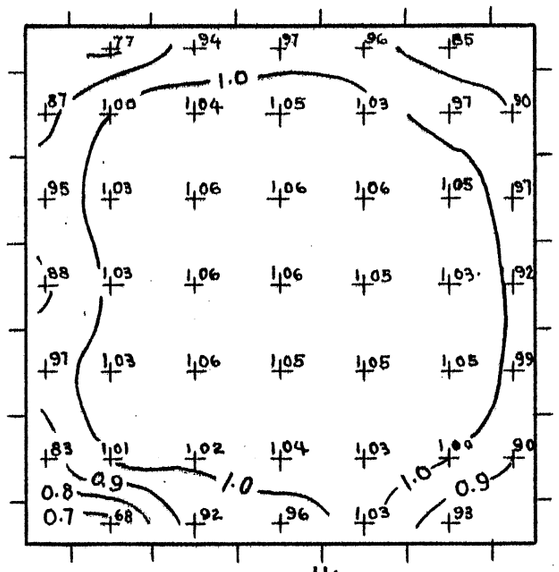

AVERAGE $\frac{H_t}{U^2 2g}$ = 1.033

SECTION K—K

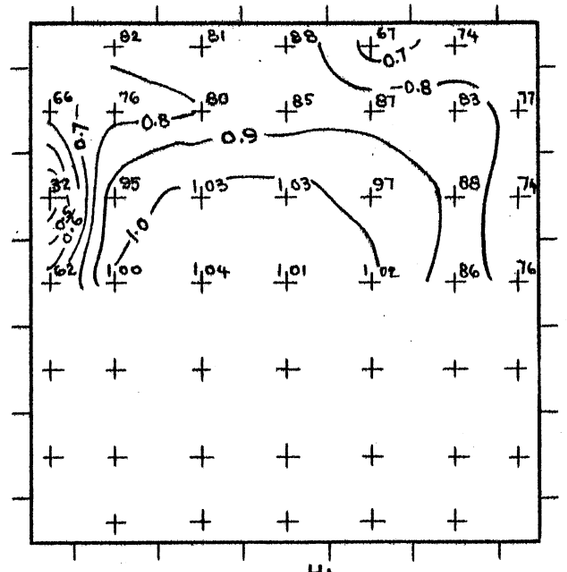

AVERAGE $\frac{H_t}{U^2 2g}$ = 0.876

SECTION M—M

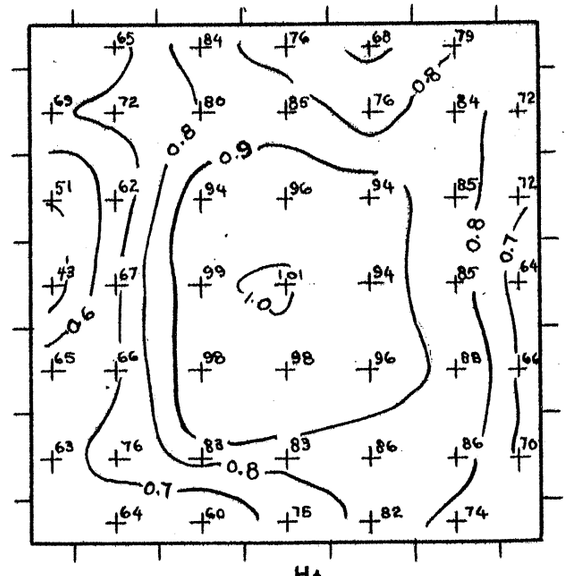

AVERAGE $\frac{H_t}{U^2 2g}$ = 0.818

TOTAL HEAD CONTOURS

(TOTAL HEADS IN FT. DIVIDED BY MEAN VEL. HEAD IN FT.)

INSIDE OF BEND

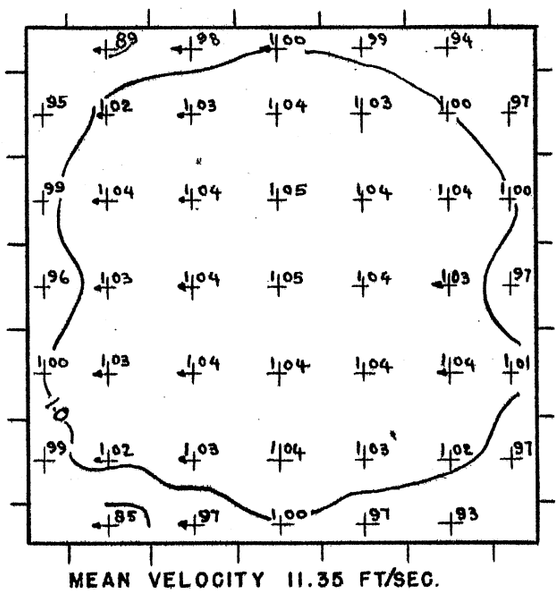

MEAN VELOCITY 11.35 FT/SEC.

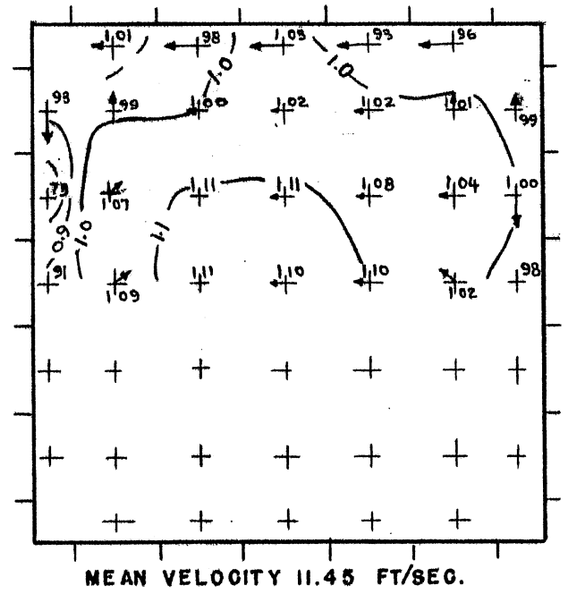

MEAN VELOCITY 11.45 FT/SEC.

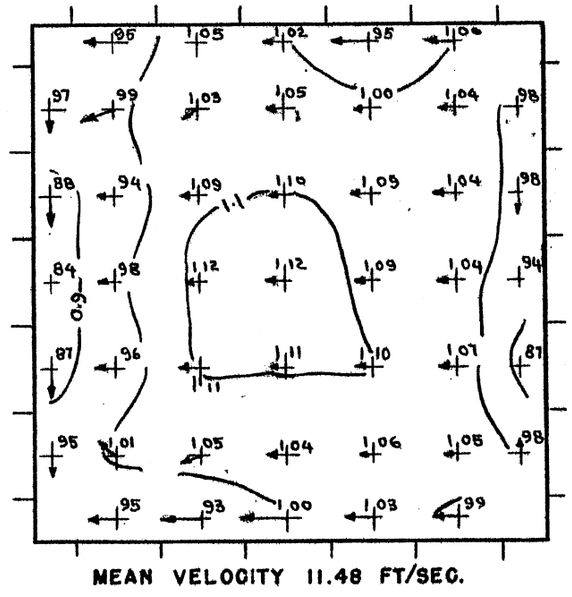

MEAN VELOCITY 11.48 FT/SEC.

OUTSIDE OF BEND

VELOCITY CONTOURS

(VELOCITIES IN FT/SEC. DIVIDED BY MEAN VELOCITY IN FT/SEC.) SCALE OF VELOCITY VECTORS 1" = 0.5 UNIT

REYNOLDS NO. 307,000 (WATER)
VANE STAGGER 96°

FIGURE NO. 15
TOTAL HEAD AND VELOCITY DATA
SERIES NO. II

SECTION D—D

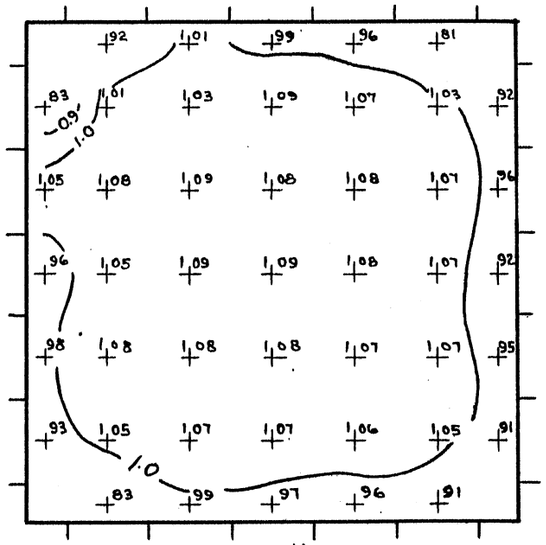

AVERAGE $\frac{H_t}{\bar{U}^2/2_g}$ = 1.027

SECTION K—K

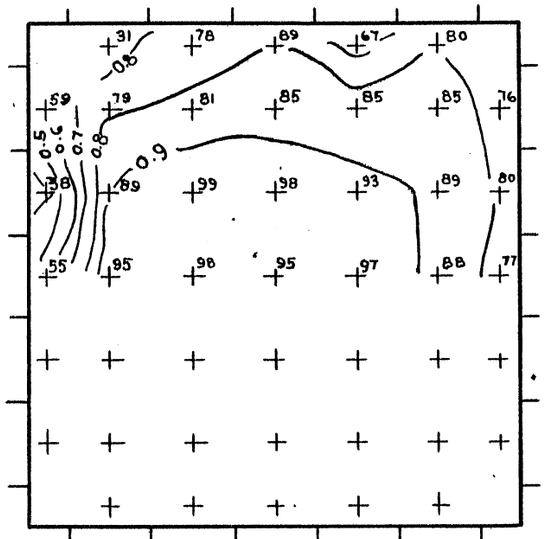

AVERAGE $\frac{H_t}{\bar{U}^2/2_g}$ = 0.850

SECTION M—M

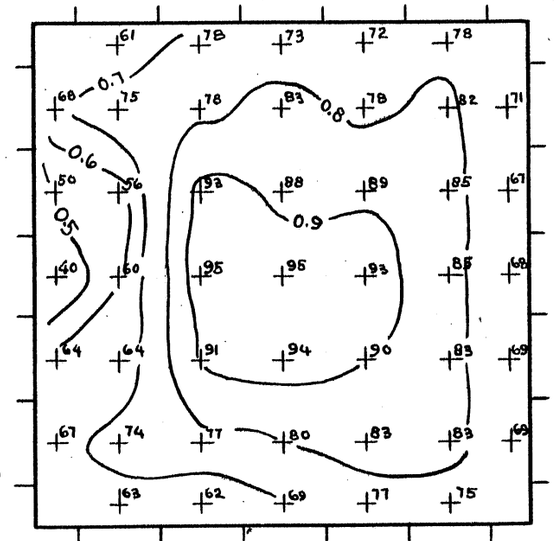

AVERAGE $\frac{H_t}{\bar{U}^2/2_g}$ = 0.785

TOTAL HEAD CONTOURS

(TOTAL HEADS IN FT. DIVIDED BY MEAN VEL. HEAD IN FT.)

INSIDE OF BEND

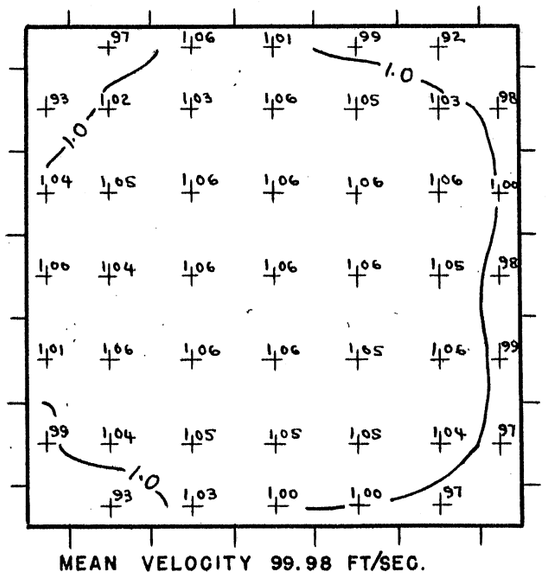

MEAN VELOCITY 99.98 FT/SEC.

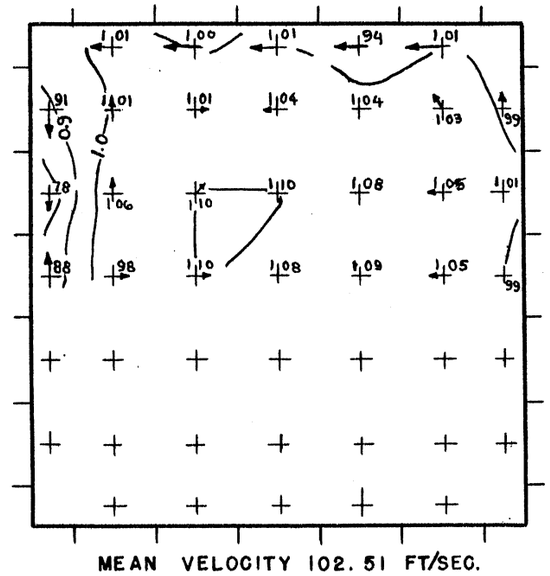

MEAN VELOCITY 102.51 FT/SEC.

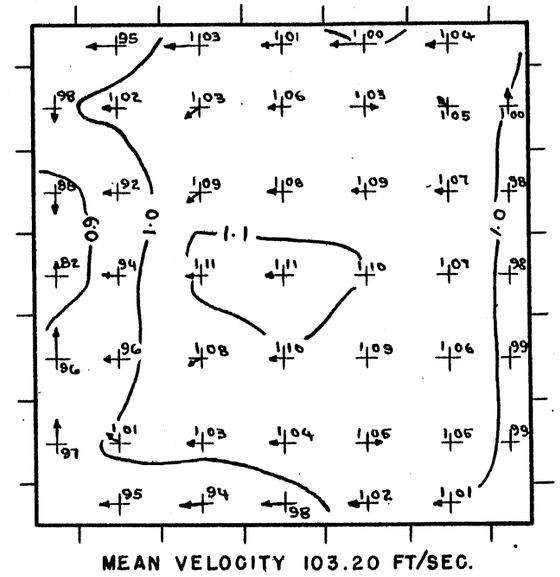

MEAN VELOCITY 103.20 FT/SEC.

OUTSIDE OF BEND

VELOCITY CONTOURS

(VELOCITIES IN FT/SEC. DIVIDED BY MEAN VELOCITY IN FT/SEC.)

REYNOLDS NO. 308,000 (AIR)
VANE STAGGER 96°

SCALE OF VELOCITY VECTORS 1" = 0.5 UNIT

FIGURE NO. 16
TOTAL HEAD AND VELOCITY DATA
SERIES NO. 12

SECTION D—D

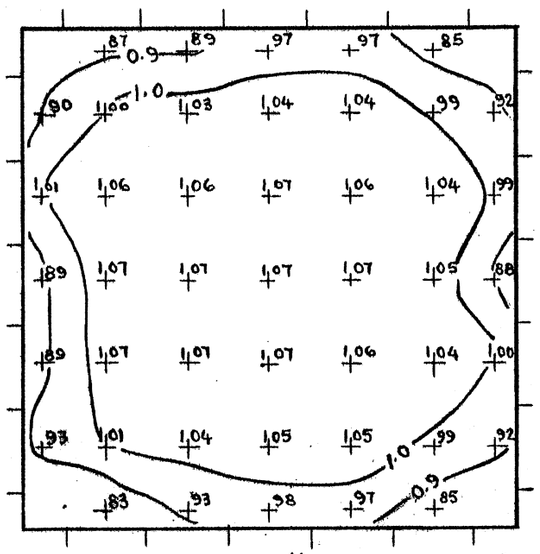

AVERAGE $\frac{H_t}{\bar{U}^2/2g} = 1.082$

SECTION K—K

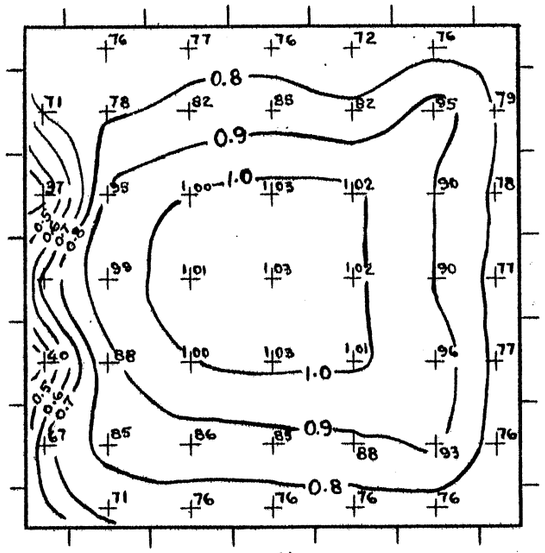

AVERAGE $\frac{H_t}{\bar{U}^2/2g} = 0.878$

SECTION M—M

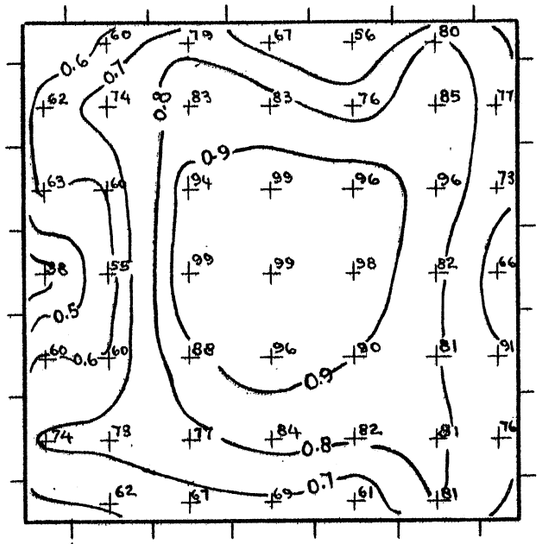

AVERAGE $\frac{H_t}{\bar{U}^2/2g} = 0.810$

TOTAL HEAD CONTOURS

(TOTAL HEADS IN FT. DIVIDED BY MEAN VEL. HEAD IN FT.)

INSIDE OF BEND

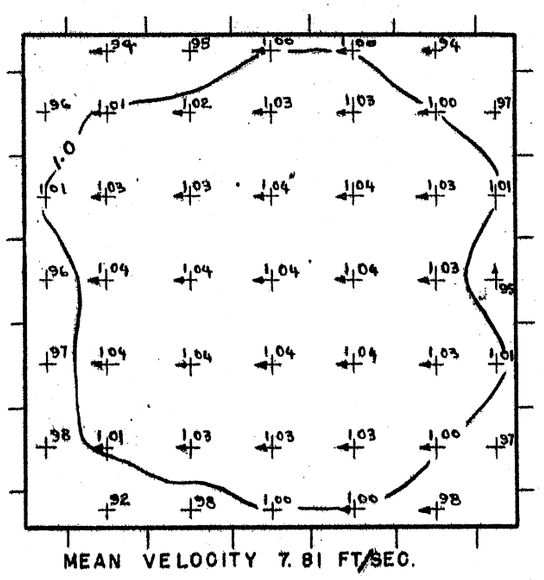

MEAN VELOCITY 7.81 FT/SEC.

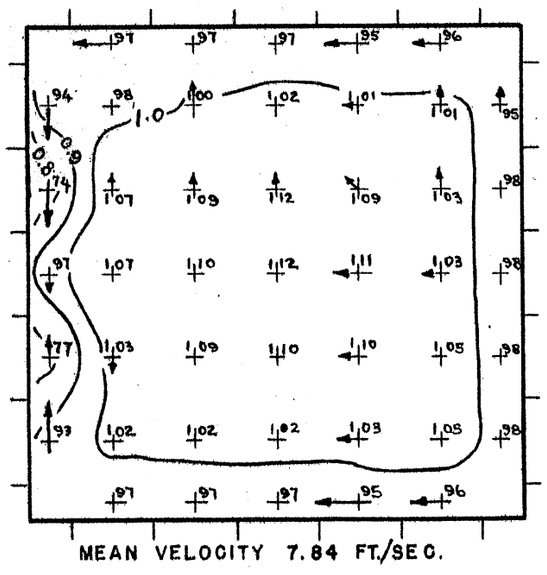

MEAN VELOCITY 7.84 FT./SEC.

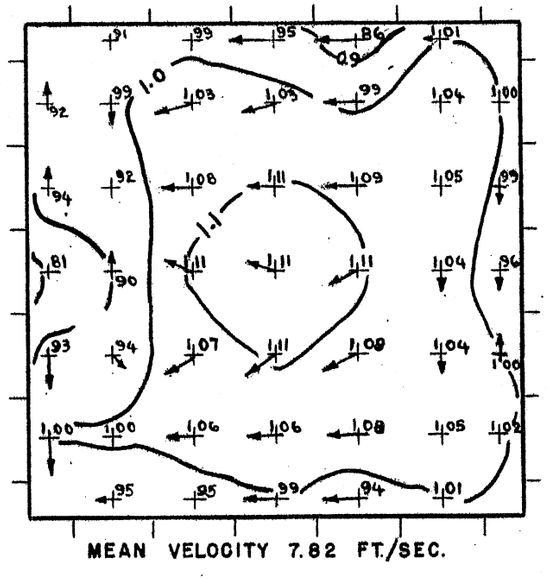

MEAN VELOCITY 7.82 FT./SEC.

OUTSIDE OF BEND

VELOCITY CONTOURS

(VELOCITIES IN FT/SEC. DIVIDED BY MEAN VELOCITY IN FT./SEC.)

REYNOLDS NO. 353,000 (WATER)
VANE STAGGER 96°

SCALE OF VELOCITY VECTORS 1" = 0.5 UNIT

FIGURE NO. 17
TOTAL HEAD AND VELOCITY DATA
SERIES NO. 13

SECTION D—D

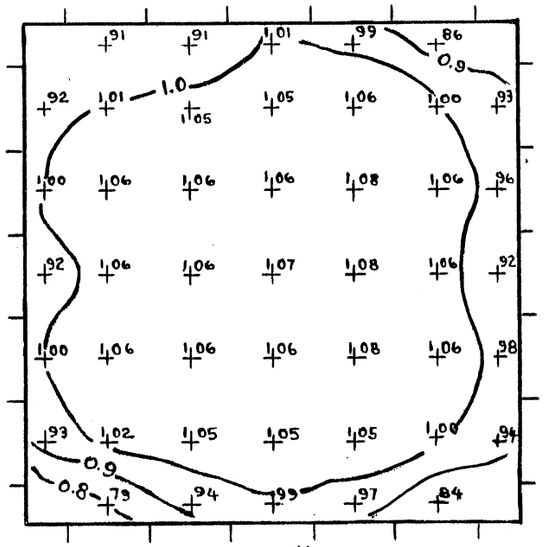

AVERAGE $\frac{H_t}{\bar{U}^2/2g}$ = 1.028

SECTION K—K

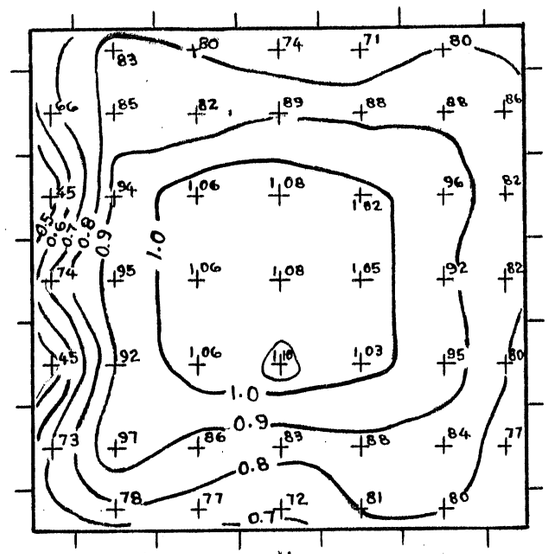

AVERAGE $\frac{H_t}{\bar{U}^2/2g}$ = 0.885

SECTION M—M

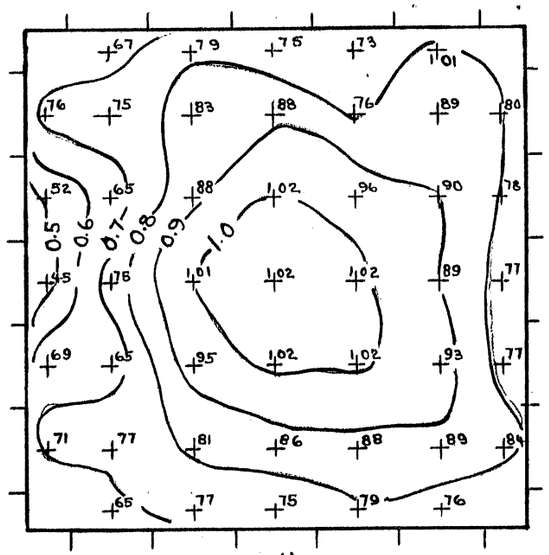

AVERAGE $\frac{H_t}{\bar{U}^2/2g}$ = 0.835

TOTAL HEAD CONTOURS

(TOTAL HEADS IN FT. DIVIDED BY MEAN VEL. HEAD IN FT.)

INSIDE OF BEND

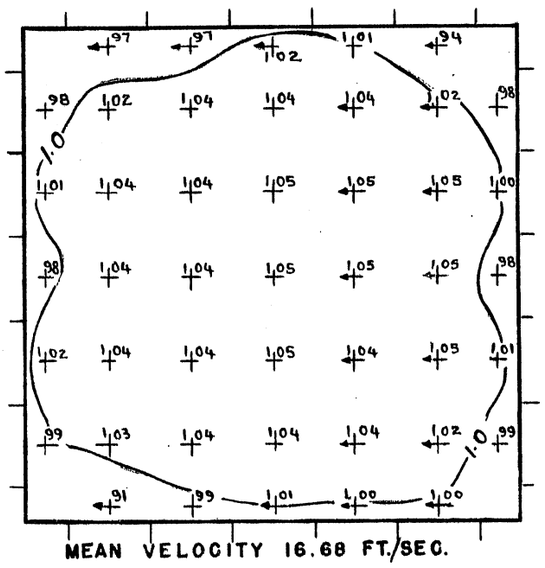

MEAN VELOCITY 16.68 FT./SEC.

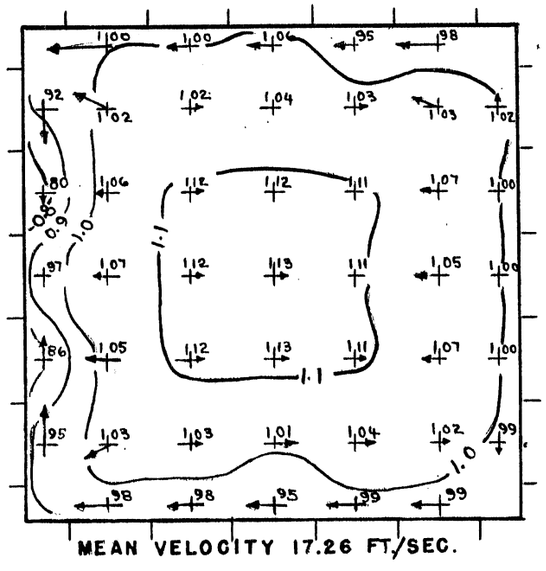

MEAN VELOCITY 17.26 FT./SEC.

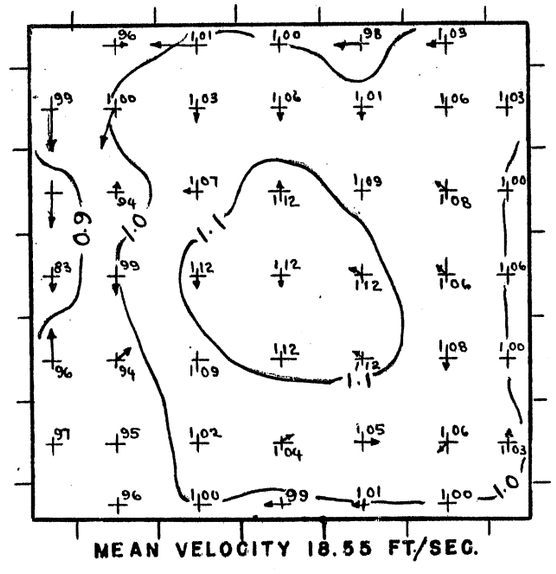

MEAN VELOCITY 18.55 FT/SEC.

OUTSIDE OF BEND

VELOCITY CONTOURS

(VELOCITIES IN FT/SEC. DIVIDED BY MEAN VELOCITY IN FT/SEC.)

REYNOLDS NO. 707,000 (WATER)
VANE STAGGER 96°

SCALE OF VELOCITY VECTORS 1" = 0.5 UNIT

FIGURE NO. 18
TOTAL HEAD AND VELOCITY DATA
SERIES NO. 14

SECTION D—D

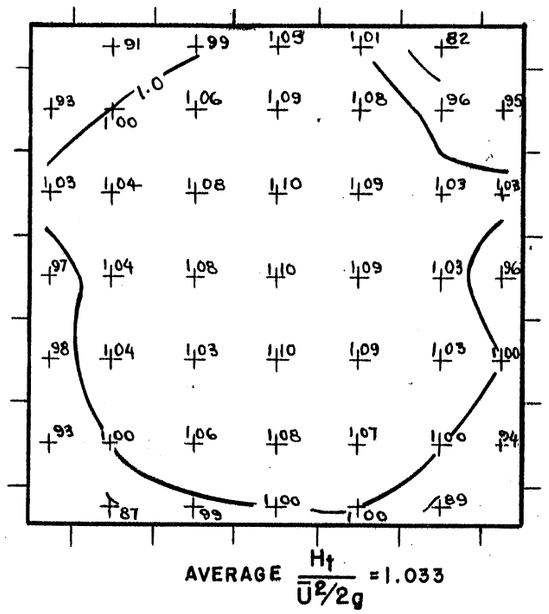

AVERAGE $\frac{H_t}{\bar{U}^2/2g}$ = 1.033

SECTION K—K

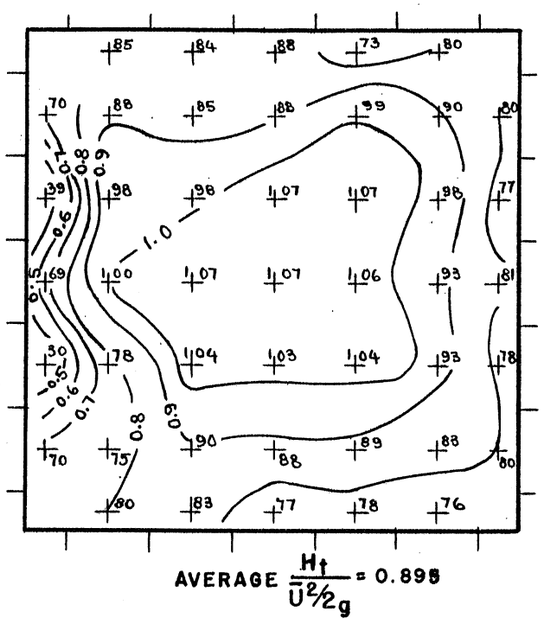

AVERAGE $\frac{H_t}{\bar{U}^2/2g}$ = 0.895

SECTION M—M

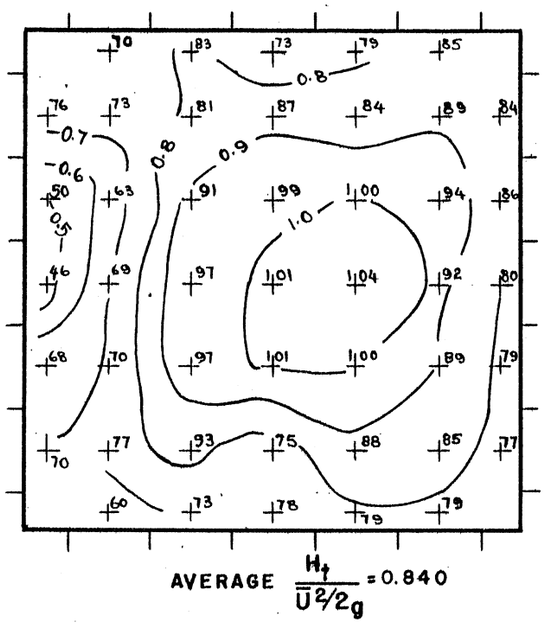

AVERAGE $\frac{H_t}{\bar{U}^2/2g}$ = 0.840

TOTAL HEAD CONTOURS

(TOTAL HEADS IN FT. DIVIDED BY MEAN VEL. HEAD IN FT.)

INSIDE CURVATURE OF BEND

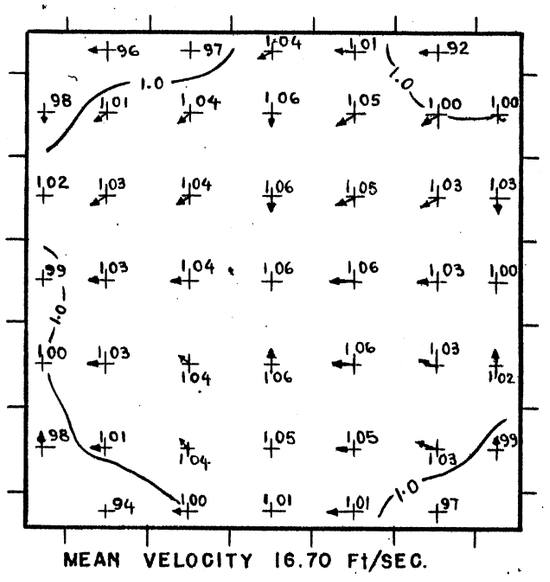

MEAN VELOCITY 16.70 Ft/SEC.

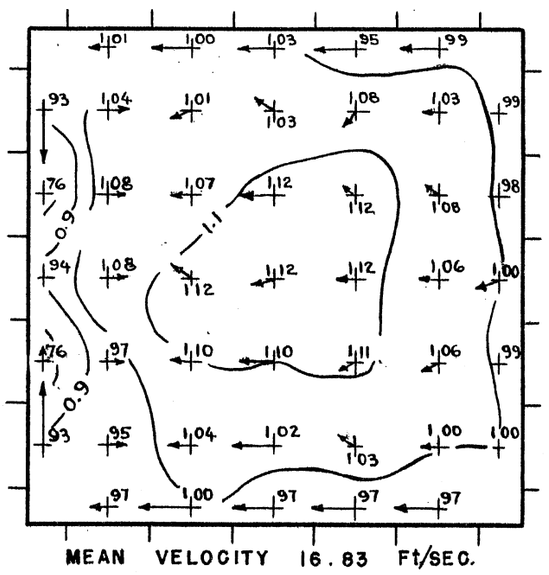

MEAN VELOCITY 16.83 Ft/SEC.

OUTSIDE CURVATURE OF BEND

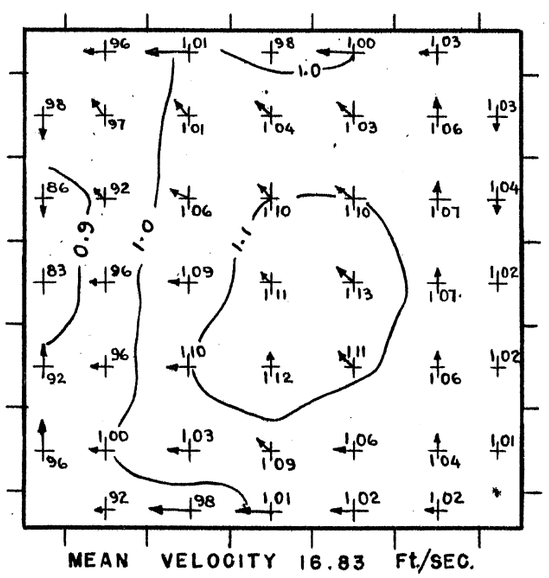

MEAN VELOCITY 16.83 Ft/SEC.

VELOCITY CONTOURS

(VELOCITIES IN Ft/SEC. DIVIDED BY MEAN VELOCITY IN Ft/SEC.)

REYNOLDS NO. 833,000 (WATER)
VANE STAGGER 96°

SCALE OF VELOCITY VECTORS 1" = 0.5 UNIT

FIGURE NO. 19
TOTAL HEAD AND VELOCITY DATA
SERIES NO. 15

SECTION D—D

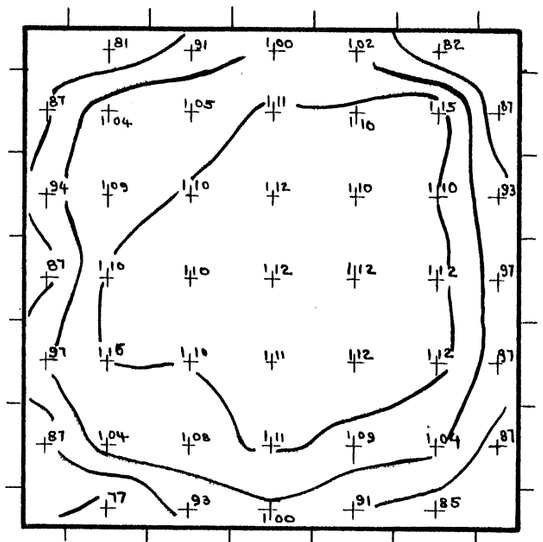

AVERAGE $\frac{H_t}{\bar{U}^2/2g} = 1.043$

SECTION K—K

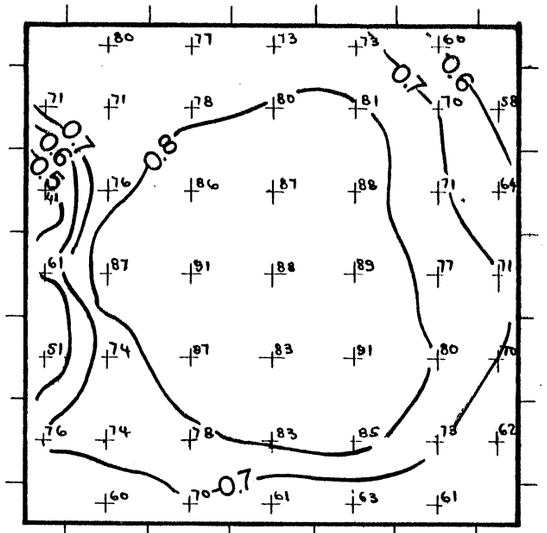

AVERAGE $\frac{H_t}{\bar{U}^2/2g} = 0.771$

SECTION M—M

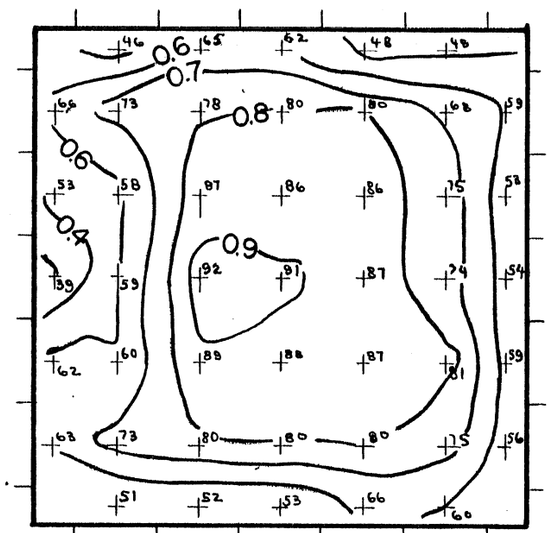

AVERAGE $\frac{H_t}{\bar{U}^2/2g} = 0.735$

TOTAL HEAD CONTOURS

(TOTAL HEADS IN FT. DIVIDED BY MEAN VEL. HEAD IN FT.)

INSIDE CURVATURE OF BEND

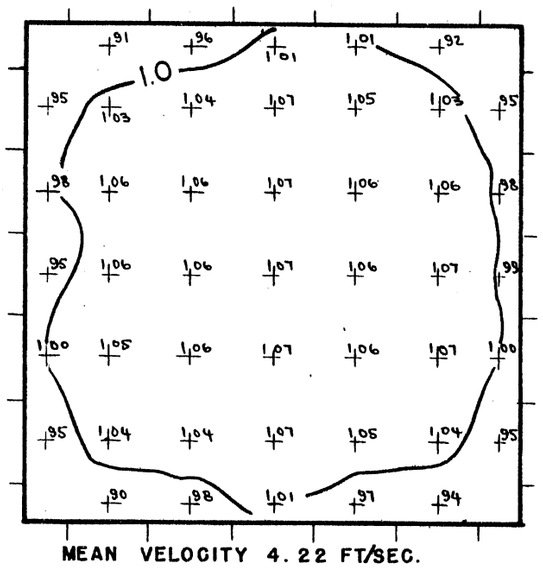

MEAN VELOCITY 4.22 FT/SEC.

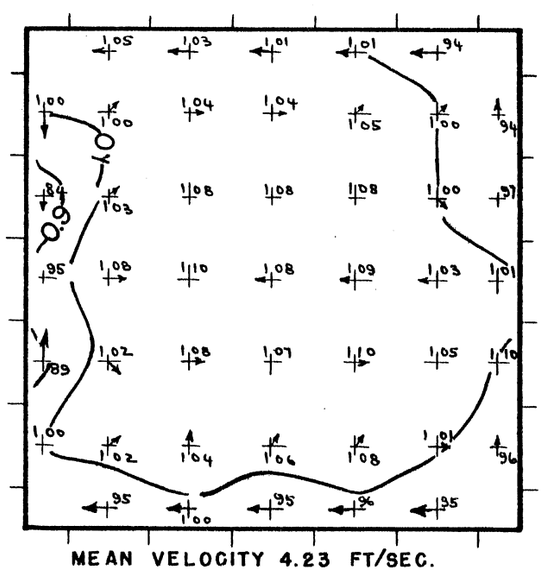

MEAN VELOCITY 4.23 FT/SEC.

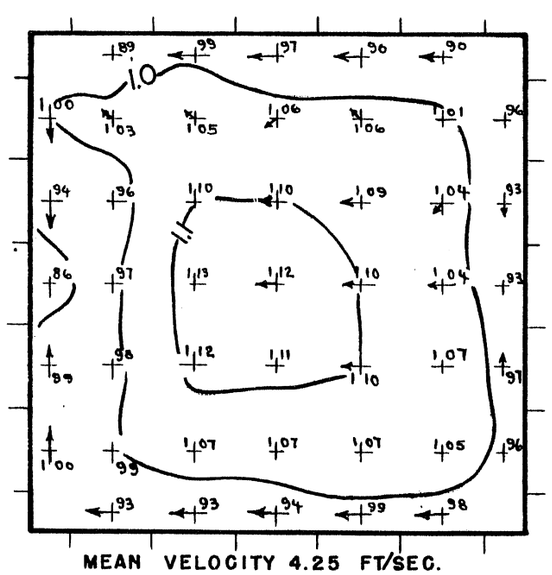

MEAN VELOCITY 4.25 FT/SEC.

OUTSIDE CURVATURE OF BEND

VELOCITY CONTOURS

(VELOCITIES IN FT/SEC. DIVIDED BY MEAN VELOCITY IN FT/SEC.)

REYNOLDS NO. 111,000 (WATER)
VANE STAGGER 101°

SCALE OF VELOCITY VECTORS 1" = 0.5 UNIT

FIGURE NO. 20
TOTAL HEAD AND VELOCITY DATA
SERIES NO. 16

SECTION D—D

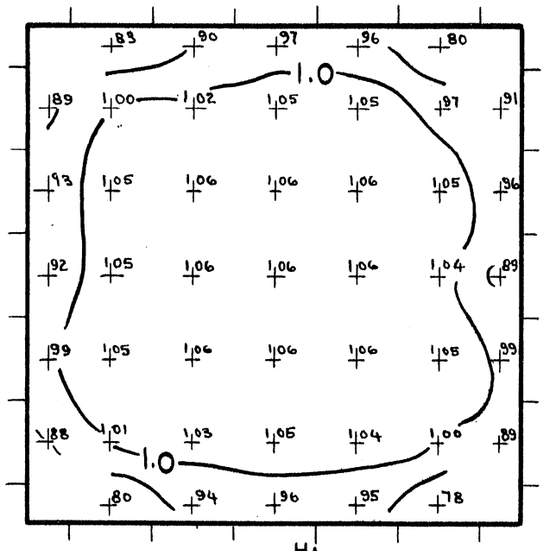

AVERAGE $\frac{H_t}{\bar{U}^2/2g}$ = 1.028

SECTION K—K

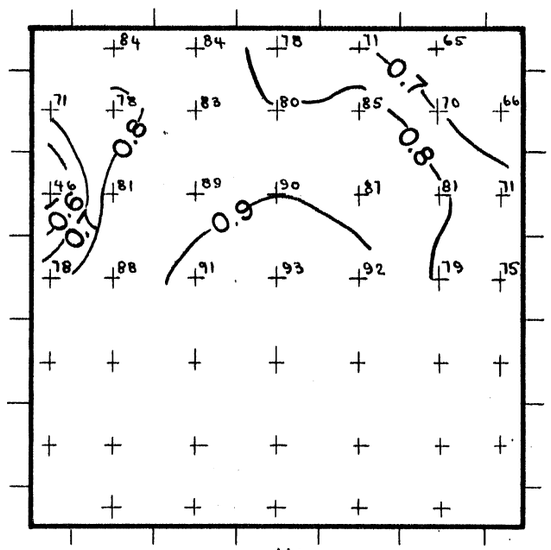

AVERAGE $\frac{H_t}{\bar{U}^2/2g}$ = 0.829

SECTION M—M

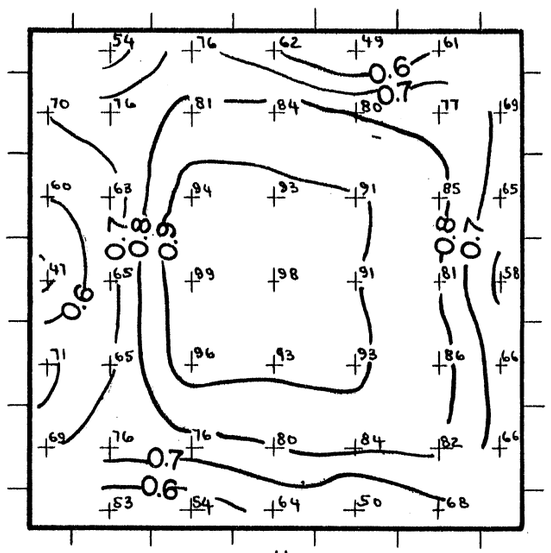

AVERAGE $\frac{H_t}{\bar{U}^2/2g}$ = 0.785

TOTAL HEAD CONTOURS

(TOTAL HEADS IN FT. DIVIDED BY MEAN VEL. HEAD IN FT.)

INSIDE OF BEND

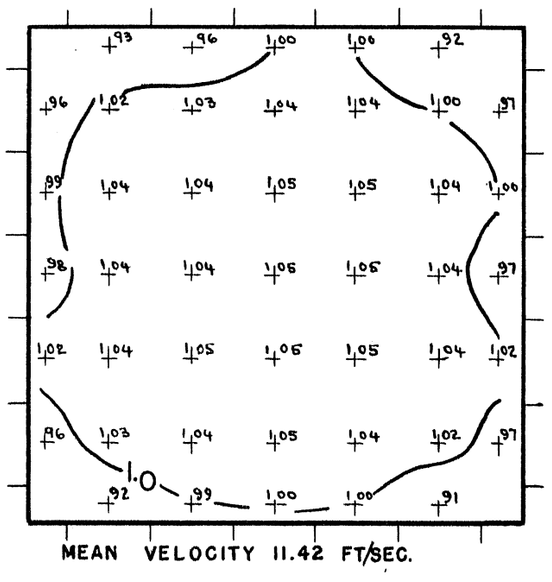

MEAN VELOCITY 11.42 FT/SEC.

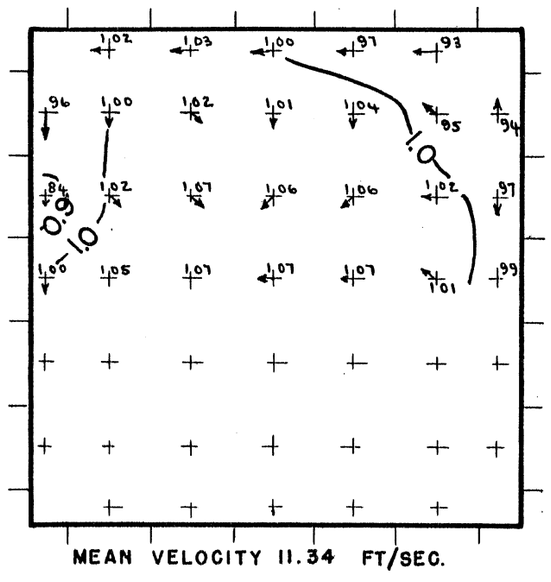

MEAN VELOCITY 11.34 FT/SEC.

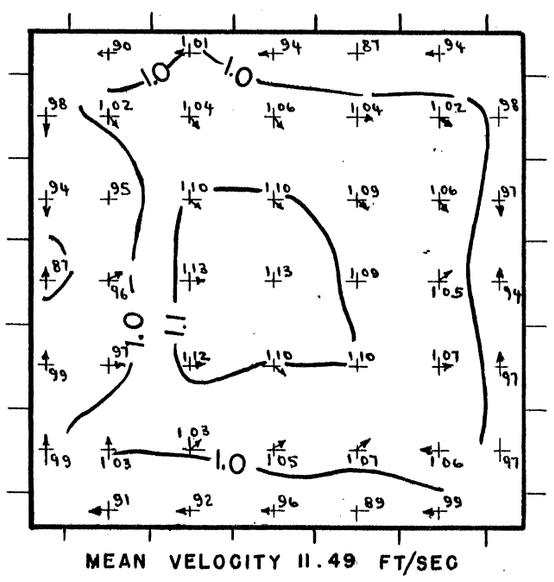

MEAN VELOCITY 11.49 FT/SEC

OUTSIDE OF BEND

VELOCITY CONTOURS

(VELOCITIES IN FT./SEC. DIVIDED BY MEAN VELOCITY IN FT./SEC.)

REYNOLDS NO. 302,000 (WATER)
VANE STAGGER 101°

SCALE OF VELOCITY VECTORS 1" = 0.5 UNIT

FIGURE NO. 21
TOTAL HEAD AND VELOCITY DATA
SERIES NO. 17

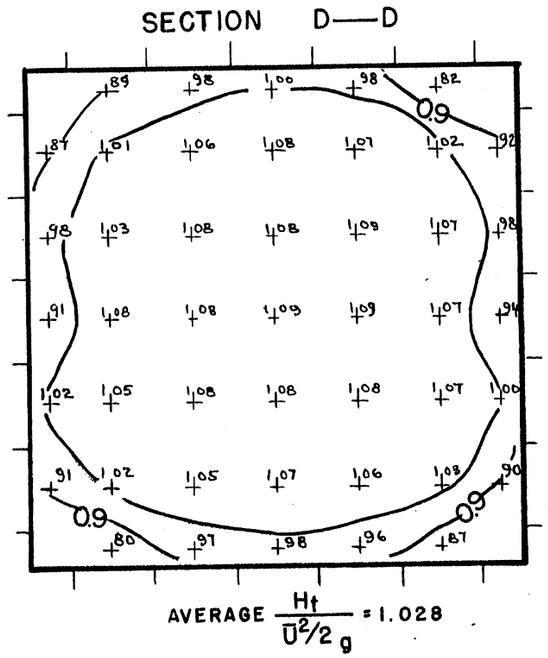

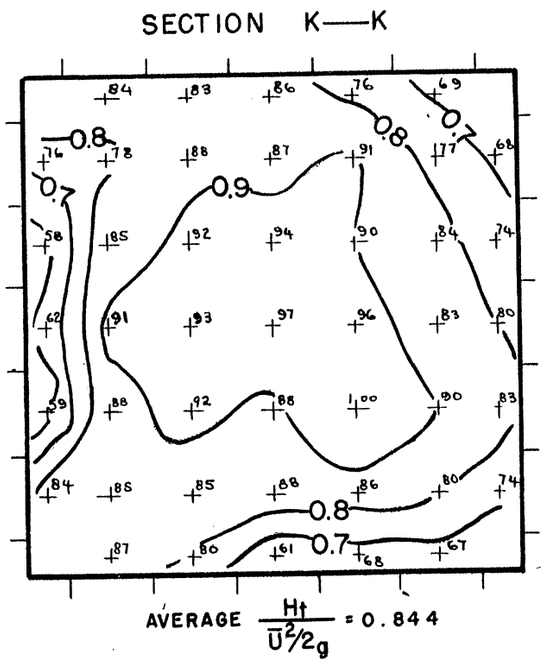

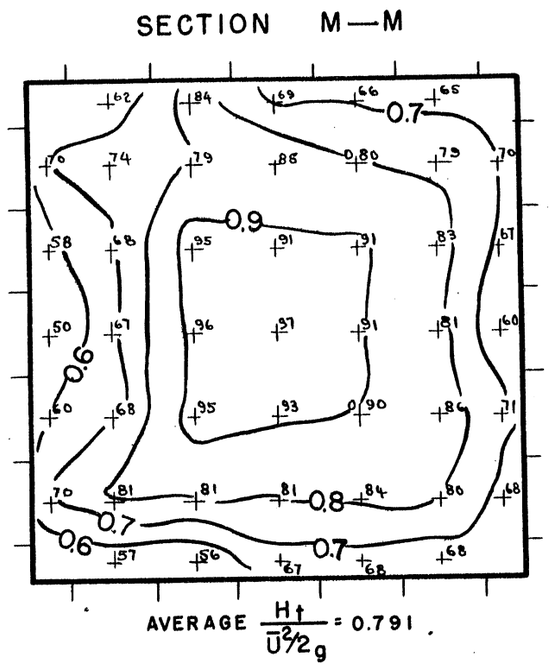

TOTAL HEAD CONTOURS

(TOTAL HEADS IN FT. DIVIDED BY MEAN VEL. HEAD IN FT.)

INSIDE OF BEND

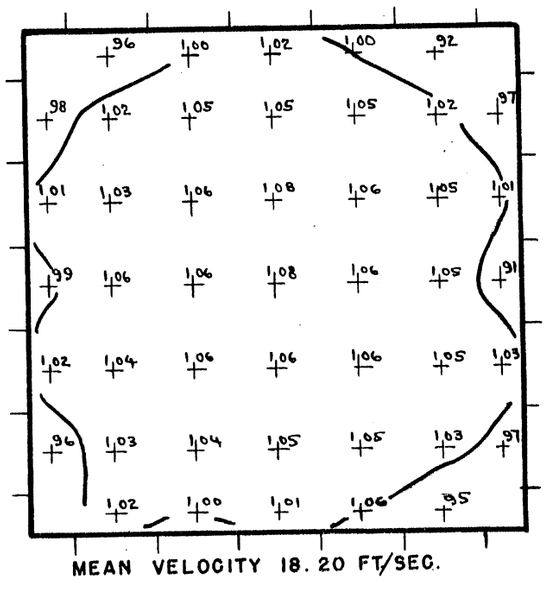

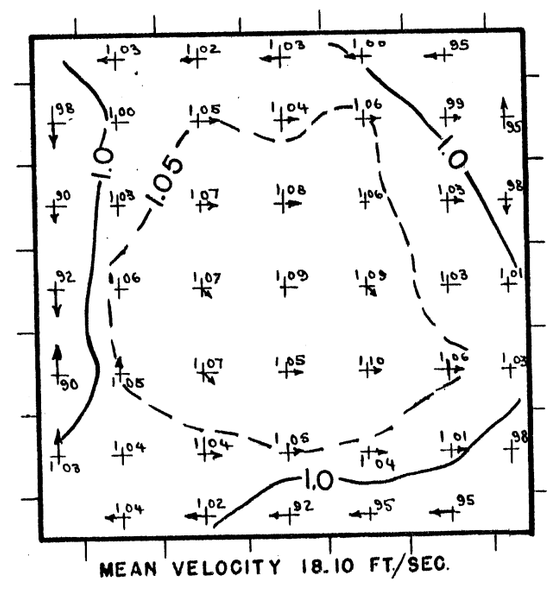

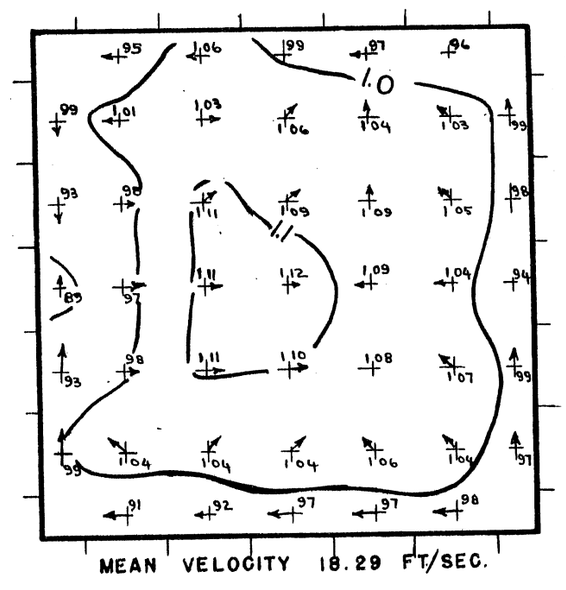

OUTSIDE OF BEND

VELOCITY CONTOURS

(VELOCITIES IN FT SEC. DIVIDED BY MEAN VELOCITY IN FT. SEC.)

REYNOLDS NO. 478,000 (WATER)
VANE STAGGER 101°

SCALE OF VELOCITY VECTORS 1" = 0.5 UNIT

FIGURE NO. 22
TOTAL HEAD AND VELOCITY DATA
SERIES NO. 18

INSIDE OF BEND

SECTION D—D

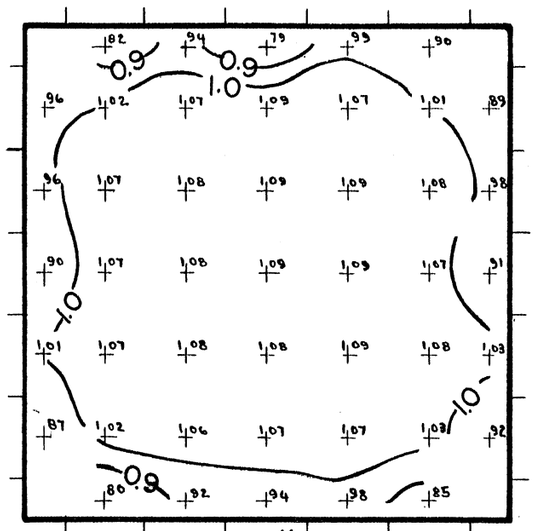

AVERAGE $\frac{H_t}{\bar{U}^2 2g}$ = 1.027

SECTION K—K

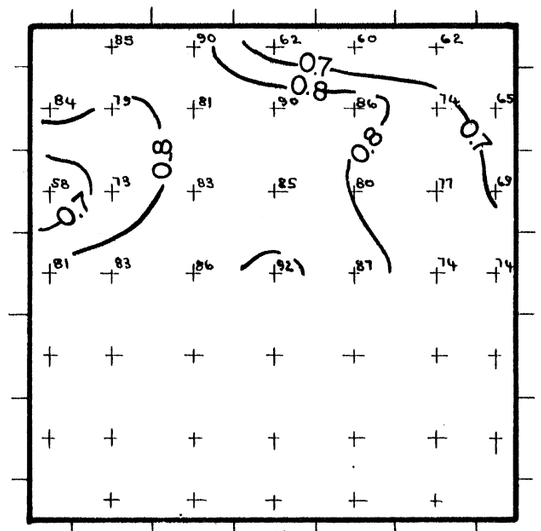

AVERAGE $\frac{H_t}{\bar{U}^2 2g}$ = 0.790

SECTION M—M

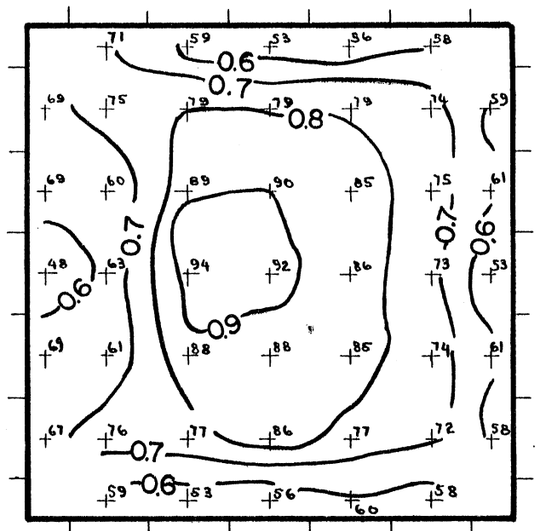

AVERAGE $\frac{H_t}{\bar{U}^2 2g}$ = 0.749

TOTAL HEAD CONTOURS

(TOTAL HEADS IN FT. DIVIDED BY MEAN VEL. HEAD IN FT.)

OUTSIDE OF BEND

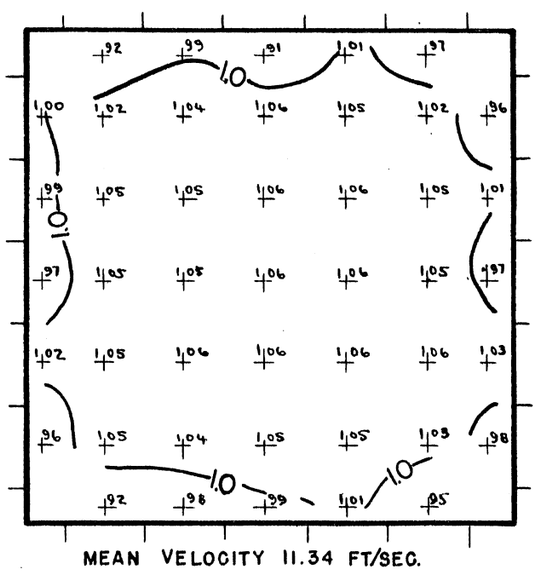

MEAN VELOCITY 11.34 FT/SEC.

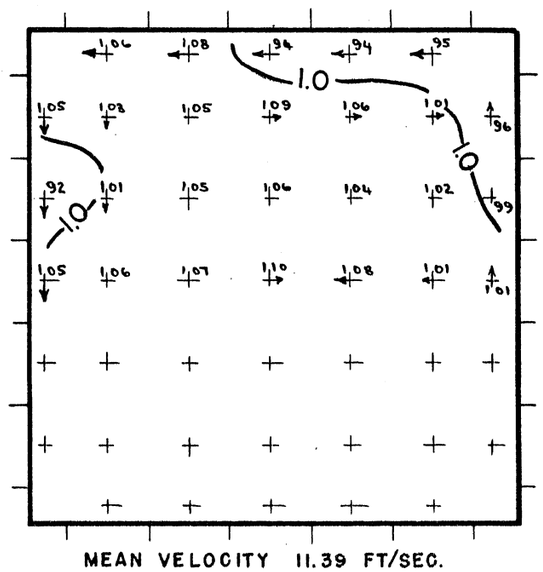

MEAN VELOCITY 11.39 FT/SEC.

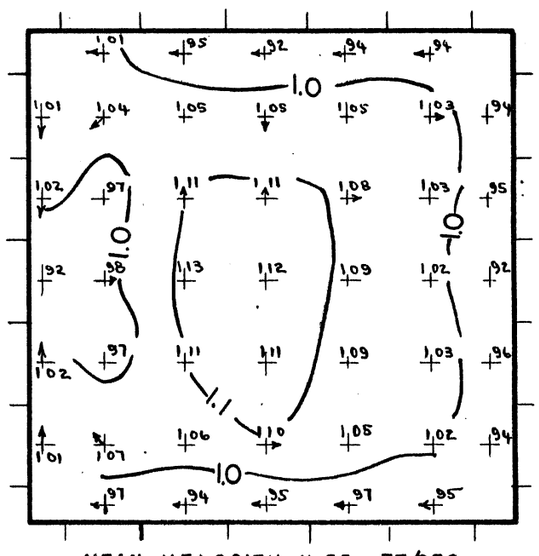

MEAN VELOCITY 11.55 FT/SEC.

VELOCITY CONTOURS

(VELOCITIES IN FT/SEC. DIVIDED BY MEAN VELOCITY IN FT/SEC.)

REYNOLDS NO. 300,000 (WATER)
VANE STAGGER 101°

SCALE OF VELOCITY VECTORS 1" = 0.5 UNIT

FIGURE NO. 23
TOTAL HEAD AND VELOCITY DATA
SERIES NO. 19

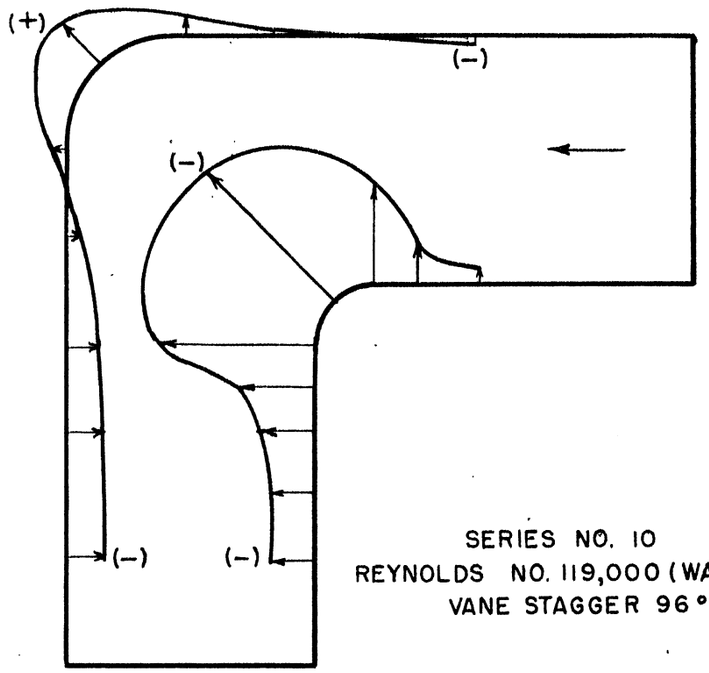

SERIES NO. 10
REYNOLDS NO. 119,000 (WATER)
VANE STAGGER 96°

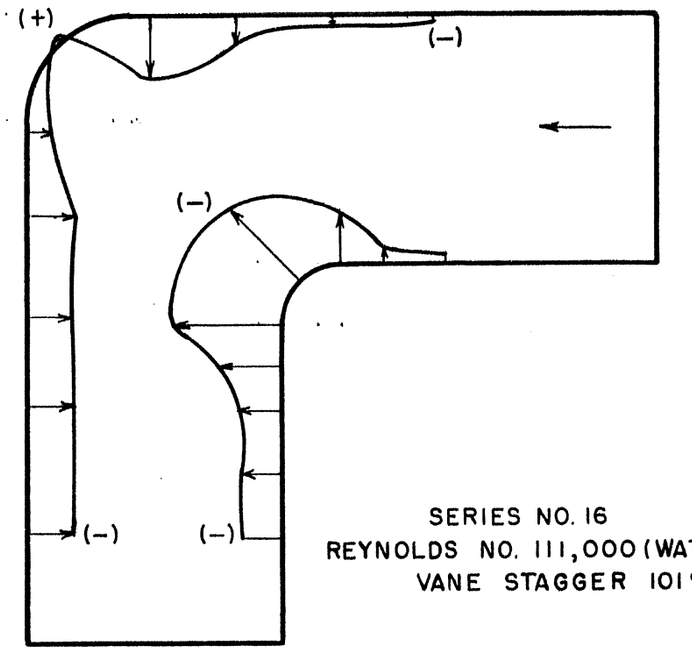

SERIES NO. 16
REYNOLDS NO. 111,000 (WATER)
VANE STAGGER 101°

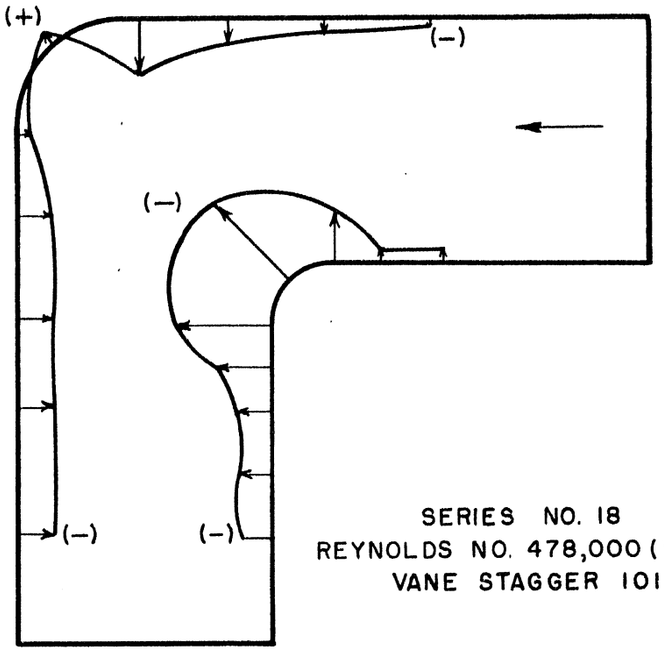

SERIES NO. 18
REYNOLDS NO. 478,000 (WATER)
VANE STAGGER 101°

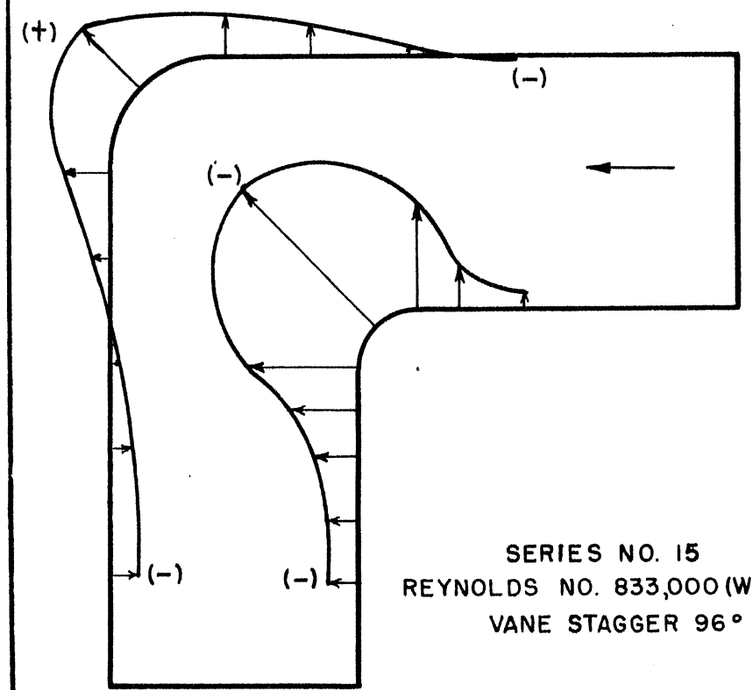

SERIES NO. 15
REYNOLDS NO. 833,000 (WATER)
VANE STAGGER 96°

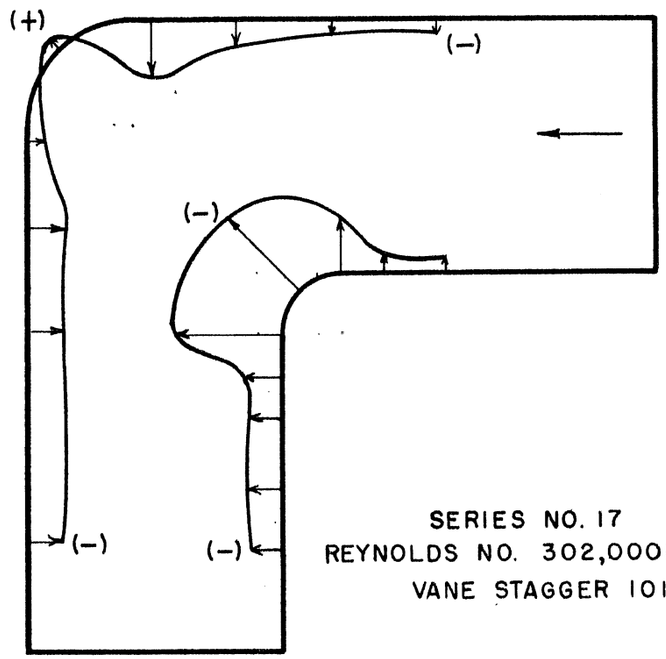

SERIES NO. 17
REYNOLDS NO. 302,000 (WATER)
VANE STAGGER 101°

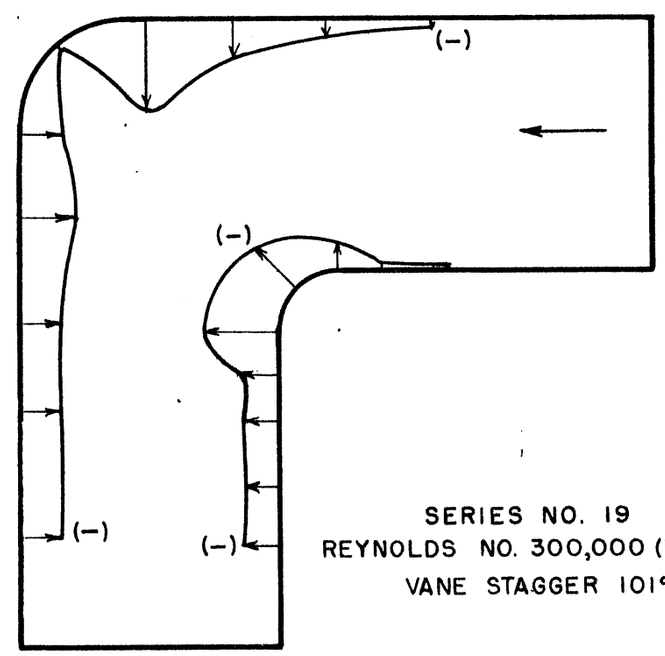

SERIES NO. 19
REYNOLDS NO. 300,000 (WATER)
VANE STAGGER 101°

S/C = 0.48
SCALE 1" = 1 UNIT

FIG. 24
WALL PRESSURES AROUND BEND AT MID DEPTH
(WALL PRESSURE IN FT. DIVIDED BY MEAN VEL. HEAD IN FT.)

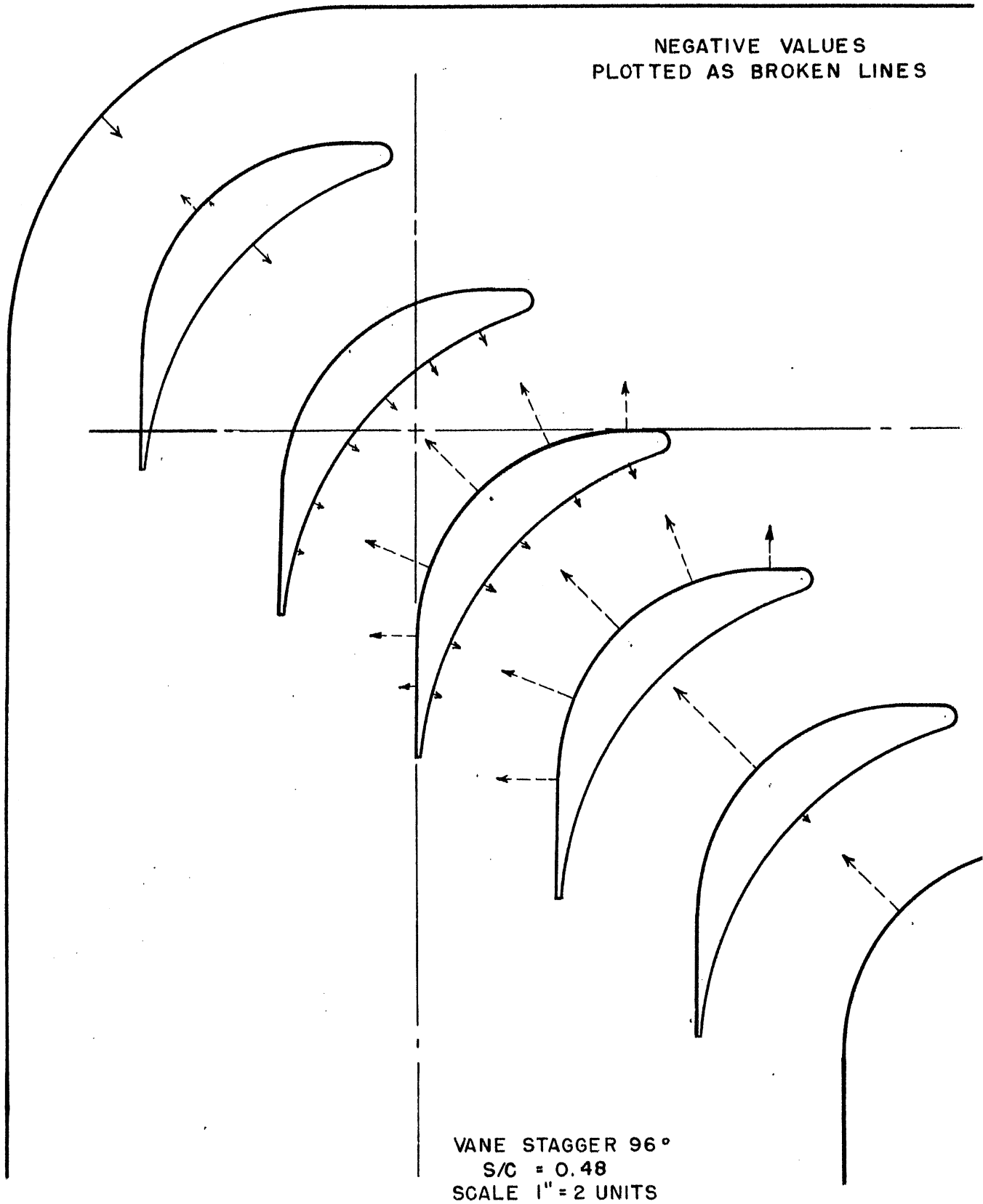

FIG. 25

PRESSURES AT MID-DEPTH ACROSS CASCADE

(PRESSURES IN FT. DIVIDED BY MEAN VEL. HEAD IN FEET)

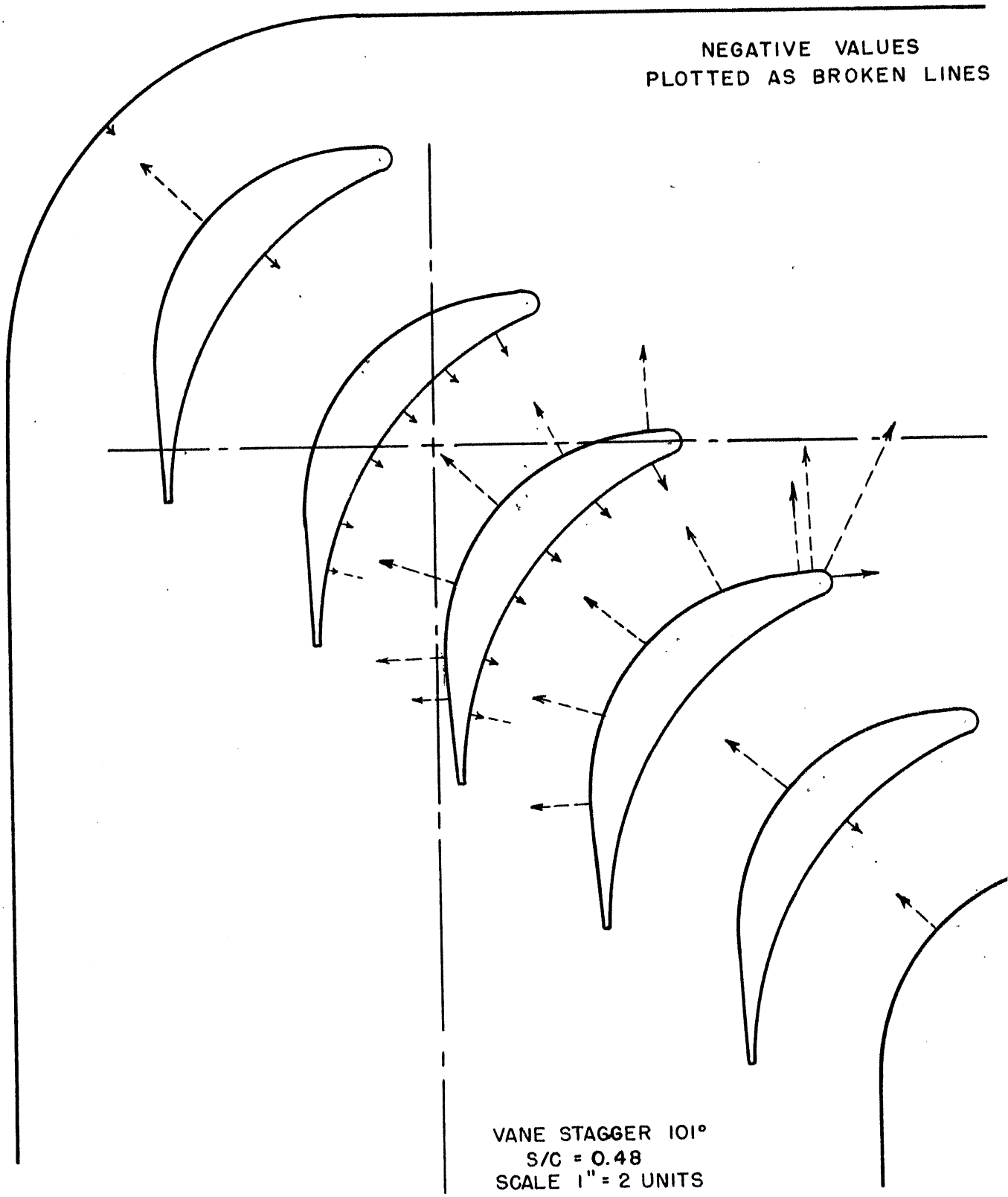

FIG. 26

PRESSURES AT MID-DEPTH ACROSS CASCADE

(PRESSURES IN FT. DIVIDED BY MEAN VEL. HEAD IN FT.)

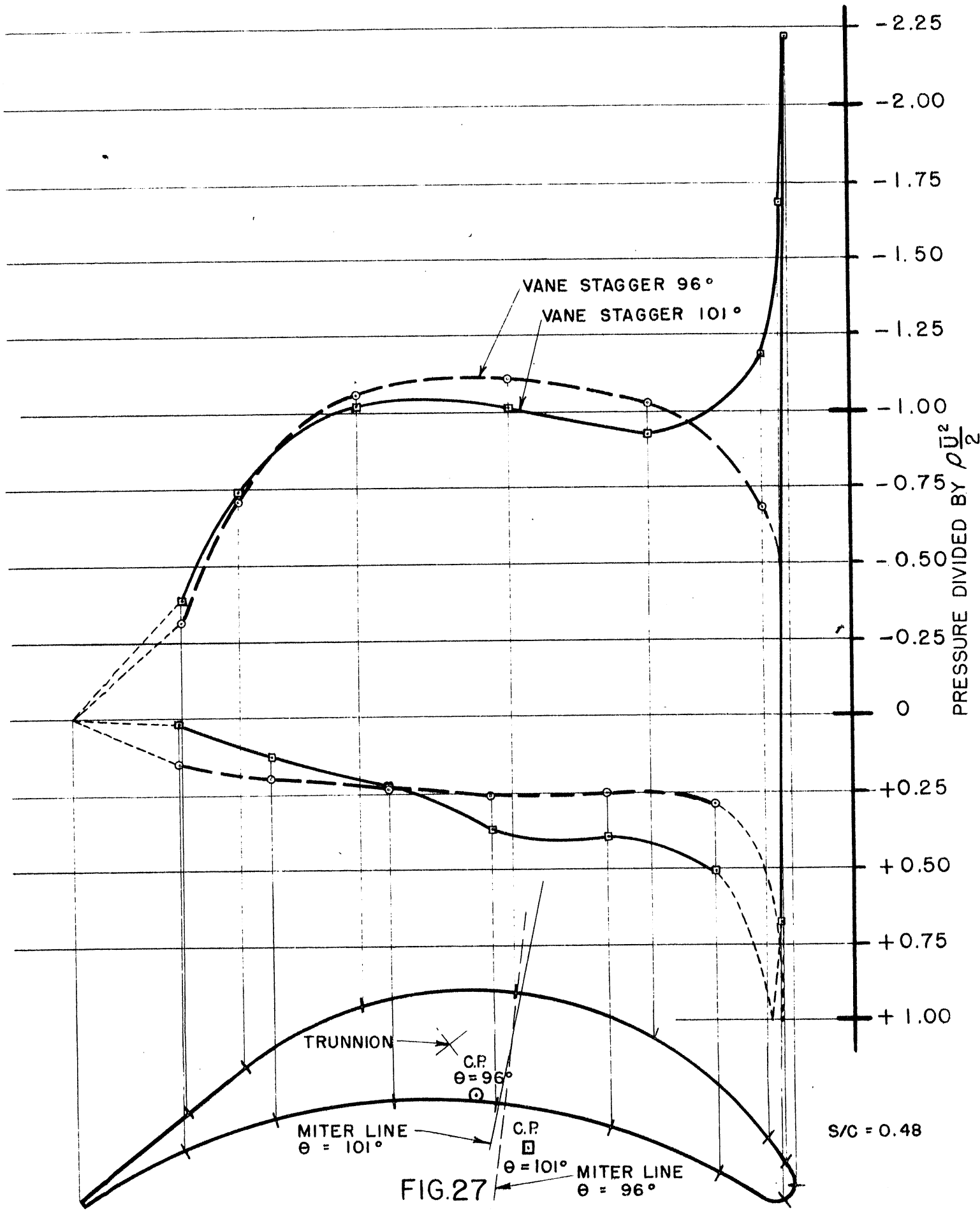

FIG.27

PRESSURE DISTRIBUTIONS AROUND TYPE I VANE IN CASCADE

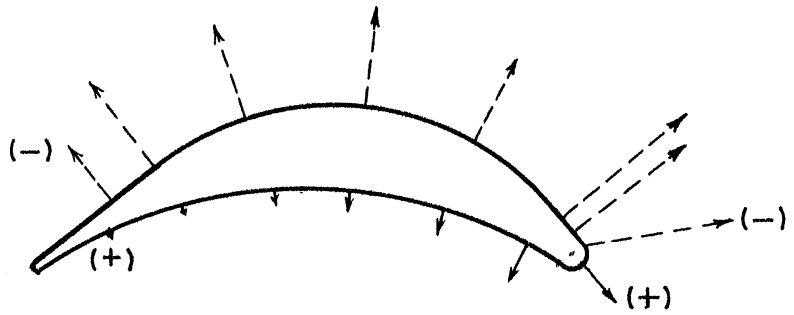

SERIES NO. 16
REYNOLDS NO. 111,000 (WATER)

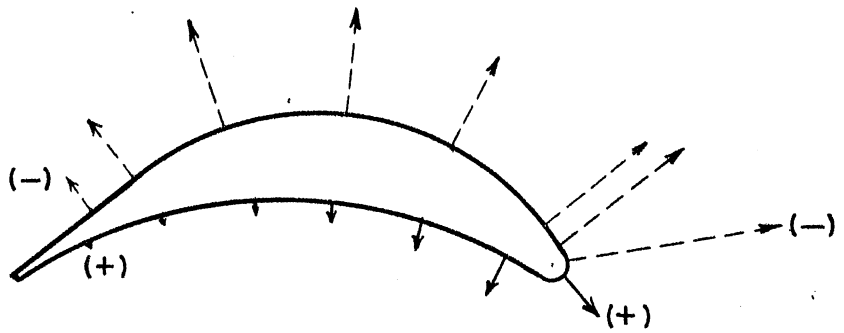

SERIES NO. 17
REYNOLDS NO. 302,000 (WATER)

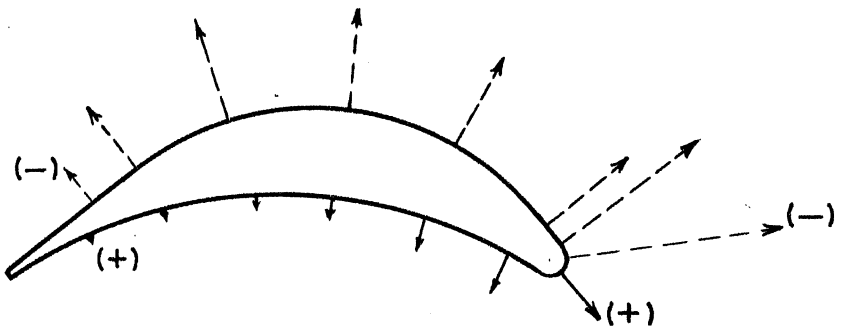

SERIES NO. 18
REYNOLDS NO. 478,000

VANE STAGGER 101°
S/C = 0.48
SCALE 1" = 2 UNITS

FIG. 28
PRESSURE VARIATION AROUND VANE WITH REYNOLDS NUMBER
(PRESSURES IN FT. DIVIDED BY MEAN VEL. HEAD IN FT.)

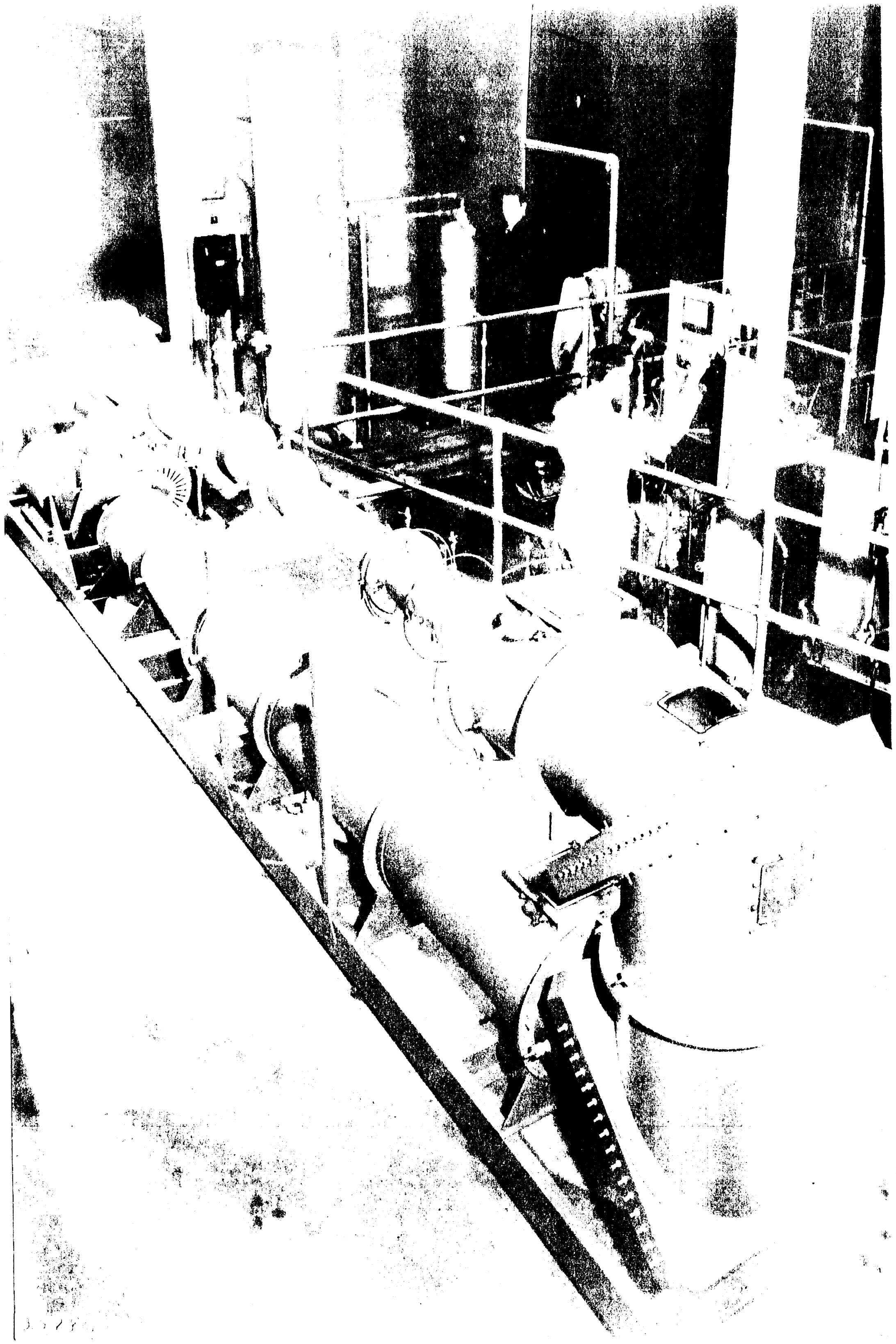

Fig. 29 Model Water Tunnel and Pressure Control Tower

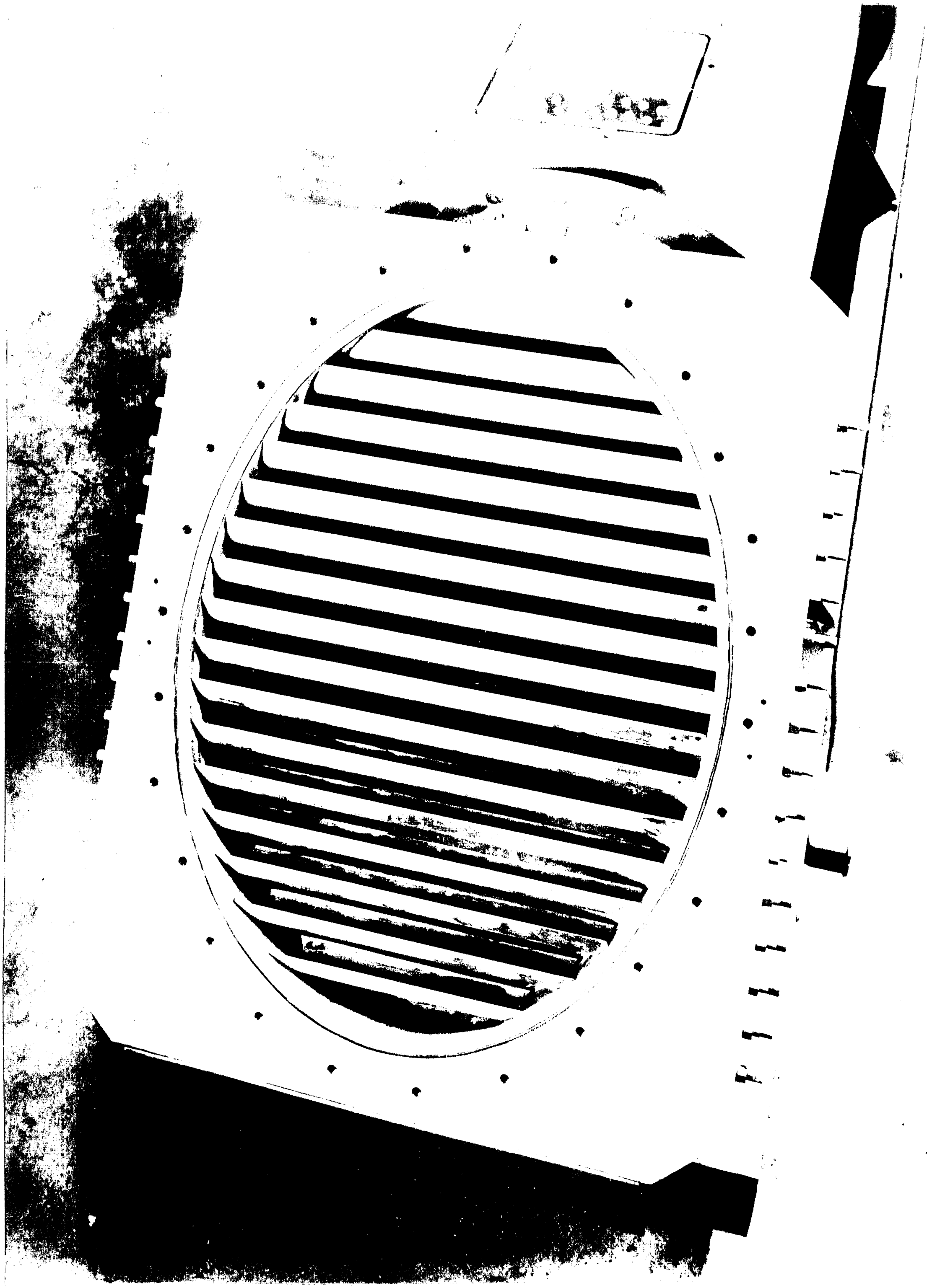

Fig. 30 Guide Vane Cascade and Elbow III
Showing Suction Surface near Trailing Edge

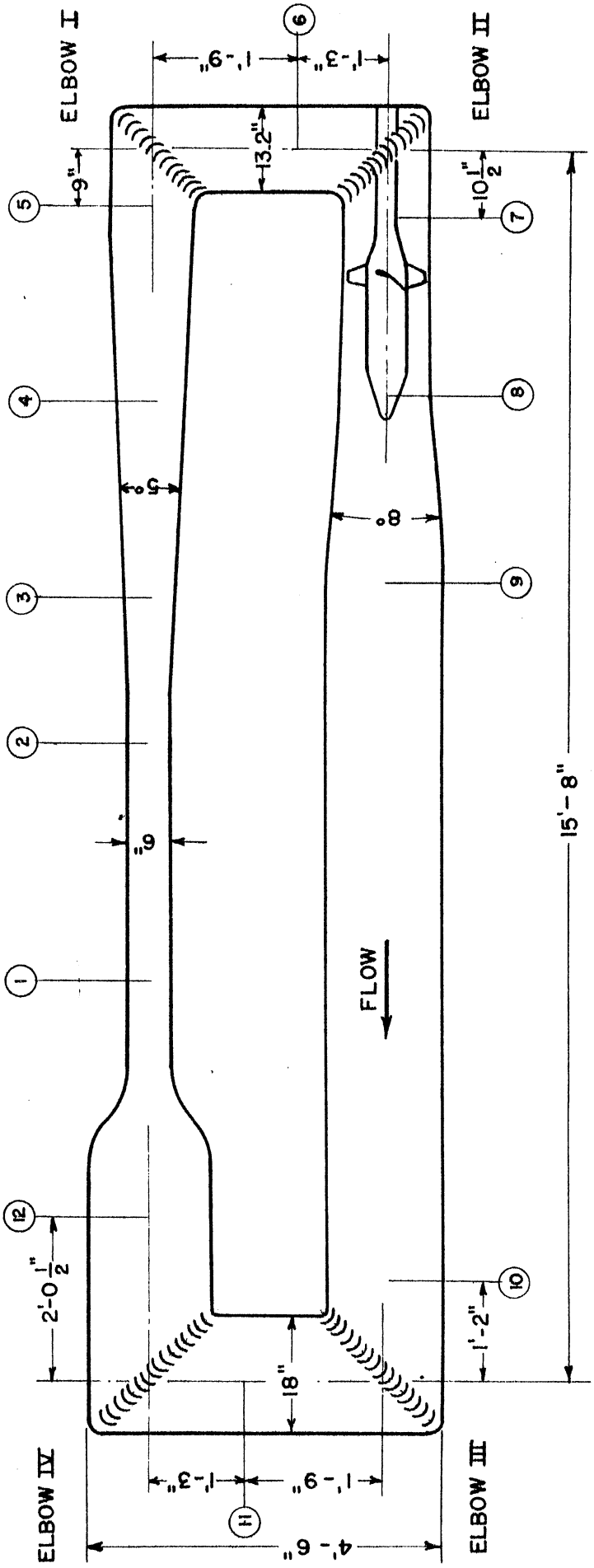

FIG. 31

DESIGNATION OF VANED TURNS AND VELOCITY TRAVERSE STATIONS

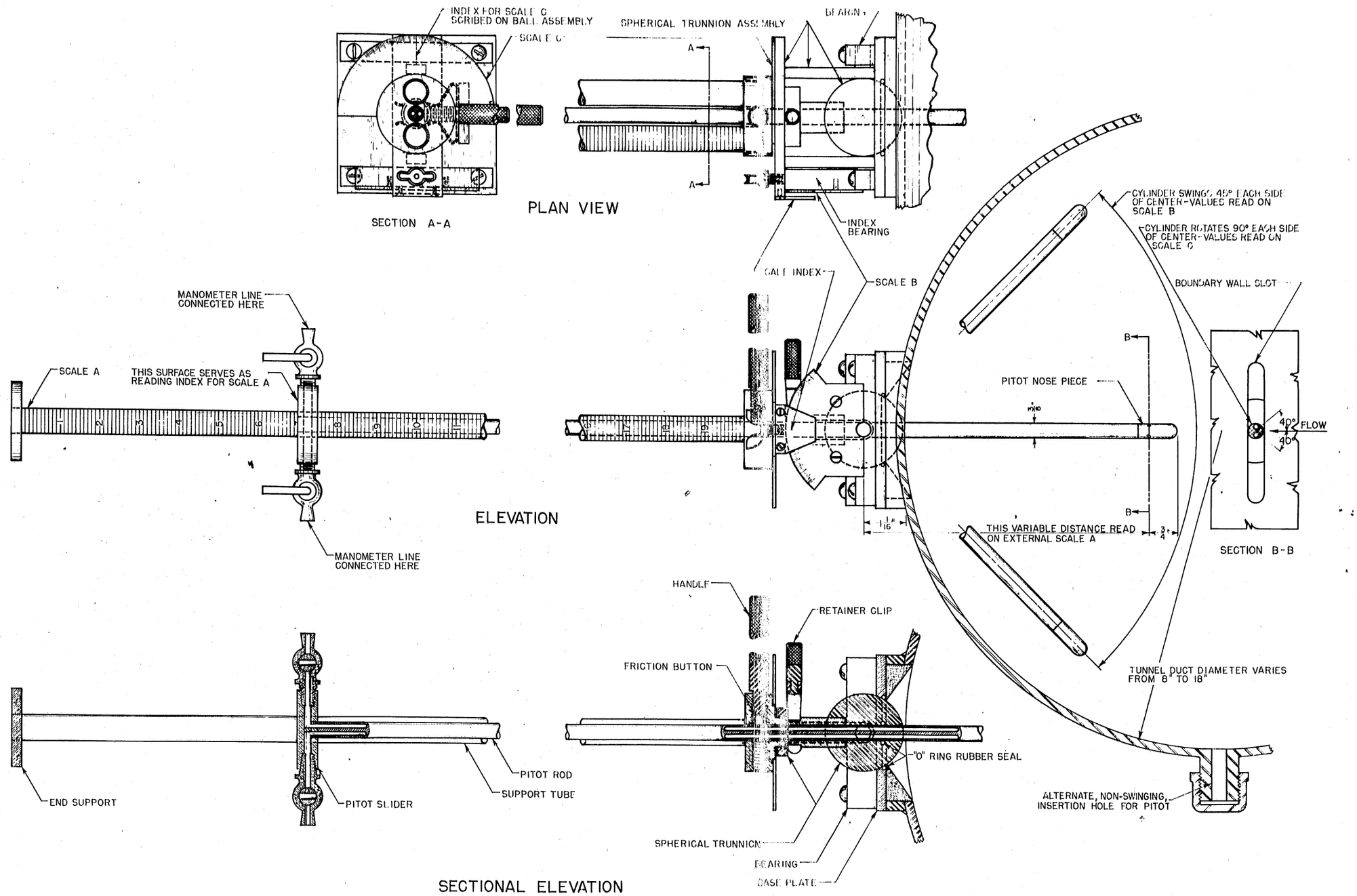

FIG. 32

PITOT CYLINDER AND MOUNTING

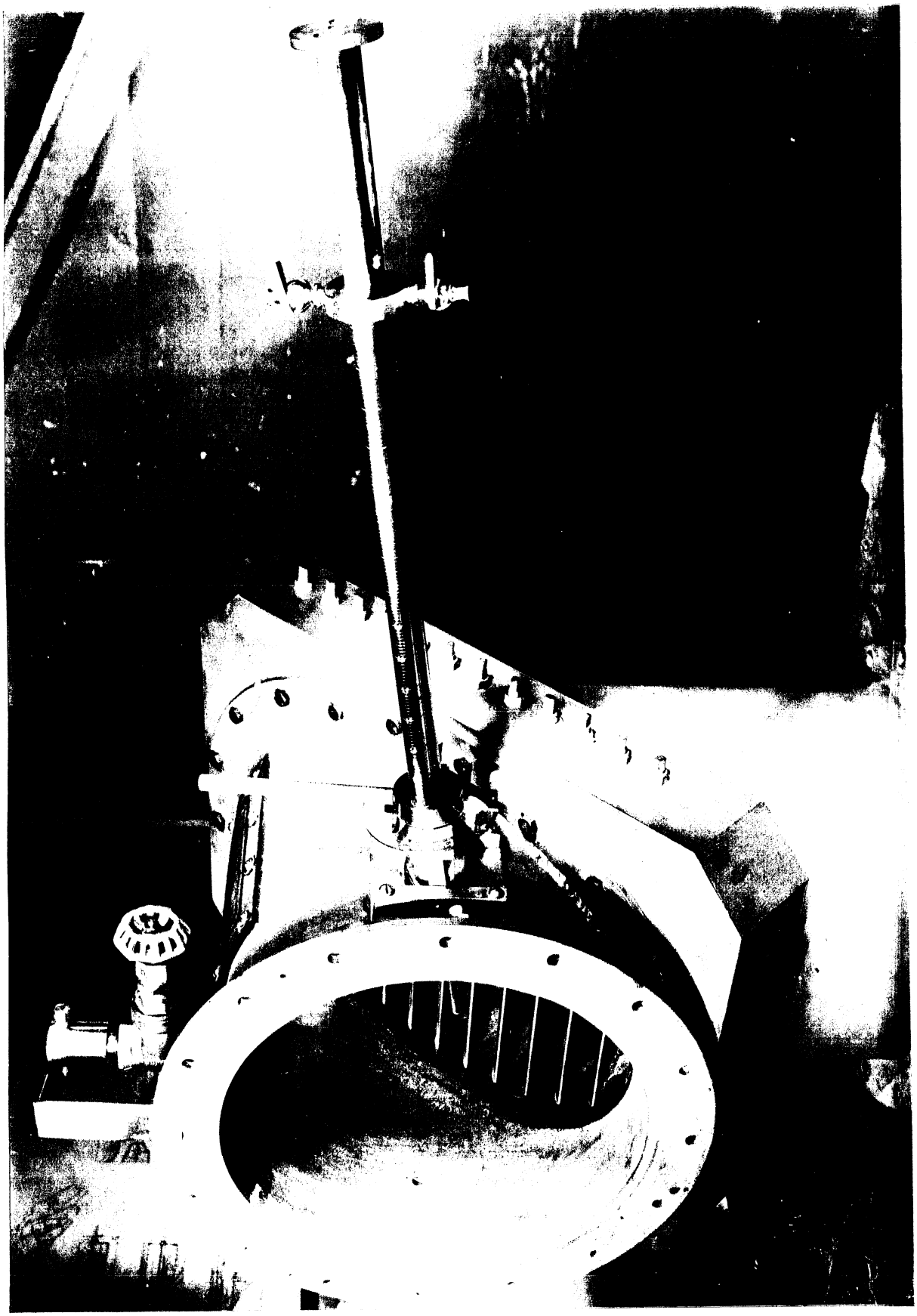

Fig. 23 Thrust Cylinder in Main Mounting at Station 5

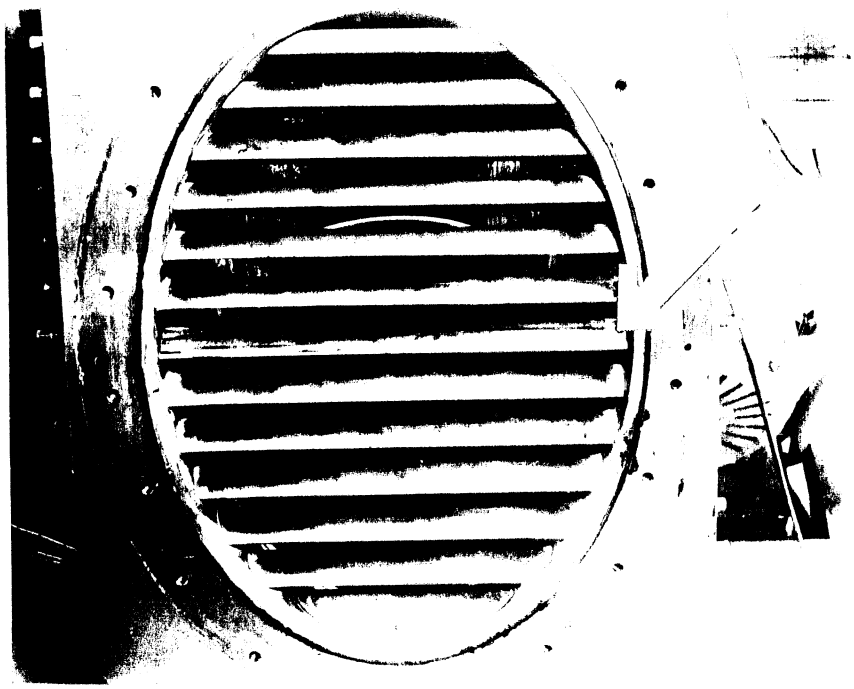

(a) Photo before pre-loading

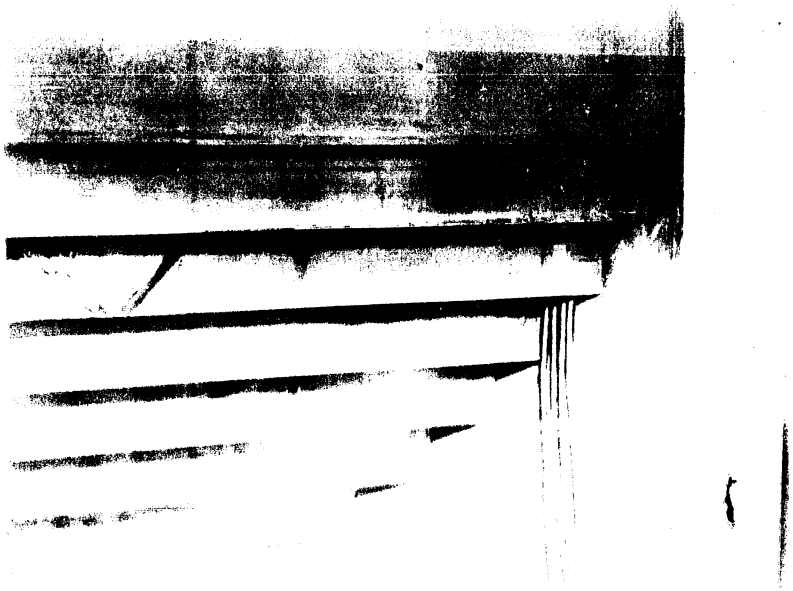

(b) Suction Surface near Trailing Edge
(Note Copper Pressure Lines from Vane Tips)

Fig. 24 Pressure Measuring Vane in Inlet of Model Water Tunnel

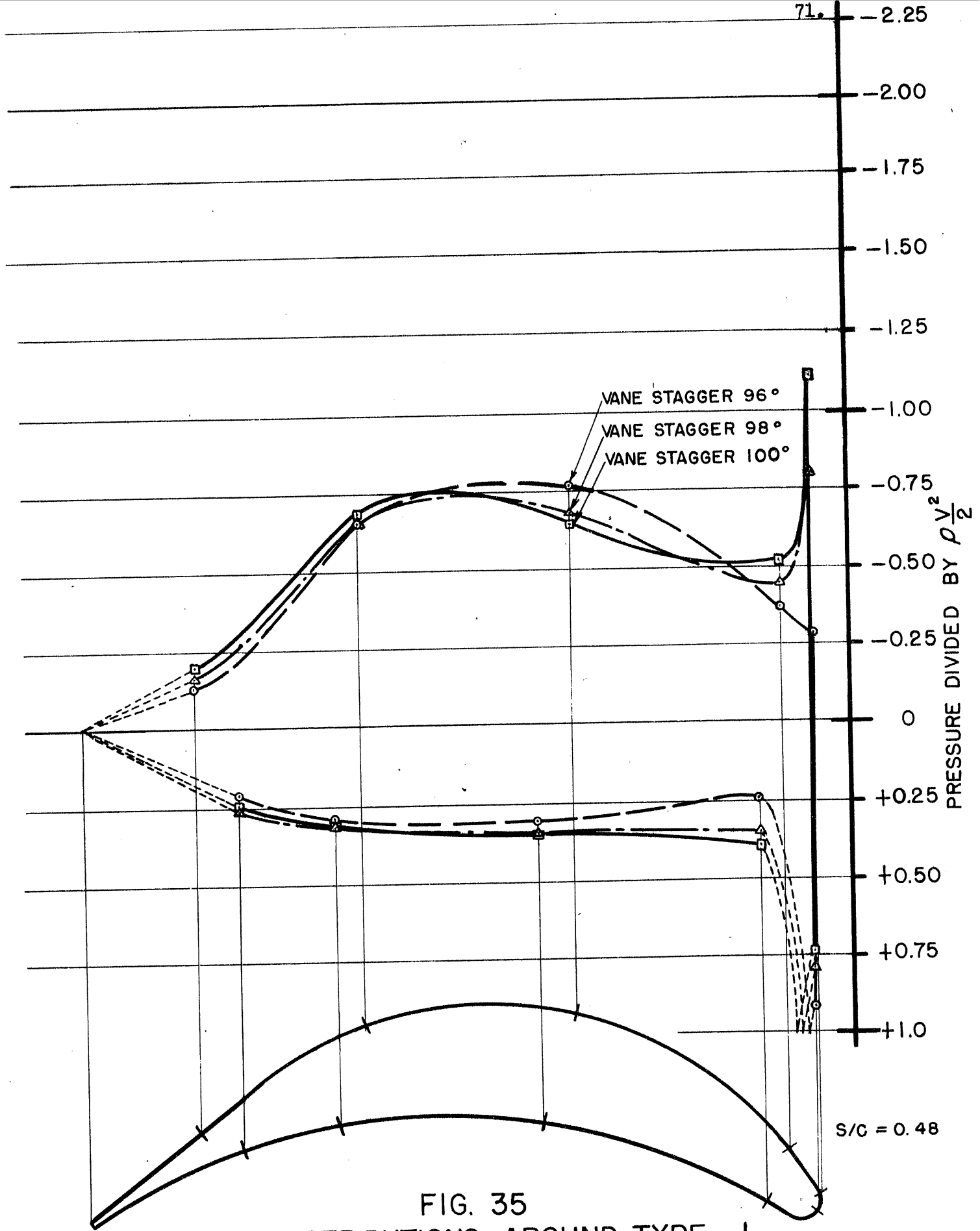

FIG. 35
PRESSURE DISTRIBUTIONS AROUND TYPE I
ALUMINUM VANE IN TUNNEL CASCADE

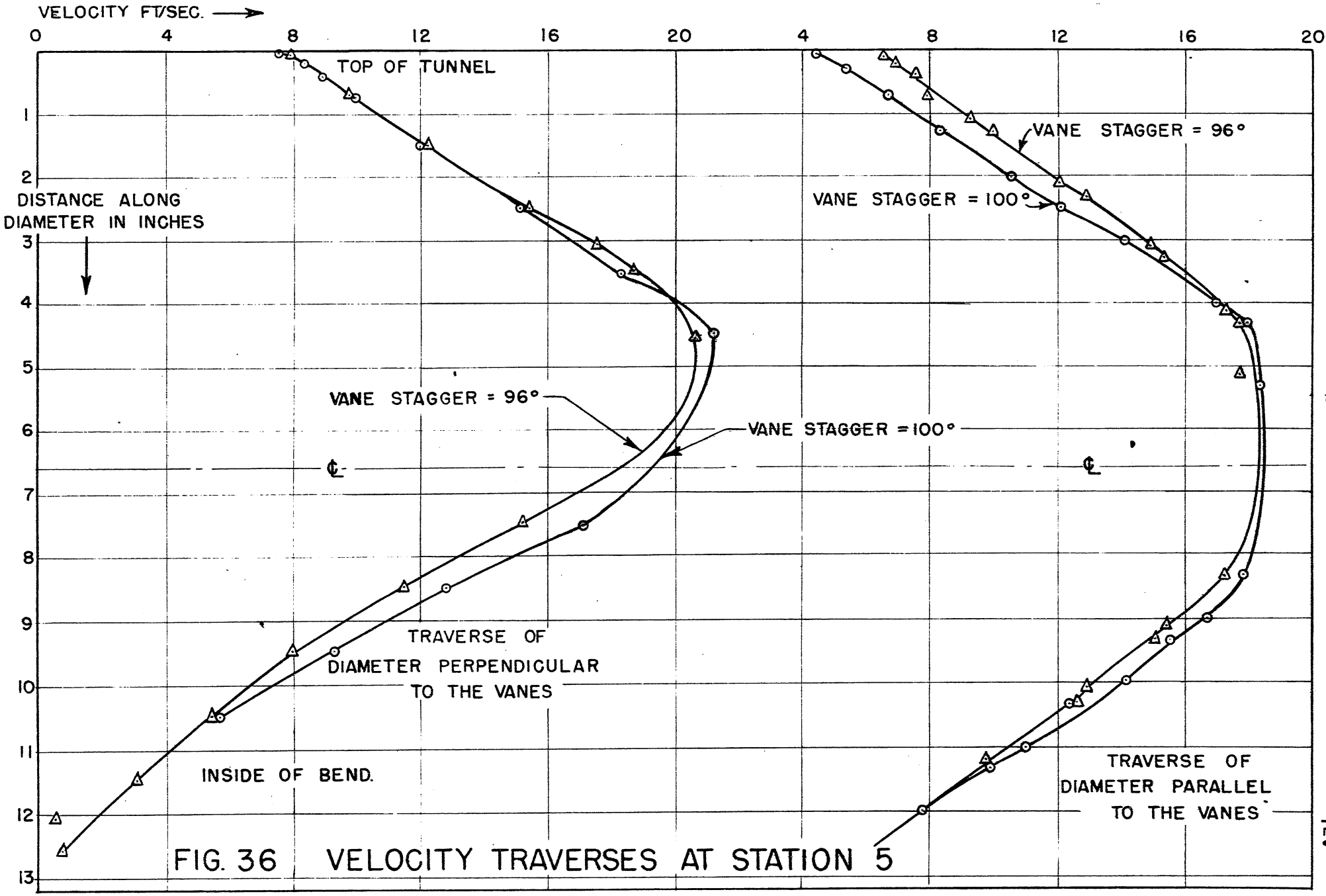

FIG. 36 VELOCITY TRAVERSES AT STATION 5

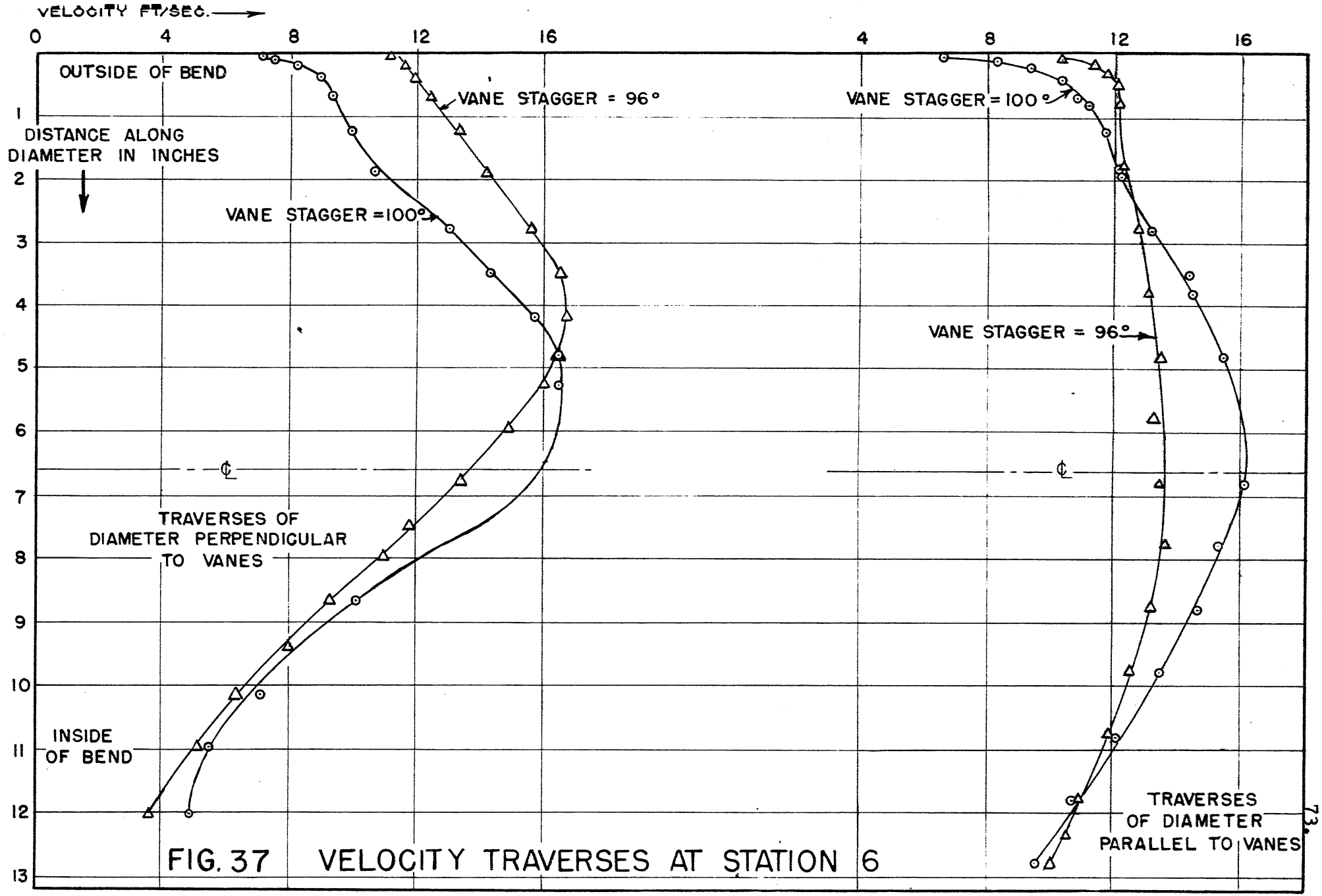

FIG. 37 VELOCITY TRAVERSES AT STATION 6

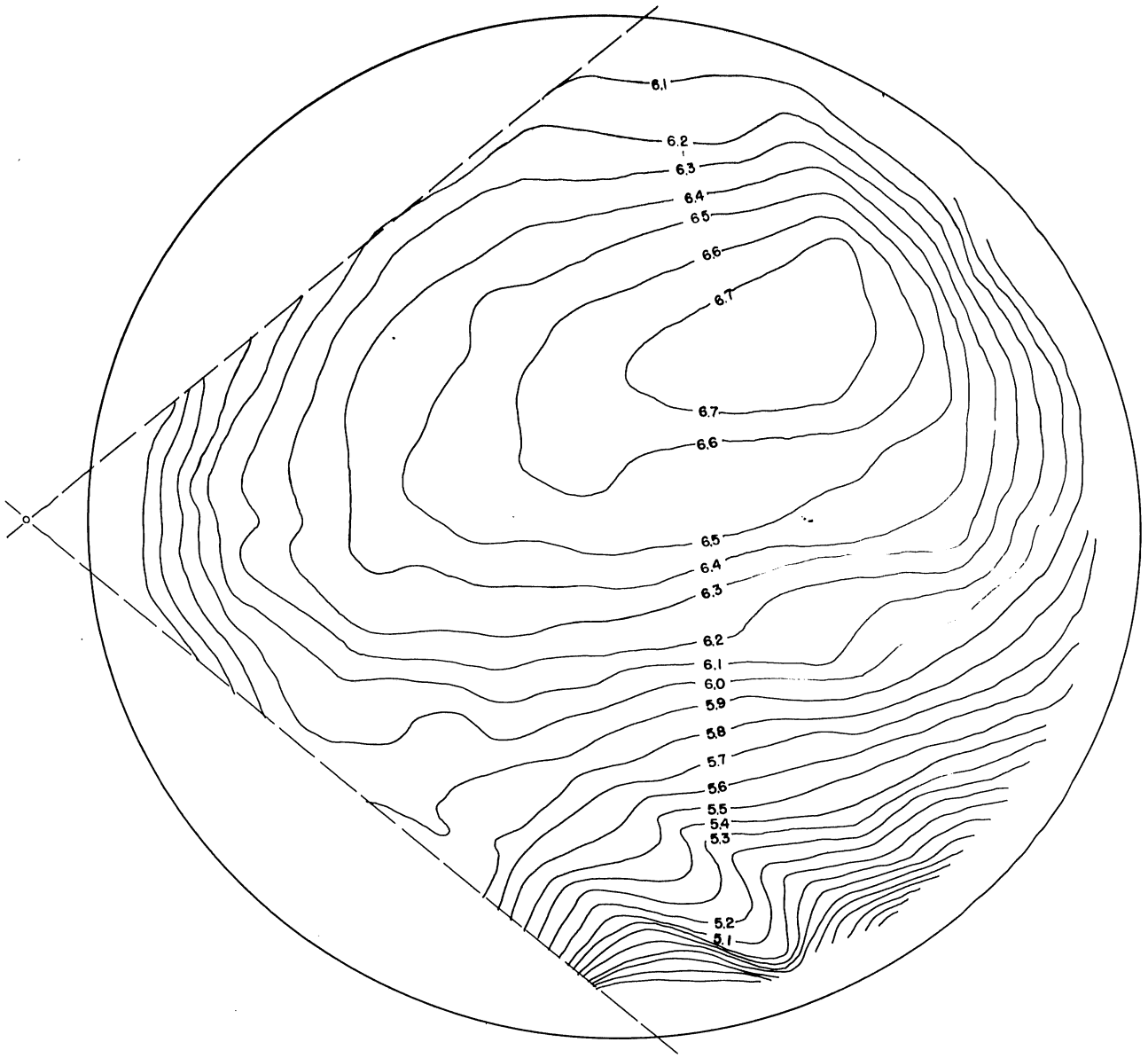

INSIDE OF BEND

FIG. 38 VELOCITY TRAVERSE AT STATION II

Velocity in Test Section = 49.6 ft./sec.
Isovel Interval = 0.1 ft./sec.
Vane stagger = 96°
$s/c = 0.48$

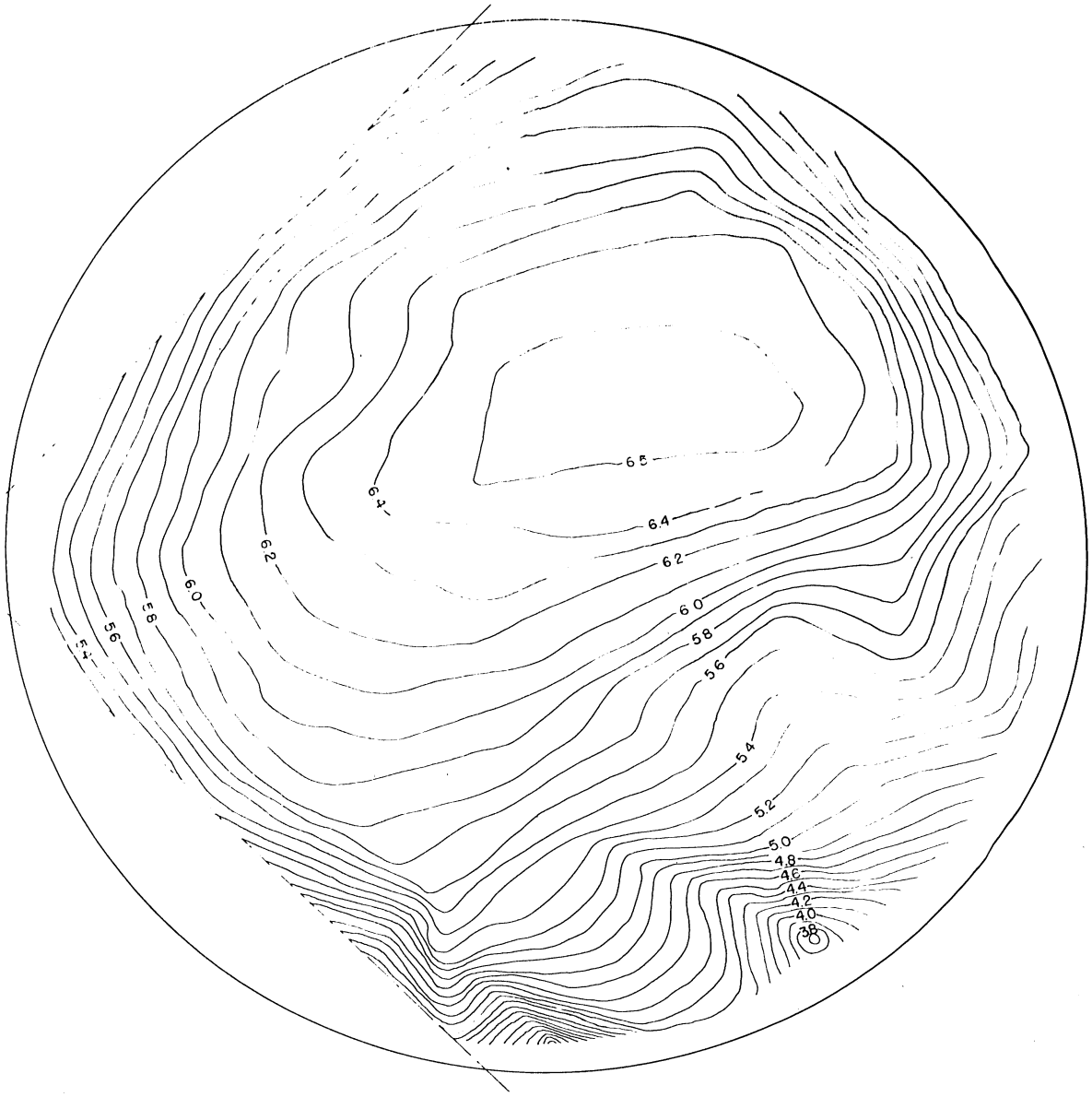

INSIDE OF BEND

FIG. 39 VELOCITY TRAVERSE AT STATION 12

Velocity in Test Section = 49.6 ft./sec.
Isovel Interval = 0.1 ft./sec.
Vane stagger = 96°
$s/c = 0.48$

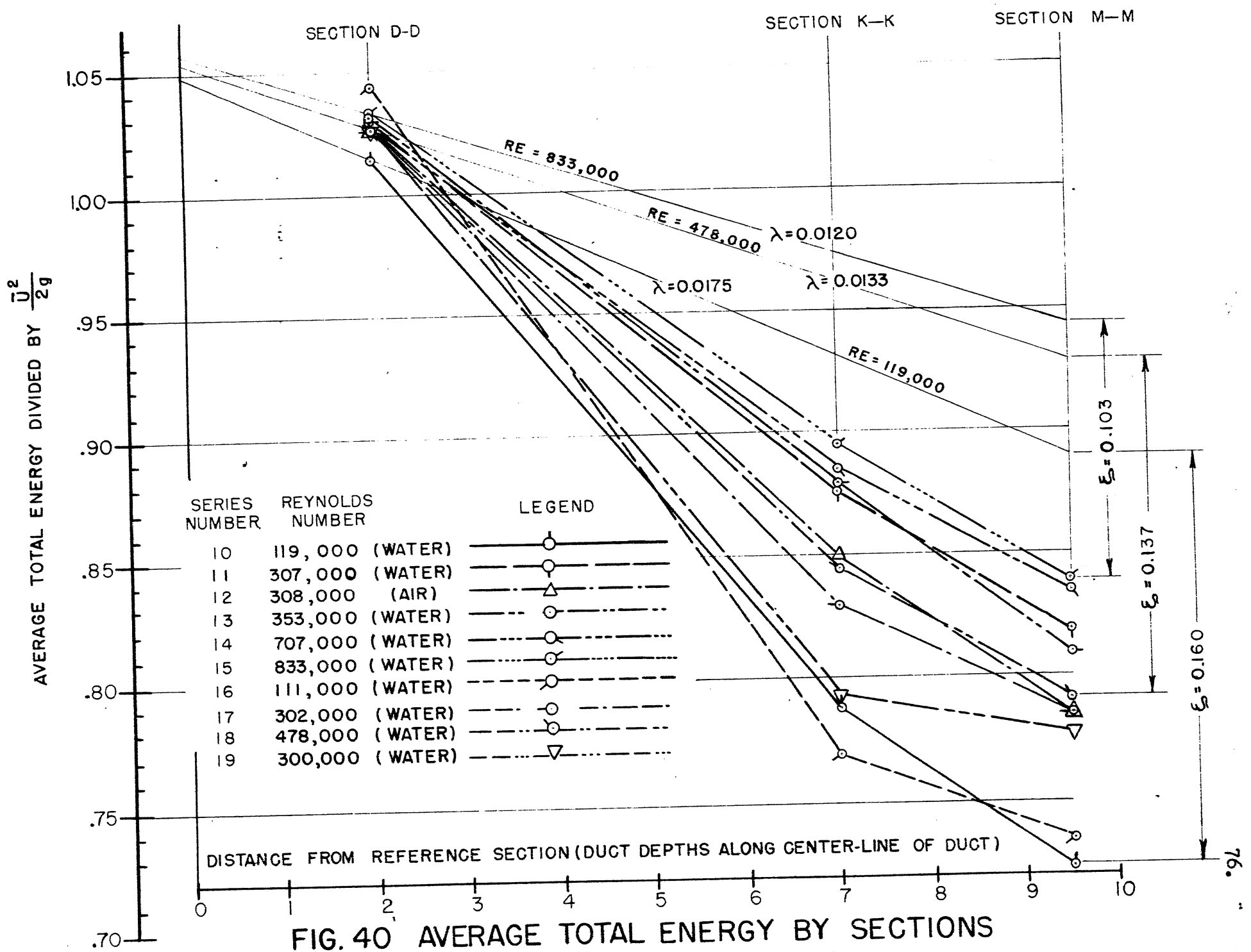

FIG. 40 AVERAGE TOTAL ENERGY BY SECTIONS

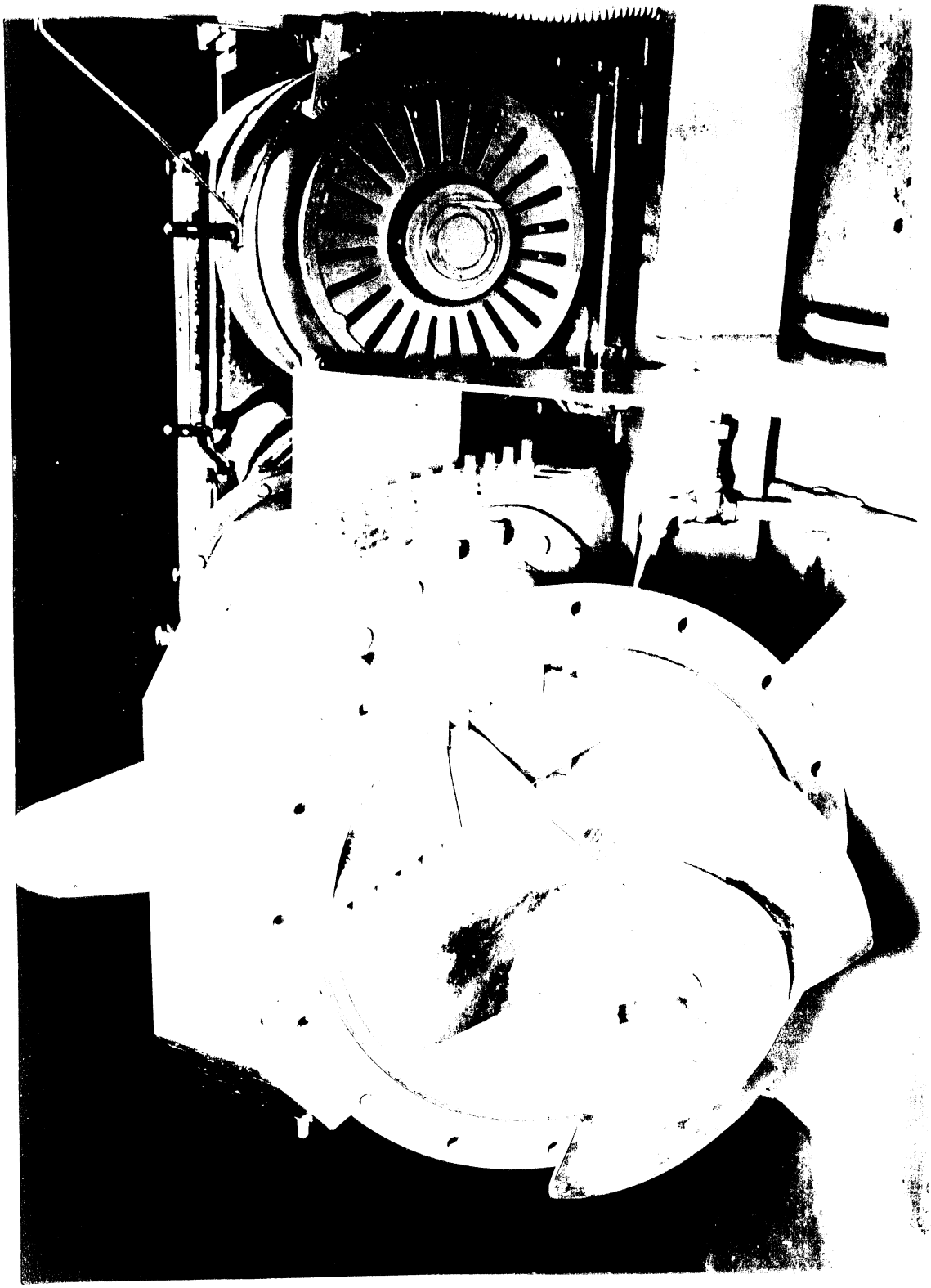

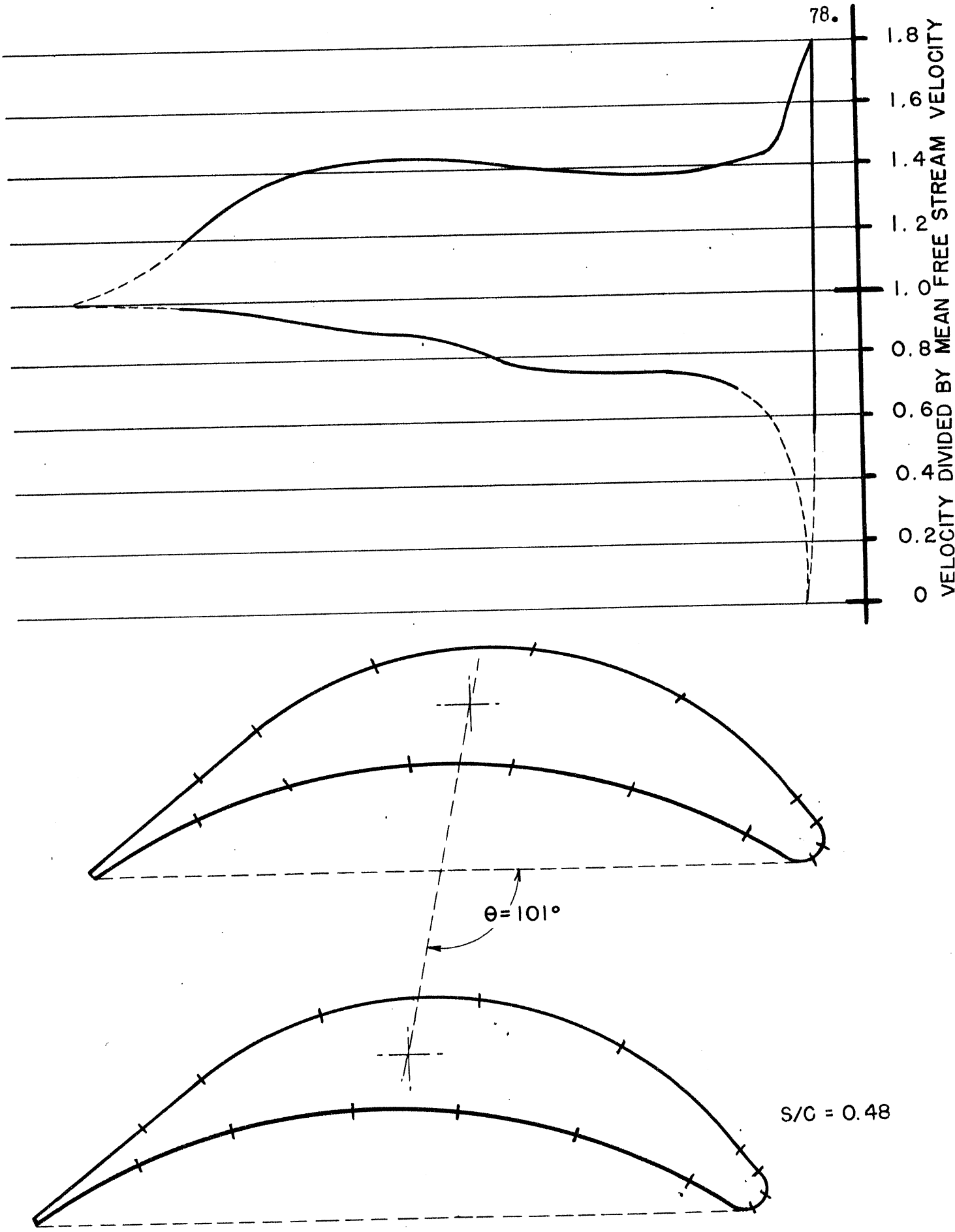

FIG. 42
RELATIVE VELOCITIES NEAR SURFACE OF TYPE I VANE IN CASCADE

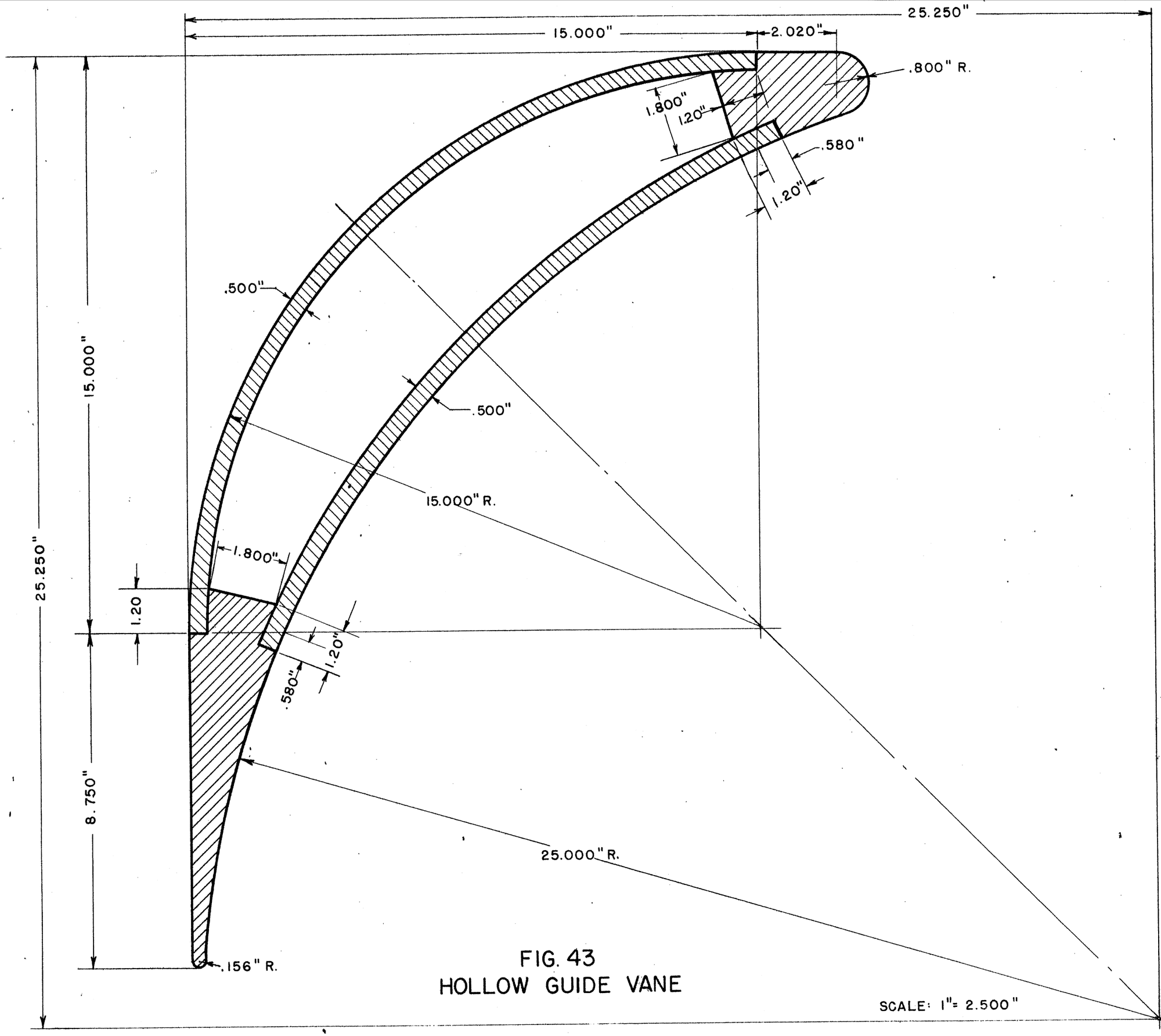

FIG. 43
HOLLOW GUIDE VANE

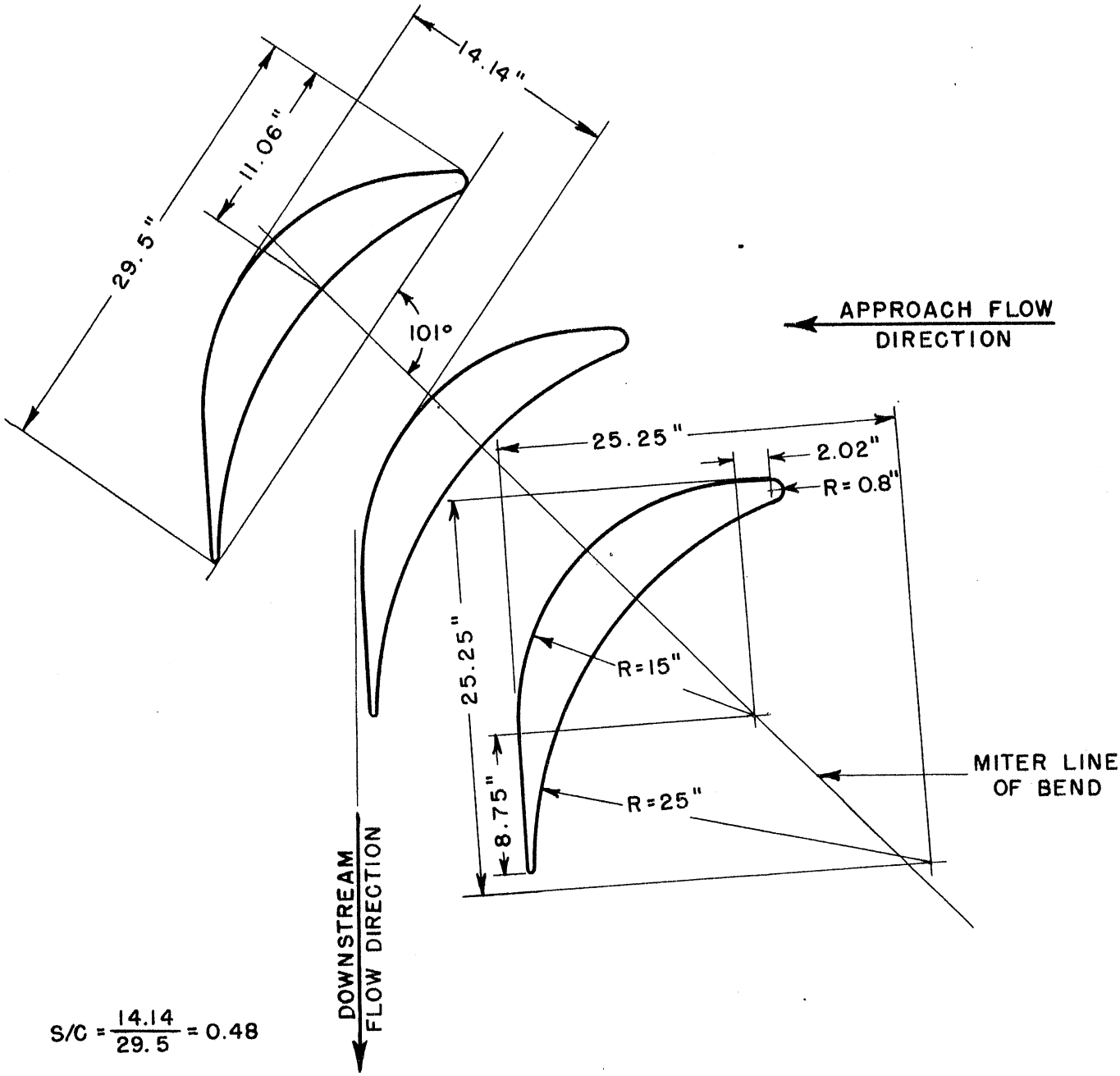

FIG. 44

VANE CASCADE WITH PROTOTYPE DIMENSIONS